BI-DIRECTIONAL BENDING FATIGUE AND STATIC TRANSMISSION CHARACTERISTICS OF POLYMER COMPOSITE GEARS

A thesis
submitted in partial fulfillment of the
requirements for the degree of

DOCTOR OF PHILOSOPHY

by

M. KODEESWARAN
(126103016)

DEPARTMENT OF MECHANICAL ENGINEERING
INDIAN INSTITUTE OF TECHNOLOGY GUWAHATI
GUWAHATI – 781039
AUGUST 2017

CERTIFICATE

It is certified that the work contained in the thesis entitled **Bi-Directional Bending Fatigue and Static Transmission Characteristics of Polymer Composite Gears** by **M. Kodeeswaran**, a student in the Department of Mechanical Engineering, Indian Institute of Technology Guwahati, Guwahati, India, for the award of the degree of **Doctor of Philosophy** has been carried out under our supervision and this work has not been submitted elsewhere for the degree.

Dr. R. Suresh
Head
Composite and Thermal Structures Section
Structural Design & Analysis Division
Vikram Sarabhai Space Centre
Thiruvananthapuram–695022, Kerala, India.

Dr. S. Senthilvelan
Professor
Department of Mechanical Engineering
Indian Institute of Technology Guwahati
Guwahati–781039, Assam, India.

ACKNOWLEDGEMENTS

I would like to express my sincere, heartiest thanks and gratitude to my research supervisors, **Dr. S. Senthilvelan, Indian Institute of Technology Guwahati** and **Dr. R. Suresh, Vikram Sarabhai Space Centre** for their valuable guidance and persistent supports throughout my Ph.D. work. I have immensely benefited from each and every moment of my association with them.

I would like to acknowledge **Dr. U. S. Dixit,** Professor, Department of Mechanical Engineering, **Dr. Sukhomay Pal**, Associate Professor, Department of Mechanical Engineering, and **Dr. A. Perumal**, Professor, Department of Physics, members of my Doctoral Committee who have directed me in right path by providing comments, suggestions and sharing their expertise at various stages of my research work.

I thank the **Honourable Director**, **IIT Guwahati** and the **Head, Department of Mechanical Engineering, IIT Guwahati** for their supports during my research work.

My sincere thanks to respected **Head**, Electro Mechanical Actuation Systems Division, **Group Director**, Control Electronics and Actuation Systems Group, **Deputy Director**, Avionics Entity, **Director**, **Vikram Sarabhai Space Centre** (VSSC), Thiruvananthapuram who have provided me an opportunity to pursue research work.

I would like to acknowledge **Mr. V. Ramachandran**, Group Director, Process Control and Product Assurance Group and **Mr. V. J. Saji**, Deputy Project Director, PSLV and **Mr. N. Narayanankutty**, Head, Library, **VSSC**, for their valuable review and comments.

I extend my sincere thanks to colleague **Mr. Hari Krishnan**, **Mr. Khuleshwar Sahu**, **Mr. Anoop Nair, Mr. Leejo**, **Mr. V. S. John Kutty, Mrs. Laija** and **Mrs. Praseeda, VSSC**, Thiruvananthapuram for their valuable supports during my research work.

I am very grateful to the technical staff of Mechanical Engineering Department, **Mr. Sanjib Sarma** for his contribution in conducting tests. I am also thankful to the office staffs of Mechanical Department **Mr. Nabajyoti Dutta** and **Mr. Raju Talukdar** who have supported me in the academic and administration works.

I thank **Mr. B. R. Singh**, M/s. OKA Basus and **Mr. Joshi**, M/s. Justi Preci Components, Thiruvananthapuram for their consistent supports in realizing specimens, gears and test rigs.

I extend my thanks to **Mr. Prasanth**, M/s. Perfect Gears, Chennai for his supports in gear metrology.

I express thanks to **Mr. Dattatray Bhilare**, ABB, Pune and **Mr. Uttam Basar**, Electro, Guwahati for their supports in realising control panel including electrical parts.

I am thankful to my friends **Dr. R. Kalidasan, Dr. A. Muthuraja, Dr. Johnney Mertens, Mr. N. Anand Mohan, Mr. Nitin S. Sarpe, Mr. Anurag Mishra, Ms. Arnika Verma, Ms. Sarita Bharti, Mr. Karthik Pandian, Mr. Sahidul Islam, Mr. R. Vignesh Babu, Dr. S. Arun, Dr. V. Satheesh Kumar** and **Mr. Kishor Kumar** for their valuable help in my thesis work**.**

I extend my sincere thanks to **my parents, my brother** and **his family** and **my family** for their enormous supports and encouragement to complete the research work.

Finally, I extend my gratitude to the **Almighty** for giving me this opportunity and good health for the successful completion of this breakthrough in my carrier.

M. Kodeeswaran

ABSTRACT

Polymer and polymer composite gears are nowadays substitute metal gears for medium load applications. In some applications such as actuators of satellite launcher, the gears experience bi-directional loads. However, gear design procedures consider only uni-directional loads, either clockwise/counter clockwise sense of rotation. In the present study, a test rig has been developed in-house with a servo motor to apply either bi-directional (ratio of minimum to maximum stresses is stress ratio, R = −1) or uni-directional (R = 0) bending loads on the gears at desired frequencies. Bi-directional and uni-directional bending fatigue performance of injection molded unreinforced and carbon fiber reinforced polyamide 66 gears were evaluated. Tests were carried out at different loads and frequencies. The torque acted on the test gear and the angular displacement of the gears were continuously measured and recorded. The net surface temperature was higher for the gears subjected to bi-directional loads compared to uni-directional loads. Carbon fiber reinforced gears exhibited lower temperature than that of unreinforced gears. Unreinforced gears exhibited both thermo mechanical and root crack failures. The straight root cracks were almost normal to tooth fillet radius and confirmed ductile failure. Mechanical fatigue failures of carbon reinforced gears exhibited tortuous crack path due to the existence of reinforced fibers. Carbon fiber reinforced gears exhibited superior bending performance compared to unreinforced gears. Significant fatigue life reduction was observed in bi-directional loading compared to uni-directional loading.

Hysteresis loop area and surface temperature increase with torque for unreinforced gears. At higher frequency, life decreases with increase in torque for both the bi-directional and uni-directional loads. The increased gear temperature at higher

frequency contributes this behaviour. Unreinforced gears exhibited both thermo mechanical and root crack failures in bi-directional loads and root crack failures only in uni-directional loads. The straight root cracks with overlapping fractured surfaces both in bi-directional and uni-directional loads at higher frequency were observed.

In this work, numerical and experimental studies were carried out on steel-polyamide gear pair to evaluate the static transmission characteristics. Two-dimensional static finite element analysis using linear and nonlinear material models was carried out using commercial finite element analysis tool, ABAQUS®. Premature and extended contacts found to occur in the mesh and were increasing with load, which increased the roll angle.

Gears experience different rates of loading during their service life. The injection molded tensile specimens made of polyamide gear material, were subjected to various rates of loading. The stress-strain performance at various rates of loading was evaluated and used to model linear and nonlinear gear materials for the numerical analysis. The bending stress and static transmission error were predicted through finite element analysis. Bending stress with nonlinear material models was lower compared to that of linear material models. The predicted static transmission error of gear pair was compared with the experimental data obtained using in-house developed gear test rig. The measured static transmission error was found to have good correlation with the static transmission error predicted with higher strain rate nonlinear material model.

KEYWORDS: Polymer composite gear; fatigue; hysteretic heating; frequency; finite element analysis; static transmission error

TABLE OF CONTENTS

LIST OF FIGURES

LIST OF TABLES

LIST OF EQUATIONS

ABBREVIATIONS

CF	Carbon fiber
CNF	Contact normal force
DTC	Double teeth contacts
DMA	Dynamic mechanical analysis
FEA	Finite element analysis
GFRP	Glass fiber reinforced plastic
iPP	Isotactic polypropylene
PA	Polyamide
PACF	Carbon fiber reinforced polyamide
PBT	Polybutylene terephthalate
PEK	Polyetherketone
PEK-C	Polyphenylene ether ketone
PEEK	Polyetheretherketone
PI	Polyimide
PMMA	Polymethylmethacrylate
POM	Polyoxymethylene
PP	Polypropylene
PPS	Polyphenylene sulphide

PTFE	Polytetrafluoroethylene
SEM	Scanning electron microscope
SiO_2	Silica
STC	Single tooth contact
STE	Static transmission error
TE	Transmission error
TiO_2	Titanium oxide
UHMWPE	Ultra high molecular weight polyethylene

NOTATIONS

English Symbols

R	Stress ratio
Fa	Total involute profile deviation (μm)
fha	Profile slope deviation (μm)
ffa	Involute profile form deviation (μm)
fp	Tooth-to-tooth spacing / pitch deviation (μm)
Fr	Radial runout variation (μm)
F_t	Tangential load (N)
m	Module (mm)
m_n	Normal module (mm)
b	Face width (mm)
Y	Lewis form factor
S_q	Critical section thickness (mm)
h_q	Height at which load acts from critical section (mm)
Y_F	Form factor
Y_S	Stress concentration factor
Y_B	Rim thickness factor
Y_{DT}	Deep tooth factor

Greek Symbols

Fβ	Total lead deviation (μm)
fhβ	Lead slope deviation (μm)

ffβ	Lead form deviation (μm)
σ_b	Tooth root bending stress (N/mm^2)
σ_{F0}	Tooth root bending stress (N/mm^2)
Y_β	Helix angle factor

CHAPTER 1

INTRODUCTION

1.1 OVERVIEW ON POLYMER AND POLYMER COMPOSITE GEARS

Gears are machine elements used in mechanisms to transmit motion and power between shafts by means of progressive engagement of teeth. Materials used for manufacturing gears range from metals to thermoplastic materials. Thermoplastic polymer and polymer composite gears are utilized in many engineering applications due to their specific advantages. Thermoplastic gears can be realized by machining from casting or by injection molding. The advantages of injection molding include cost effectiveness and elimination of machining operations. Thus, injection molded thermoplastic gears are most widely used as compared to machined thermoplastic gears. On the other hand, limitations such as higher initial mold cost and poor quality are associated with the injection molded thermoplastic gears. The use of reinforced thermoplastics as gear materials is increased to improve the structural, tribological and thermal properties. Glass and carbon fibers are the most commonly used reinforcement in the thermoplastic gears.

Extensive investigations have been carried out to understand the fatigue and wear performance of polymer composite gears under uni-directional cyclic bending and contact loads (Kurokawa *et al.* (1999, 2003), Senthilvelan and Gnanamoorthy (2004b, 2007), Mao *et al.* (2007, 2009), Imrek (2009), Duzcukoglu (2009a, 2009b), Kirupasankar *et al.* (2012), Hoskins *et al.* (2014), Pogacnik and Tavcar (2015)). Mohan

and Senthilvelan (2014) evaluated the bi-directional bending fatigue performance of polymer composite gears under constant deflection mode.

Investigations were also carried out to understand the influence of fiber reinforcement and fiber orientation, on the mechanical properties of polymers including the fatigue behavior and failure mechanisms at the specimen level (Zhou *et al.* (1994), Zainudin *et al.* (2002), Bernasconi *et al.* (2007), Goel *et al.* (2009), Mortazavian *et al.* (2015c), Mortazavian and Fatemi (2016)).

Extensive research works have been carried out to evaluate the bending fatigue performance of steel gears with the aid of single tooth bending fatigue test facility, but these investigations were also limited to uni-directional loading (Eyercioglu *et al.* (1997), Daniewicz and Moore (1998), Akata *et al.* (2004), Handschuh *et al.* (2007), Stringer *et al.* (2011), Zhang *et al.* (2013)). In this research work, a test rig has been developed and bi-directional bending fatigue loads were applied on the unreinforced and carbon fiber reinforced polymer gears and studied the bending fatigue performance.

Polymer gears generate significant heat due to material hysteretic effect. Hence, it is important to assess the performance of polymer gears under different loads and speed ratings. Investigations for the effects of frequency and stress magnitude on hysteretic self-heating and fatigue life were carried out on the polymer specimens for both bi-directional (stress ratio, $R = -1$) and uni-directional ($R \geq 0$) loads (Goel *et al.* (2009), Mortazavian *et al.* (2015c), Mortazavian and Fatemi (2016)). Hysteretic self-heating and the effect of loading frequencies on the fatigue life due to bending loads under bi-directional and uni-directional loadings on the gear mesh were not investigated, which is attempted by the researcher.

In the recent years few researchers (Yelle and Burns (1981), Walton *et al.* (1994), Ming and Ying (1997), Meuleman *et al.* (2007), Letzelter *et al.* (2009), Karimpour *et al.* (2010), Atanasiu *et al.* (2011), Cathelin *et al.* (2013)) have carried out numerical, analytical as well as experimental works on polymer gears transmission characteristics. Polymer materials have strain rate dependent nonlinear material behaviour. Extensive investigations were carried out on the polymer and polymer composite materials under different strain rate conditions (Mourad *et al.* (2004), Guo and Li (2007), Nitta and Nomura (2014)). Analytical works and finite element analyses carried out on the polymeric gears used linear material model only. Hence there is a scope to understand transmission characteristics of polymer gears comprehensively.

1.2 MOTIVATION

The transmission characteristics of gears are functional requirements in precision motion applications. Polymer gears undergo large nonlinear deflection due to low material modulus which motivate to investigate their bending and transmission characteristics. Additionally, in some applications such as actuators of satellite launcher and robotics, the gears experience bi-directional loads. Also, hysteretic heating affect the performance of polymer gears significantly. Hence, it is important to investigate the performance of polymer composite gears under such bi-directional loads at different speeds to widen their applications.

1.3 HYPOTHESIS

The following are the prepositions

- Loading pattern controls fatigue life of polymer material
- Hysteretic heating controls the fatigue life of polymer material

- Thermo mechanical failure is significant mode for polymeric parts

1.4 OBJECTIVES

The main objectives of present work are to investigate the bending fatigue and static transmission characteristics of polymer composite gears for precision bi-directional applications.

1.4.1 Methodology

Following methods were carried out to achieve the main objectives

- Investigation of mechanical behaviour of the gear material (unreinforced and carbon fiber reinforced polyamide 66) using standard servo hydraulic test facility.
- Metrological inspection of driver gear (ground standard steel gear) and driven gears (injection molded unreinforced and carbon fiber reinforced test gears).
- Design and development of fatigue test rig simulating actual gear mesh to exert bi-directional and uni-directional loads.
- Evaluation of bi-directional and uni-directional bending fatigue performance of unreinforced and carbon fiber reinforced polyamide gears using gear test rig.
- Evaluating the effects of frequency on hysteretic heating and fatigue performance of unreinforced polyamide gears.
- Numerical investigation on the bending and transmission characteristics of unreinforced polyamide gears using linear and nonlinear material behaviours obtained at different strain rates.
- Experimental investigations on static transmission error using an in-house developed test rig and comparison with the numerical results.

1.5 ORGANISATION OF THE THESIS

First chapter briefly discusses the motivation of the present work which includes research on polymer and polymer composite gears including the numerical and experimental investigations on the transmission and bending characteristics, fatigue evaluations using uni-directional gear test rigs and requirement and evaluation using bi-directional gear test rig. Objectives and major methodologies adopted are outlined in this chapter.

Brief literatures on polymer and polymer composite gears are discussed in the second chapter. Prior work related to assessment of uni-directional bending fatigue life evaluation of polymer gears, uni-directional and bi-directional bending fatigue performance of polymers at specimen level including hysteretic heating and transmission characteristics using numerical and experimental evaluations, are also discussed in this chapter.

Third chapter deals with the materials used to develop gears, manufacturing details, test rig details and methodologies adopted for evaluating mechanical, metrology of gears and performance of gears.

Fourth chapter deals with the uni-directional and bi-directional bending fatigue performance of unreinforced and carbon fiber reinforced polyamide spur gears. Effects of frequency (rate of loading) on the hysteretic heating and bending fatigue life are reported in fifth chapter.

In the sixth chapter, the transmission and bending characteristics of unreinforced polyamide gears evaluated numerically and experimentally, are discussed. The effect of strain rate on these characteristics is also discussed in this chapter.

Major conclusions drawn from the work and scope for the future work are the outline of the last chapter.

CHAPTER 2

LITERATURE SURVEY

2.1 INTRODUCTION

The gears made up of thermoplastic polymer materials are being considered for many engineering applications due to many advantages such as less weight and dynamic forces, self lubrication, reduced noise and lower manufacturing costs. The candidate thermoplastic materials are polyetherketone (PEK), polyphenylene sulfide (PPS), polyoxymethylene (POM), polybutylene terephthalate (PBT), polymethyl methacrylate (PMMA), polypropylene (PP), polyimide (PI), polyamide (PA), polyetheretherketone (PEEK). As the polyamide (PA) material has good mechanical properties such as strength, damping, rigidity, fatigue strength, wear and sliding resistance, it is preferred for the gear applications over other thermoplastic materials.

The polyamide gears generate heat by material hysteretic effect predominantly. The performance of polymer gears is significantly affected by this heat generation and it varies with the load magnitude, load pattern and rate of loading. The carbon fiber reinforcement in polyamide gears improve the mechanical strength, material modulus and thermal properties to obtain superior load carrying capability and bending fatigue life. The transmission characteristics of polyamide gears become critical parameter in precision motion applications. In addition, the mechanical properties of polymer materials are improved with increase in the rate of loading.

The research and development on the polymer and polymer composite gears have been progressing significantly in the last few decades. The present work is attempted to widen the scope of using polymer composite gears in bi-directional precision applications. In this chapter, the prior works to understand the relevant behaviours of polymers, polymer composites, polymer composite gears and their fatigue performance including transmission characteristics and hysteretic self-heating, are discussed.

2.2 BENDING FATIGUE PERFORMANCE OF POLYMER COMPOSITES, POLYMER COMPOSITE GEARS AND METAL GEARS

Gears are subjected to uni-directional (clockwise or counter clockwise) bending fatigue loads in automobile gear application. However, in the actuators of launchers, the gears are subjected to bi-directional (both clockwise and counter clockwise) bending loads. The bending fatigue performance of polymer composite/metal gears subjected to uni-directional loads and bending fatigue performance of polymer composites subjected to both the uni-directional and bi-directional loads were studied by many researchers and are discussed in the subsequent sections.

2.2.1 Bending fatigue performance of polymer composite gears under uni-directional loads

The bending fatigue alongwith the contact fatigue, wear, surface temperature and durability performances of polymer composite gears were investigated by simulating actual gear mesh. The test gears were subjected to various uni-directional loads at different speeds. The same polymer composite/metal gears were used for mating with the test gears. The test rigs used for the studies include power absorption type and

power circulation type. Effects of fiber reinforcement on the performance and failure modes were also reported.

Breeds *et al.* (1993) investigated the wear behaviour of nylon-nylon and acetal-acetal gear pairs. Novel test rig with back-to-back arrangement was used for exerting loads on the test gears. Tests were carried out for different loads (3–17 Nm) at 1000 rpm speed. Wear process was found to be complex. Life was limited by wear and thermal failure at low and high loads respectively.

Hooke *et al.* (1993) experimentally investigated the wear behaviour of polymer gears using test rig with back-to-back arrangement. Wear was continuously monitored and recorded and related to the surface temperature of gears. Gears made up of acetal, nylon 66 and glass fiber reinforced nylon 66 materials were considered. The same material gears were used as mating gears. Tests were carried for different loads (3–17 Nm) at different speeds (500–2500 rpm). The wear behaviour was dependent on gear materials and load. The temperature rise was found to be proportional to load applied. A mathematical model was developed to predict the temperature rise and was closely agree with the measured values.

Crippa and Davoli (1995) experimentally studied the fatigue behaviour of polymer-polymer and steel-polymer gear pairs. Test rig with back-to-back arrangement was used for exerting load on the test gears. Unreinforced and glass/carbon reinforced polyamide gears were considered for the evaluation. The tests were carried out in different lubrication condition (dry, grease and oil). Fatigue tests were conducted at a speed of 1500 rpm for different loads (8.8–45 Nm). Plastic gears failed due to wear and fatigue breakage. Type of lubrication affected fatigue life significantly. Carbon fiber reinforcement improved the torque transmission capability of polymer with lesser wear.

Kurokawa *et al.* (1999, 2000a) evaluated the load carrying capabilities and the wear behaviour of carbon fiber reinforced polyetheretherketone (PEEK/CF) using the power absorption type gear test rig. The mating gears were made up of different surface finish/materials such as hobbed steel gear, ground steel gear, unreinforced PEEK and PEEK/CF. The lithium base grease was used in some test cases. The tests were carried out under uni-directional loads (2 Nm at 200 rpm). The load carrying capability of PEEK/CF gears was found to vary depending on the mating gear and running conditions (grease). The affinity between PEEK and CF affected the wear rate. Kurokawa *et al.* (2003) studied the load carrying performance of carbon fiber reinforced polyamide 12 (PA12/CF) gears and compared with the performance of gears made up of different polyamides reinforced with carbon fibers (PA6/CF, PA66/CF and PA46/CF). The power absorption loading gear test rig was used for exerting uni-directional loads on the test gears. The mating gears made up of same materials were used in the tests under dry or lithium grease applied condition. It was observed that the PA12/CF gears exhibited highest load capability, better wear property and noiseless property over PA6/CF, PA66/CF, and PA46/CF gears.

Teisuke *et al.* (2001) investigated the wear behaviour of injection-molded polymer composite gears such as nylon 66, polyacetal, PEEK and glass fiber reinforced nylon, polyacetal and polyphenylene sulphide. Unreinforced nylon and reinforced polyacetal gears exhibited higher wear. Unreinforced PEEK and polyacetal gears shown lower wear.

Senthilvelan and Gnanamoorthy (2004b) investigated the wear characteristics of unreinforced and glass fiber reinforced nylon 6 spur gears. The uni-directional loads (0.8–2.5 Nm; 800–1200 rpm) were applied on the test gears. The hobbed steel gear

(AISI 1040) was used as driver. The reinforced gears exhibited better wear resistance because of the improved material modulus and strength. At higher rotation speeds, the test gears exhibited lesser wear because of the reduced contact period of single tooth contact. Senthilvelan and Gnanamoorthy (2007, 2009) investigated the effect of rotation speeds on the performance of unreinforced and glass fiber reinforced nylon 6 gears by applying the uni-directional loads (0.8–3 Nm; 600–1200 rpm) under unlubricated dry condition. The load was applied by the hobbed steel driver gear (AISI 316). The gear running speed influenced the performance of both the unreinforced and reinforced gears. At low stress level, the tooth root cracking and wear were the failure modes and no influence of speeds on the gear life was observed. At higher stress level, thermal induced failure was observed and the surface temperature of gear was increasing with speed increase.

Mao *et al.* (2007, 2009, 2010) proposed a new design method for the polymer composite gears based on the gear surface temperature and gear wear rate. Power circulation type gear test rig was used for exerting the uni-directional loads (7–16.1 Nm at 1000 rpm) on the tests gears (acetal and glass fiber reinforced nylon with polytetrafluoroethylene (PTFE) as an internal lubricant). The test gears were paired with the same gears as mating gear in the tests. The performance of acetal gear was load dependent. The critical loads were observed for each running speed. Beyond the critical load, the surface temperature rises to the level of melting point of gear material and rapid wear occurred. The critical loads were predicted using the thermal model and validated in the tests. Mao *et al.* (2015) used power circulation type gear test rig for evaluating the wear and thermal mechanical contact behaviour of machine cut acetal and polyamide gears. The tests were carried out for different loads (6–9 Nm) at 1000

rpm. The same material gears were used as mating gears. The critical load controlled the wear and thermal behaviour.

Hoskins *et al*. (2011) investigated the acoustic noise generated from polymer composite gears through tribological investigation with the aid of power recirculation type test rig. Polyamide, polyoxymethylene, polyetheretherketone, glass fiber reinforced polyamide and carbon fiber reinforced polyetheretherketone were considered for the studies. The mating gears were made up of same / steel materials. Tests were carried out at different loads (5, 7 and 10 Nm) and speeds (1000, 1500 and 2000 rpm). The influence of various polymer materials and operating conditions on the frequency spectrum of sound was investigated. The fiber reinforcement, geometry and material flow effected the tribological behaviour which was used to predict the noise generation. Surface roughness influenced the sound power level and volumetric wear loss for all the materials tested.

Hoskins *et al.* (2014) studied the rolling-sliding wear behaviour of PEEK material in twin-disc configuration which simulates the gear mesh. Tests were conducted at different loads (100–400 N) and slip ratios (3.92–28.57 %) without lubrication. The friction, wear and temperature were recorded during tests. Surface melting and contact fatigue were the failure modes.

Pogacnik and Tavcar (2015) used servo motor driven gear test rig to evaluate the performance of unreinforced polyamide, short glass fiber reinforced polyamide and acetal gears in accelerated testing mode. Hysteresis brake was used for loading the gears. This accelerated testing mode reduced the testing time and cost. Polymer gears were used as mating gears and the tests were carried out for different loads (0.21–0.82

Nm) at a speed of 1176 rpm. Load influenced the failure modes (wear, fatigue and sudden melting).

2.2.1.1 Effect of reinforcement on the performance of polymer composite gears under uni-directional loads

Investigations were carried out to understand the effect of fiber orientation and distribution on the tooth stiffness (Weale *et al.* (1999)) and the tribological properties (Kurokawa *et al.* (2000b), Wright and Kukureka (2001)) of polymer composite gears.

Walton *et al.* (2002a) investigated the influence of material combination of polymer composite (POM, nylon 6.6, PEEK, glass fiber reinforced nylon, carbon fiber reinforced nylon) gears on their friction and efficiency performance. A specially made test rig was used for exerting the loads (3–10 Nm) on the test gears at different speeds (upto 3000 rpm). The tests were carried out at different lubrication (dry and grease) conditions. The efficiency and friction performance were dependent on the material combination and lubrication condition.

Senthilvelan and Gnanamoorthy (2004a) investigated the type of failures exhibited by the unreinforced, glass fiber and carbon fiber reinforced nylon 66 spur gears. The power absorption type gear test rig was used to exert the uni-directional loads (1.5–3.0 Nm at 1000 rpm) on the test gears by hobbed steel gear (AISI 316). The failure modes exhibited by unreinforced nylon gears include surface wear, gear tooth deformation, surface cracking near pitch region and cracking at the tooth root region. However, tooth deformation failures were not observed in both the glass and carbon fiber reinforced nylon gears, because of their improved thermal conductivity of materials. At higher loads, thermal softening of material was observed for glass fiber reinforced nylon gears.

Senthilvelan and Gnanamoorthy (2006c, 2008) investigated the orientation of fibers in the glass fiber reinforced nylon 6/6 spur gears. The orientation of fibers near the tooth profile, weld line region and injection points were observed using optical microscope. The gear metrology confirmed that the incorporation of fibers in the nylon gears has reduced the overall volumetric shrinkage in the reinforced gears. The tooth profile form error and lead error deviations observed were due to presence of fibers in the molded skin surface. The presence of fibers across the tooth section affected the material homogeneity in the reinforced gears and was responsible for more deviations as compared to the unreinforced gears.

Hakimian and Sulong (2012) analysed the warpage and shrinkage behaviour of injection molded micro gears made up of polymer composite materials. Amorphous polycarbonate/acrylonitrile–butadiene–styrene blend, amorphous polyphenylene–ether/polystyrene, and crystalline polyoxymethylene filled with glass fibers were considered. Warpage and shrinkage were affected by cooling temperature, packing time, molding temperature, melting temperature, packing pressure, injection pressure and fiber volume fraction.

Kirupasankar *et al.* (2012) investigated the transmission efficiency of pristine polyamide 6 and clay incorporated polyamide nanocomposite spur gears using power absorption the gear test rig. The effect of load on the transmission efficiency was studied. A hobbed stainless steel gear was used as mating gear. The tests were conducted at various loads (1.5–2.5 Nm) at 1200 rpm. The frictional and hysteresis losses were less for nanocomposite gears as compared to the pristine polyamide gears due to their superior mechanical and thermal properties. Nanocomposite gears exhibited lesser load dependent efficiency.

Kim *et al.* (2012) developed mathematical model to predict the efficiency of steel worm and polymer (nylon 6) worm wheel. The tests were carried out for different output torques (2–60 Nm) and speeds (30–360 deg/s). The predicted efficiencies were agreeing with the experimental results. The mathematical model was proposed to be used for predicting efficiency with different plastic gear materials.

Pogacnik and Tavcar (2015) reported that wear, fatigue crack and thermal melting of polymer gears as failure modes and were controlled by the load applied.

2.2.1.2 Effect of geometry modifications on the performance of polymer composite gears under uni-directional loads

Investigations were carried out to understand the geometry modifications on the performance of polymer composite gears. Walton *et al.* (2002b) investigated the influence of gear geometry of polymer gears on their friction and efficiency performance. The geometry modification included speed ratio, module, pressure angle, addendum and tip relief. The sensitivity of center to center distance variation on the performance was also reported. The efficiency and friction performance were dependent on the geometry parameters.

Kim (2006) experimentally studied the wear and durability performance of polymer (acetal and nylon) gears. Steel gear was used to exert the load on the test gears. Investigation to improvement the wear and durability of the polymer gears were carried out with holes and steel pins insertion on the tooth centerline. Tests were conducted at different loads (9.8, 19.6 and 29.4 N/mm and at a pinion speed of 1273 rpm). The surface temperature and wear were reduced for the nylon gears with pin holes / pins

insertion and improved the durability. For the acetal gears, the wear increased for the modified gears.

Senthilvelan and Gnanamoorthy (2006a) evaluated the service life of nylon 6/6 gears, with different teeth fillet radius (0.25 and 0.75 mm). The uni-directional loads (1.5–3.0 Nm at 1000 rpm) on the test gears were exerted by hobbed steel gear (AISI 316). The gears with high fillet radius exhibited more life. The gear tooth deflection and heat generation were more for the gears with less fillet radius. The gear with less fillet radius was more prone to stress concentration zone near the fillet which affected the life of the polymer gears.

Imrek (2009) used the power circulation loading test rig for the evaluation of service life and wear rate of nylon 6 gears driven by steel gear (AISI 1045). The tests were conducted at a constant speed (1000 rpm) for different loads (4.41, 6.62 and 8.82 Nm). Tooth width modified gear shown lesser wear rate and decreased heat generation. Increased heat dissipation prevented the premature failure and shown longer life.

Duzcukoglu (2009a) investigated the durability improvement with tooth width modification of glass fiber reinforced polyamide gears. Tests were conducted at two loads (8.5 and 13 Nm) and two speeds (1000 and 1500 rpm). Steel gear made of AISI 8620 was used as mating gear. The rise in tooth temperature and wear were less for the tooth width modified gears as compared to the unmodified gears, which increased the surface durability of modified gears. Duzcukoglu (2009b) used the power circulation loading test rig and developed the polyamide gears by introducing drilled holes for improving the load carrying capacity. Drilled cooling holes on the tooth body decreased the tooth surface temperature and led to an increase in the load carrying capacity/service life and wear resistance of polyamide gears.

Li *et al.* (2011) investigated the friction and wear behaviour of gears made up of different materials (acetal-nylon, nylon-nylon, PEEK-steel, steel-PEEK, PEEK-PEEK gear pairs). The nonlinear finite element analysis was carried out to understand the contact behaviour of gears. The tests were conducted using test ring with back-to-back arrangement. Geometry modification (tip relief) reduced the friction force and wear of gear tip.

2.2.2 Bending fatigue performance of steel gears under uni-directional loads

Investigation were carried out to understand the bending fatigue performance of steel gears under uni-directional loads. Stand alone test rigs were used for exerting load on the gears. Eyercioglu *et al.* (1997) carried out single tooth bending fatigue test with the aid of Amsler high frequency vibrophore push-pull fatigue testing machine and test fixture. Hardened and induction hardened steel (EN 24) gears were subjected to tests at different frequencies (105–115 Hz). The exerted loads were sinusoidal and fluctuated between maximum and preload (0.5 kN). In all the failures, fatigue crack initiated from fillet and propagated into the root. Machined gears shown inferior life as compared to the forged gears.

Daniewicz and Moore (1998) observed the improved fatigue life of AISI 1040 steel gears by introducing beneficial compressive residual stress using single tooth loading test rig. Fluctuating bending loads at a stress ratio of 0.1 and a frequency of 15 Hz, were applied only on highest point single tooth contact of individual gear tooth. Number of test trials were carried out on the same gear by re-fixing another tooth for the tests.

Akata *et al.* (2004) used the three points bending test fixture for the stand alone tests to evaluate the bending fatigue performance of steel gears cut by hobbing and shaving. Bending load was applied only on the highest point single tooth contact of individual gear teeth during the tests with the servo hydraulic fatigue testing machine. For all the tests, the alternating load was varied between 0.25 kN and a predetermined value (9.75 and 20.7 kN). Due to the strengthening effect of heat treatment, increased fatigue strength was reported for the case hardened gears as compared to fully machined gears / machined gears from upset blanks.

Handschuh *et al.* (2007) investigated the low cycle bending fatigue of spur gears made of AISI 9310 steel. Sinusoidal cyclic loading at 0.5 Hz was applied under uni-directional load control mode. Authors performed the finite element analysis (FEA) for estimating maximum principle tensile stresses for a load applied at highest point of single tooth contact. Linear relationship of stress to crack propagation cycles was reported. The fatigue crack was observed at gear tooth root.

Xi (2010) studied the region of fatigue crack initiation of gear made of MnCr steel. The details of residual stress and hardness at different distance from the surface were used for the assessment of fatigue limit of single tooth bending. It was reported that surface strengthening control the region of fatigue crack initiation.

Stringer *et al.* (2011) evaluated high cycle bending fatigue of AISI 9310 steel spur gear teeth. The frequency of loading was varied from 50−1000 Hz and load was varied from high stress to low. The fatigue root crack at tooth root was reported.

Gorla *et al.* (2012) used BS ISO 6336 standard to compute the bending stresses induced in the coated and non-coated steel spur gears with different geometries. Single tooth

bending fatigue tests were carried out at the stress ratio of 0.1 were carried out on these gears for evaluating the bending fatigue strength.

Zhang *et al.* (2013) evaluated the bending fatigue strength of 20CrMoH carburized steel gears. Experiments were carried out with the aid of Amsler high frequency resonance fatigue testing machine. The grade of test gear was ISO 7. The surface hardness and core hardness of gear were 62 HRC and 39 HRC, respectively. The tests were carried out at different pulsating loads (76–96 kN). The failure criterion was either crack/fracture of the gear tooth or load/frequency decreased by 5 %. The bending fatigue limits were obtained for the reliability of 99 % and 50 %.

The above methods of evaluating the bending performance of gears are suitable for the gears, experiencing uni-directional loading during their service life. In-addition, from the literature it is observed that the gear test rig used for bending fatigue evaluation do not simulate the actual gear meshing condition.

2.2.3 Bending fatigue performance of polymer gears subjected to bi-directional loads under constant deflection control mode

Mohan and Senthilvelan (2014) evaluated the bending fatigue performance of symmetric (20º / 20º) and asymmetric (20º / 34º) unreinforced and glass fiber reinforced polypropylene gears. A special fixture was designed and integrated with the servo hydraulic fatigue testing machine for applying bi-directional bending fatigue loads under constant deflection control mode. A stainless steel (AISI 316) gear manufactured by wire cut electrical discharge machining process, was used for loading polymer composite gears. Tests were conducted for different angular deflections (1.7º, 2.5º, 3.4º, 4.2º and 5º) at different frequencies (1, 1.5 and 2 Hz). Both the gears

exhibited gradual load drop with increase in cycles to maintain constant angular deflection. The root crack failures at gear tooth were reported as a failure modes for all gears. Reinforced gears exhibited higher load carrying capacity as compared to the unreinforced gears. In this configuration, test gears were not subjected to bi-directional bending load under constant load control mode and no attempt was made to compare with uni-directional loads.

2.2.4 Bending fatigue performance of polymer composites under uni-directional and bi-directional loads

Investigations were carried out to understand the fiber orientation, influence of fiber reinforcement on the mechanical properties of polymers including the fatigue behaviour and failure mechanisms at specimen level. Zhou *et al.* (1994) investigated the flexural fatigue behaviour and failure mechanism of short fiber reinforced a blend of polyphenylene ether ketone (PEK-C) and polyphenylene sulfide (PPS). Four point bending tests under load controlled mode, at different stress ratios (R = 0.1, 0.3 and 0.5) and frequencies (0.89–7.0 Hz) were conducted. The stress levels were corresponding to 0.35 to 0.9 times the measured static strength. The trend of S-N curve was stress dependent. The matrix yielding and crack growth dominated fracture were the failure modes at higher and lower stress levels, respectively.

Takahara *et al.* (1994) studied the effect of fiber-matrix interaction on the fatigue behaviour of glass fiber-reinforced poly butylene terephthalate. Interfacial adhesion between fiber and matrix affected the fatigue strength significantly. Fatigue failure criterion was established based on the hysteresis energy loss during fatigue cycles.

Fatigue behaviour of injection-molded blends of polypropylene and a liquid-crystalline polyester was studied by Kawagoe *et al.* (1997). Under loading, polypropylene and liquid-crystalline polyester closely attach each other which improved the fatigue life.

Handa *et al.* (1999) predicted the temperature rise in the stress controlled fatigue tests of glass fiber reinforced polyamide composites based on the viscoelastic properties, load and frequency. This temperature rise was used for assessing the fatigue life of composites.

The fatigue characteristics of glass fiber reinforced polypropylene composites was studied by Pegoretti and Ricco (2000). The volume fraction of fiber, mean load and test frequency influenced the fatigue behaviour.

Zainudin *et al.* (2002) reported that the injection speed, cavity thickness, convergent flow, divergent flow, fiber concentration, wall and gate locations affect the distribution of fiber orientation in the short glass fiber reinforced injection molded thermoplastic composites.

Bernasconi *et al.* (2007) evaluated the effect of fiber orientation (0º, 30º, 60º and 90º) on the fatigue behaviour of unreinforced and short glass fiber reinforced polyamide 6 under tension-tension axial fatigue tests. Load tests were carried out at a stress ratio of 0.1 and frequency of 4 Hz. The elastic modulus, ultimate tensile strength and fatigue strength were found to be decreasing for increasing values of orientation angle of fiber.

Bernasconi and Kulin (2009) studied the effect of frequency on the fatigue strength of glass fiber reinforced polyamide 6. A reduction of fatigue strength for increasing frequency was reported. Bernasconi *et al.* (2015) investigated the combined effect of notch size and fiber orientation on the fatigue strength of the injection molded short

glass fiber reinforced polyamide 6 specimens. The tests were conducted with different notch tip radius (0.5, 1 and 2 mm) at a frequency of 4 Hz. A negligible influence of notch tip radius on the static and fatigue strength of notched injection molded specimens were observed.

Goel *et al.* (2009) investigated the fatigue behaviour of unreinforced and long glass fiber reinforced polypropylene. The fatigue tests were conducted at a stress ratio of 0.2 for different frequencies (10, 15 and 20 Hz) under tension-tension load control mode. Decrease in fatigue life and higher temperature rise for increasing frequency were reported. The temperature rise was less on the reinforced polymer as compared to the unreinforced polymer. Fiber pull-out, fiber fracture and matrix fracture were the failure modes for the reinforced polymer.

Koricho *et al.* (2014) studied the bending fatigue behaviour of twill fabric glass/epoxy composite specimens. The tests were conducted at a stress ratio of 0.1 under displacement control mode for different stress levels (corresponding to 30–75 % of average ultimate flexural strength). The S-N curves drawn were indicating stiffness loss. The mean tensile stress was detrimental while compressive stress was beneficial.

Brunbauer *et al.* (2014) investigated the effects of fiber orientation on tensile and bending fatigue behaviour of short glass fiber reinforced polyamide 66. Two types of specimens such as 0º and 90º directions with respect to the mold flow direction, were selected for the tests. Fatigue strength decreased for 90º specimens than 0º specimens. Decreased fatigue strength was reported when the temperature increased from 23 ºC to 150 ºC. The slope of S-N curves was found to be independent of temperature and specimen angle.

Brunbauer and Pinter (2015) studied the effects of mean stress combining with fiber volume fraction with respect to the fatigue behaviour and damage mechanisms in carbon/epoxy specimens. Specimens with different orientation angles (0º, 45º and 90º) were selected. Fatigue tests were conducted at a stress ratio of 0.1 and –1 for the tension-tension and tension-compression loads, respectively. The smooth fracture surface with steeper slope of S-N curve was reported for tension-compression load tests. The fiber volume fraction and orientation angles controlled the fatigue behaviour and damage mechanisms.

Mortazavian and Fatemi (2015a, 2015b) investigated experimentally the effects of fiber orientation and anisotropy on the tensile strength and elastic modulus of short fiber reinforced polymer composites (1. polybutylene terephthaplate with 30 wt. % glass fibers and 2. polyamide 6 with 35 wt. % glass fibers and about 10 wt. % rubber impact modifier). The mechanical properties were affected by flow direction. The properties reduced significantly in perpendicular-to-flow direction as compared to in-flow direction for all the temperatures and strain rates.

Mortazavian *et al.* (2015c) studied the effects of cycling frequency and self-heating on fatigue behaviour of unreinforced and reinforced thermo plastic polymer composites. The fatigue tests were conducted under fully reversed (R = -1) and repeated (R = 0.1) conditions on the specimens made up of unreinforced polypropylene, polypropylene blended with 25 wt. % elastomer and filled with 30 wt. % magnesium silicate, polybutylene terephthalate reinforced with 30 wt. % short glass fibers and polyamide-6 reinforced with 35 wt. % short glass fiber with addition of about 10 wt. % rubber. The tests were conducted at two temperatures (23 and 125 ºC) for different frequencies (0.063–20 Hz). The temperature rise (>10 ºC) shortened the fatigue life for both the

unreinforced and glass fiber reinforced polymer composites. The unstable temperature rise was observed beyond the critical frequency at any stress amplitude.

Mortazavian and Fatemi (2016) experimentally investigated the effects of mean stress and stress concentration on the fatigue behaviour of unreinforced polypropylene and short fiber glass reinforced polybutylene terephthalate and polyamide. Effect of mean stress on the fatigue life was found to be significant and the surface temperature rise was found to be material, frequency and stress dependent.

Chandran (2016) studied the mechanical fatigue behaviour of polymers through continuum based approach. With negligible thermal effect, the remaining life of polymer was related to size of uncracked section. The constitutive equation was derived to predict S-N details of various polymers based on the macroscopic mechanism approach.

Naebe *et al.* (2016)) provided the overview of crack damages in polymer and polymer composites. Principal causes for cracking and the non-destructive techniques used for crack detection in the polymer composites were reported.

In all the above investigations, the effects of fiber orientation, stress magnitude, cyclic frequency and stress ratio on the fatigue performance of polymer composites at specimen level only were reported.

2.3 HYSTERETIC HEATING OF POLYMER COMPOSITES AND POLYMER COMPOSITE GEARS

Polymer gears generate heat by the surface interaction of driver and driven gears and material hysteretic heating due to large tooth deflection. Unlike metallic gears, performance of polymeric gears is significantly affected by this heat generation and it

varies with the load and rate of loading (frequency). Gears in real life application subjected to different loads and frequencies. Load magnitude and rate of loading (speed) are responsible for the heat generation characteristics and influences the surface durability and wear performance of polymer gears. In those studies (Yousef *et al.* (1973), Kurokowa (1999), Senthilvelan and Gnanamoorthy (2006a, 2007), Mao *et al.* (2009), Imrek (2009), Duzucukoglu (2009a), Letzelter *et al.* (2010), Hoskins *et al.* (2011), Pogacnik and Tavcar (2015)), temperature of test gears was monitored using non-contact infrared thermal sensor/camera. At low stress levels, gear tooth root cracking and gear wear were the dominant failure modes and no influence of speed on gear life. At high stress levels, the local temperature rise led to weakening of gear material and reduced the performance and was dependent on rotational speed. Geometry of polymer gears were modified by increasing the tooth thickness near pitch and introducing cooling holes for better heat dissipation in order to improve the performance of polymer gears. Thermal induced deformation, tooth root cracking and wear were the failure mechanisms and were dependent on stress levels and rate of loading. Mathematical models have been developed to predict the surface temperature rise of polymer composite gears mating with same material/steel gears (Koffi *et al.* (1985).

2.3.1 Effect of frequency on hysteretic heating and bending fatigue performance of polymer composites

Investigations were carried out on the polymer composite specimens for both the bi-directional (stress ratio, $R = -1$) and uni-directional ($R \geq 0$) loads at constant/different frequencies.

Temperature measurement methodology was used for rapid determination of the fatigue limit of polymer composite components (Takahara *et al.* (1994), Handa *et al.* (1999)) steel materials and mechanical components (Rosa and Risitano (2000)).

Rittel *et al.* (2003) investigated the hysteretic response of polymethyl-methacrylate (PMMA) and tougher modified PMMA with N-methyl glutarimide under high stress compressive cyclic loading. Load control cyclic testing was carried out on cylindrical specimens (9.5 mm diameter, 15 mm height) at 15 Hz frequency. Temperature was continuously measured during the test with thermocouple. Temperature rise and bulging were the failure modes for both the materials.

Goel *et al.* (2009) assessed the fatigue behaviour including thermal response of the unreinforced and glass fiber reinforced polypropylene specimens subjected to different frequencies at a stress ratio of 0.2. Decrease in fatigue life with increased frequency was reported. Temperature rise was increasing with increase in frequency and stress for both the materials. Temperature rise was more for unreinforced polypropylene.

Katunin *et al.* (2010) conducted the experimental investigations on glass fiber reinforced polymers using dynamic mechanical analysis (DMA) technique. The tests were performed under constant excitation amplitude (20 μm) for different frequencies (1–200 Hz). The influence of temperature and frequency on the loss rigidity for linear viscoelastic laminate was determined.

Jegou *et al.* (2013) investigated the fatigue behaviour of glass fiber reinforced polyamide composites based on the heat build-up measurements. The stress controlled tests were conducted on the specimens at a stress ratio of 0 and 1 Hz frequency. The

temperature rise was measured using infrared camera. Good correlation between the temperature rise and fatigue life was reported.

Florin *et al.* (2013) and Munier *et al.* (2014) also used self-heating methodology for the rapid assessment of fatigue behaviour of steel components. Infrared camera was used for recording temperature rise which was used for fatigue life computation.

Mathieson and Fam (2014) evaluated the high cycle fatigue of sandwich panels with glass fiber reinforced plastic (GFRP) skins and polyurethane foam core under fully reversed bending load (stress ratio of −1). The tests were conducted at different loads (30−70 % of ultimate static load) for a stress ratio of −1 and compared with the results of tests conducted at a stress ratio of 0 (loads: 45−70 % of ultimate static load). Fatigue life reduced significantly for the fully reversed bending loads.

Wang *et al.* (2014) experimentally evaluated the multiaxial fatigue behaviour of PEEK under four loading paths. Micro tubes (2.4 mm outer diameter × 0.2 mm thickness) were used for the experiments. Mixed fatigue cracking of material was reported. Fatigue life prediction criterion were evaluated based on the experimental data.

Peyrac *et al.* (2015) used self-heating method for fatigue limit determination on carbon fibers and polyamide 66 matrix composite specimens. Infrared thermal camera was used for measuring the temperature rise due to self-heating while subjecting the specimen to bi-directional loads, which was used for assessing fatigue life in a shortest time frame. Boccardi *et al.* (2015) also used infrared thermography to evaluate bending behaviour of the polypropylene matrix thermoplastic composites under cyclic load at different frequencies (0.1, 0.5 and 2 Hz).

Mortazavian *et al.* (2015c, 2016) studied the self-heating and fatigue behaviour of unreinforced polypropylene specimens under both the stress ratio conditions. Effect of mean stress on the fatigue life was found to be significant and the surface temperature rise was found to be material, frequency and stress dependent.

Shrestha *et al.* (2016) evaluated the fatigue behaviour including cyclic deformation of PEEK. The uni-axial monotonic tests (tension and compression) at different stain rates and uni-axial fully reversed strain controlled cyclic tests (0.02–0.04 mm/min strain amplitudes) at various frequencies (0.4–3 Hz) were conducted. Frequency influenced the fatigue lives of unreinforced PEEK. Load controlled fatigue tests were also carried out. Strain based model, stress-strain based model and an energy based model were used to correlate the data. The energy based model was found to better correlate the experimental results of PEEK.

From the above, it was observed that the hysteresis self-heating studies due to bending loads under bi-directional and uni-directional loadings at different frequencies on the gear mesh were not carried out.

2.4 BENDING AND TRANSMISSION CHARACTERISTICS OF POLYMER GEARS

Investigation of path of contact, transmission error and gear mesh stiffness of polymer gears become important in precision motion applications such as robotics, actuators of satellite launchers, etc,. Prediction/measurement of static transmission error (STE) of polymer gear provide a measure of gear tooth deflection and in turn the position accuracy. Hence there is a need to understand the transmission characteristics of polymer gears systematically and comprehensively to suitably choose safe loading or

gears can be suitably designed to operate at appropriate load levels in order to limit STE within the acceptable limit.

2.4.1 Analytical and numerical evaluations on bending and transmission characteristics of polymer gears

Studies were carried out on the polymer-polymer and metal-polymer gear pairs to understand the bending and transmission characteristics. Yelle and Burns (1981) proposed analytical model to predict real contact ratio of acetal-acetal and acetal-steel gear pairs and compared with experimental results. Springs analogous to the polymer gear material modulus were modeled between gear tooth surfaces and compliance was estimated along the length of contact from beginning to end. The calculations of contact ratio show that load sharing increases with increase in load.

Walton *et al.* (1994) investigated tooth deformation and load sharing in metallic and non-metallic gear pairs. A finite element analysis employing the flexibility method for contacting bodies was used to model tooth deflections and contact patterns between meshing gears. For metallic gears, the change in contact ratio between the theoretical and running values was small. However, for low modulus non-metallic gears, the change in contact ratio was large which affected bending and contact characteristics significantly.

Ming and Ying (1997) analyzed the static transmission error and load sharing ratio of nylon 66-nylon 66 and steel-nylon 66 gear pairs with the help of commercial finite element software, MARC®. Multi-tooth contact analysis with isotropic linear elastic material model was considered to estimate transmission error and compared with modified Houser's method of analytical model. Because of larger tooth deflection of

polymer gears, it was proposed to consider the influence of the premature and delayed meshing of teeth for plastic gears.

Wang and Howard (2004) used two dimensional plane stress finite element model to evaluate torsional mesh stiffness of aluminium gear driven by rigid gear. FEA results identified handover region (transition region between single tooth contact and double pair of teeth contacts). From tooth contact zone, contact ratio of gear pair was estimated and found to increases with the load. Torsional stiffness had shown its load dependency for both the single and double teeth contact zones.

Taburdagitan and Akkok (2006) carried out the coupled thermo-elastic finite element analysis using MARC® software. Tooth surface temperature rise during meshing of metallic spur gear pair due to frictional heat was investigated. Results of FEA and analytical computation were compared.

Senthilvelan and Gnanamoorthy (2006a) studied the effect of tooth fillet radius on polymer gear performance by using numerical model of single tooth. The gear tooth deflection and bending stress were assessed and were found to be higher in tooth with smaller fillet radius.

Meuleman *et al.* (2007) analyzed the deformation, transmission error (TE) and mesh stiffness on the steel-polyoxymethylene (POM) and POM-POM gear pairs. The tip relief and change in pressure angle of tooth were considered to reduce TE. An experimental test facility was used to measure TE and the measured TE was more as compared to the FEA prediction.

Lin and Kuang (2008) analytically studied the dynamic interaction between tooth wear and contact loads of nylon 66-nylon 66 and POM-POM gear pairs. The model included

the effects of position varying tooth mesh stiffness, load sharing ratio, damping ratio, tooth profile wear and temperature on the dynamic contact load. The simulation results indicated that wear has significant effect on the contact load.

Hossan and Hu (2008, 2013) numerically evaluated the strength of gears made up of glass/carbon fiber reinforced nylon. A commercial finite element analysis software (ANSYS®) was used for the three dimensional simulation of steel-polymer gear pair with isotropic and anisotropic material models. The root stresses were more for reinforced gears as compared to the unreinforced gears.

Letzelter *et al.* (2009) developed the computational method for predicting the mechanical behaviour of polymer gears. The viscoelastic properties of polyamide 6.6 material at its linear region was considered in the method. Rheological model considering the effect of temperature, humidity and time was used. Load sharing was solved with local meshing to include the displacement history. Transmission error and mesh stiffness were computed.

Karimpour *et al.* (2010) investigated the kinematic and kinetic behaviour of the POM-POM gear pair. The isotropic linear elastic material model was considered and the path of contact, load sharing, bending stress and contact stress were analyzed. The premature and extended contacts occurred in the path of contact due to the difference in tooth stiffness of meshing gear pair. The deviation of maximum bending stress predicted with respect to the stress computed using BS ISO 6336 standard was found to increase with the load increase.

Atanasiu *et al.* (2011) developed the analytical model with time varying mesh stiffness and load sharing ratio for the high gear ratio steel/nylon 66 gear pair. In order to have

high gear ratio, reduced weight and compact structures, the combination of steel pinion with lesser number of teeth and a driven gear which was made of plastic have been considered. Dynamic transmission error and load sharing along the line of contact during meshing cycle were computed using the model for different teeth numbers, addendum modification coefficients and input torques.

Cathelin *et al.* (2013) developed a quasi-static load sharing model to predict the mechanical behaviour of polyamide 66 gears. Viscoelastic material model in its linear domain was considered and load sharing, tooth root stress and transmission error were predicted. Experiments were conducted to validate the predicted transmission error and good correlation was seen between them.

Bravo *et al.* (2015) used models which considered the behaviour of polymer gear meshing, properties of gear material and application. The models were combined with finite element analysis to obtain the critical failures of polymer gears and the corresponding maintenance aspects. It was reported that damaging modes of gears were mainly influenced by the normal load on gear tooth. Wear and root cracks were the failures at low and high stresses, respectively.

Trobentar *et al.* (2015) investigated the tooth deflection behaviour of steel-polymer gear pair using finite element analysis tool, ABAQUS®. In the numerical analyses, the gear deflection behaviour was determined using the linear elastic model and the hyper-elastic Marlow model. From the results it was confirmed that an appropriate nonlinear material model should be considered for the higher contact forces, and consequently the large deflections.

It is observed from literature that extensive numerical and analytical works have been carried out to understand transmission characteristics of steel gears. However, very few numerical and experimental works have been carried out on the transmission characteristics of polymer gears. Hence there is a need to understand transmission characteristics of polymer gears systematically and comprehensively.

2.4.2 Experimental evaluations on transmission error

Experimental investigations were carried out to measure the transmission error of gear pair. Sweeney and Randall (1996) used both the angular accelerometer and encoder for measuring the transmission error of automotive helical gears. Walton *et al.* (2002a, 2002b) developed a servo motor based test rig with optical encoder for the measurement of transmission error of polymer composite gears. Meuleman *et al.* (2007) measured transmission error (TE) on the steel-POM, POM-POM gear pairs with the help of experimental test facility using encoders. Letzelter *et al.* (2009) and Cathelin *et al.* (2013) experimentally measured the transmission error of polyamide 66 gears with the help of optical encoders and good correlation was seen with the analytically/numerically predicted results.

2.4.3 Effect of strain rates on performance of polymer composites and polymer composite gears

Polymeric materials have strain rate dependent nonlinear material behaviour, which affects the bending characteristic of polymer gears significantly. Gears in application, experience different loading rate during their service life. Hence, it is important to investigate the bending characteristics of such gears before they are considered for such applications.

Extensive investigations were carried out on the polymer and polymer composite materials using standard specimens under different strain rate conditions. Mourad *et al*. (2004) presented the experimental and numerical results of plain and notched ultra-high molecular weight polyethylene UHMWPE and polyoxymethylene (POM) specimens. The experimental results for plain specimens showed that the materials under investigation were sensitive to strain rate changes.

Guo and Li (2007) experimentally studied the quasi-static and dynamic characteristics of SiO_2–epoxy at different loading rates (10^{-4} to 10^{4} s^{-1}). Results showed that strain-rate hardening plays a dominate role in the stress–strain behaviour of the composites.

Shan *et al.* (2007) investigated the effects of the draw temperatures (15, 25, 35, 50, 65 and 80 ºC) and the strain rates (1, 5, 10 and 50 mm/min crosshead speeds correspond to 0.33×10^{-3}, 1.67×10^{-3}, 3.33×10^{-3} 1.67×10^{-2} and s^{-1}, respectively) on the tensile deformation of polyamide 6. The yield strength was increasing with increase in strain rate. The special double yielding phenomenon was present in PA6 at certain temperature, strain rate and initial structure.

Starkova *et al.* (2008) estimated the limits of linear viscoelastic behaviour of TiO_2 nanoparticle-filled polyamides quantitatively using uniaxial tension tests. The stress limit of the filled polymer was higher than that of the unfilled polymer. Their values were lower for lower strain rate, higher moisture content and higher temperature of test specimen.

Cao *et al.* (2010) investigated the effect of strain rate (from 0.001 s^{-1} upto 1700 s^{-1}) on the tensile behaviour of polycarbonate under uniaxial tension loading conditions. The

strain rate greatly influenced the tensile behaviour of polycarbonate, and the yield strength was found to increase with increasing strain rate.

Nitta and Nomura (2014) studied the uniaxial tensile properties of cold-drawn isotactic polypropylenes (iPP) subjected to various drawn histories to understand the effect of strain-hardening in the uniaxial stress-strain behaviour of polymers. The yield stress, Young's modulus, and strain-hardening modulus were found to linearly increase with strain rate.

Fan *et al.* (2015) studied the dynamic tensile mechanical response of a soft polymer material (Clear Flex 75). Under static loading, the polymer exhibited an elastomeric behaviour, while under dynamic loading, the response was elasto-plastic. The critical strain rate for transition from a rubbery-like behaviour at low strain rates to a glassy-like behaviour at high strain rates at room temperature was reported.

It is observed from the above investigations, that the deformation behaviour of polymer gears is nonlinear and strain rate dependent. Analytical works and finite element analyses carried out on the polymeric gears mentioned in section 2.4.1, used linear material model only and recommended to use nonlinear material model due to large deflections of gear teeth. In this work, finite element analysis is carried out on the steel-polymer gear pair with linear and nonlinear material behaviour obtained at different strain rates to study its effect on static transmission error and bending stress. Experiments using in-house test rig developed with encoder have been conducted on the gears for the transmission error and compared with numerical results.

2.5 SUMMARY

From the literature, it is observed that the investigations were carried out for (i) bending and contact fatigue behaviour of polymer composite gears subjected to uni-directional loads (ii) fatigue behaviour of polymer composite specimens subjected to both bi-directional and uni-directional loads, (iii) single tooth bending fatigue behaviour of metallic gears under uni-directional loads, and (iv) bi-directional bending fatigue behaviour of polymer composite gears simulating actual gear mesh condition under position control mode. Hence, there is a need to evaluate the bi-directional bending fatigue performance of polymer gears under load controlled mode to extend their application. Additionally, hysteresis self-heating studies due to bending loads under bi-directional loadings at different frequencies on the polymer gear were not carried out and compared with uni-directional loading performance. Also, the effect of loading frequencies, simulating near practical load applications, on the fatigue life of polymer gear was not also studied, as the similar loading conditions are experienced in few applications.

It is observed that the extensive numerical and analytical works have been carried out to understand the bending and transmission characteristics of metallic gears. However, very few numerical and experimental works have been carried out on the bending and transmission characteristics of polymer gears. It is also observed from the investigations that the deformation behaviour of polymer gears is nonlinear and strain rate dependent. Analytical works and finite element analyses carried out on the polymeric gears mostly used linear material model only and recommended to use nonlinear material model due to large deflections of gear teeth.

CHAPTER 3

MATERIALS, MANUFACTURING, INSPECTION AND PERFORMANCE EVALUATION METHODOLOGY

3.1 INTRODUCTION

Good mechanical properties such as strength, rigidity, damping characteristic, fatigue strength, wear and sliding performance of polyamide 66 (PA) material makes it to use in many engineering and gear applications. Reinforcing polyamide polymer using carbon fibers further enhance the mechanical and thermal properties such as strength, rigidity, wear and thermal conductivity. Hence, unreinforced and carbon fiber reinforced polyamide are preferred over other polymer materials (Kurokawa *et al.* (2003), Senthilvelan and Gnanamoorthy, (2007)). Materials, processing conditions, inspection, evaluation of mechanical properties and the details of gear test rigs used for the performance evaluation of test gears, are reported in this chapter.

3.2 MATERIALS AND MANUFACTURING

A commercial master batch, 40 wt. % long carbon fiber reinforced polyamide 66 (Celstran, USA) and an unreinforced polyamide 66 (SRF, India) were considered for the development of composite and are shown in Figures 3.1(a) and 3.1(b) respectively.

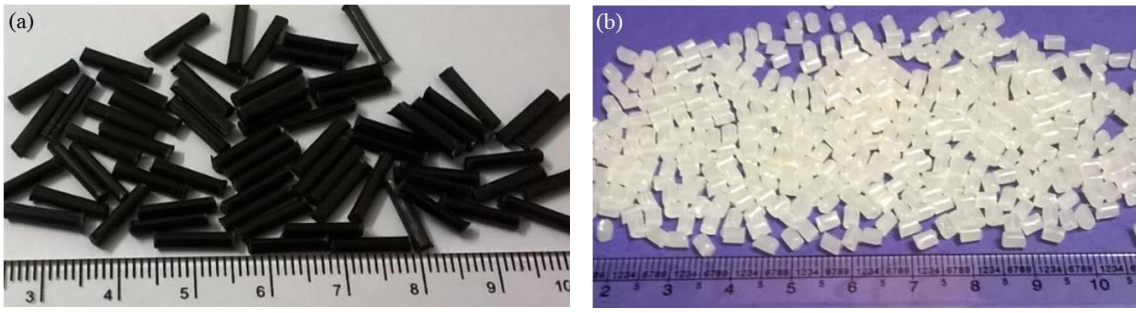

Figure 3.1 Gear materials (a) master batch long carbon fiber reinforced polyamide 66 and (b) polyamide 66 pellets

Using the considered materials, unreinforced polyamide 66 (PA) and 20 wt. % long carbon fiber reinforced polyamide 66 (PACF) were injection molded into the tensile specimens (as per ASTM D638-10) and test gears using injection molding machine (DGP Windsor, ST50). The injection molding machine and schematic of injection molding process are shown in Figure 3.2(a) and 3.2(b) respectively. The injection molding dies used for the manufacturing of tensile specimens and test gears are shown in Figures 3.3(a) and 3.3(b), respectively. The materials were preheated at 353 K for 4 h to remove the moisture content before injection molding. The injection pressure of 7 MPa and screw speed of 11.51 rad/s, were maintained. The injection temperatures of 558, 563, 568 and 573 K were kept at barrel zones indicated by 4, 3, 2 and 1 respectively. The geometry of tensile specimen and test gear are shown in Figures 3.4(a) and 3.4(b) respectively. The injection molded tensile specimens and test gears are shown in Figures 3.4(c) and 3.4(d), respectively. The ground finished gear made of AISI 316 stainless steel material was used as driver gear, considering the following aspects

a. Driver gear is a pinion which is generally smaller in size and lesser in weight as compared to driven gear. To obtain weight advantage especially for applications

in space industry, the driven gears made up of polyamide and carbon fiber reinforced polyamide materials are attempted in this study.

b. Due to higher thermal conductivity of steel (more than 100 times) as compared to polyamide gear materials, the usage of steel gear will dissipate the heat generated in the contact region of steel-polyamide gear pair during bending fatigue loads to some extent. Thus increases the fatigue life of polyamide gears.

The parameters of gears are shown in Table 3.1.

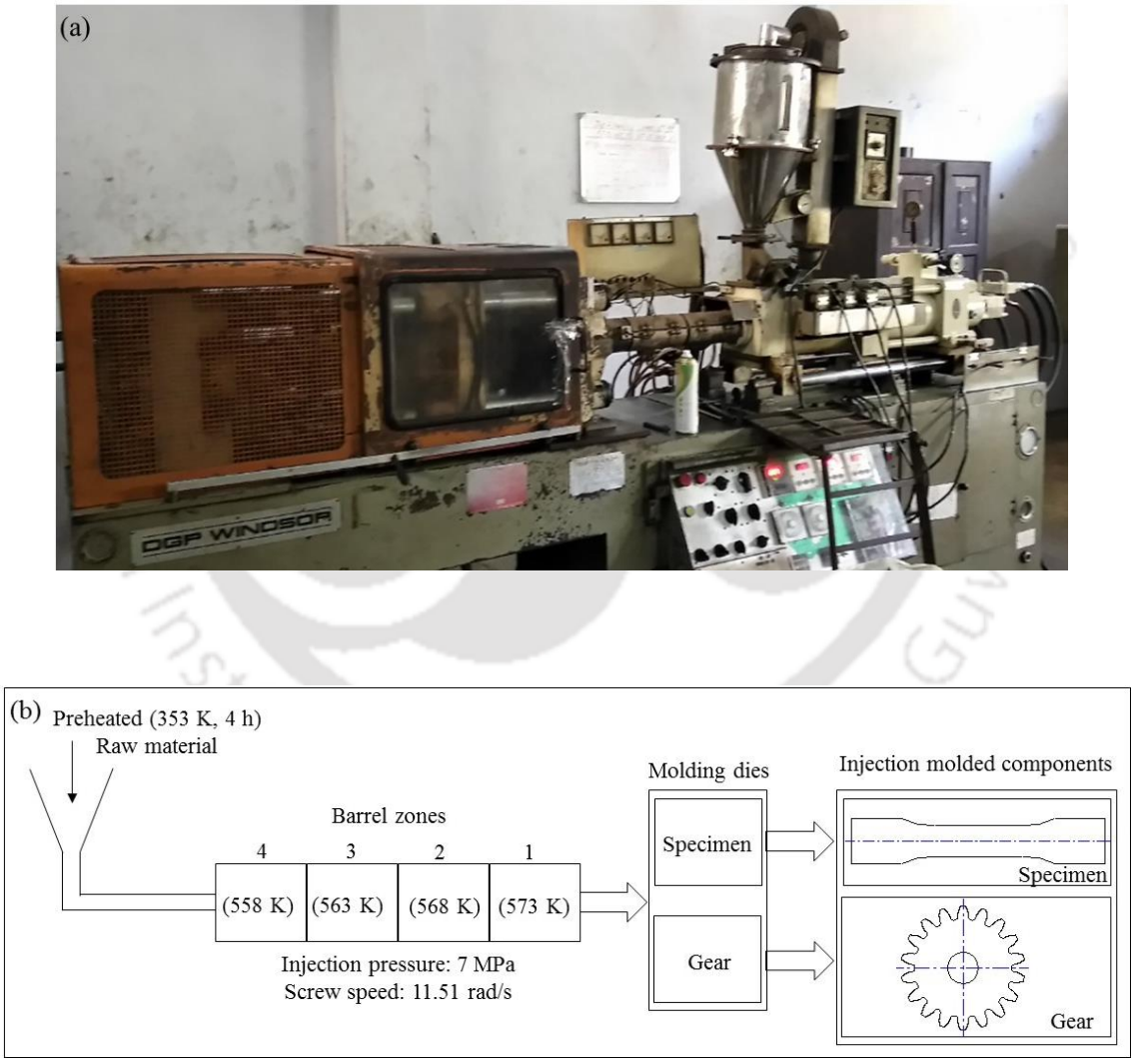

Figure 3.2 Injection molding (a) photograph of injection molding machine and (b) schematic of injection molding process

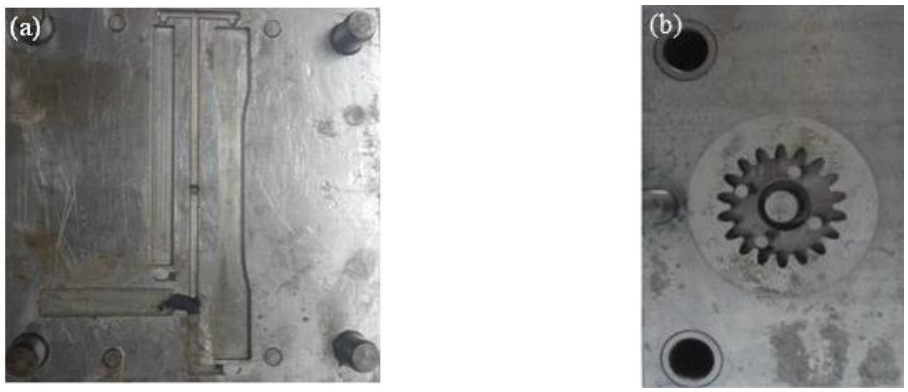

Figure 3.3 Injection molding dies for (a) tensile specimen and (b) test gear

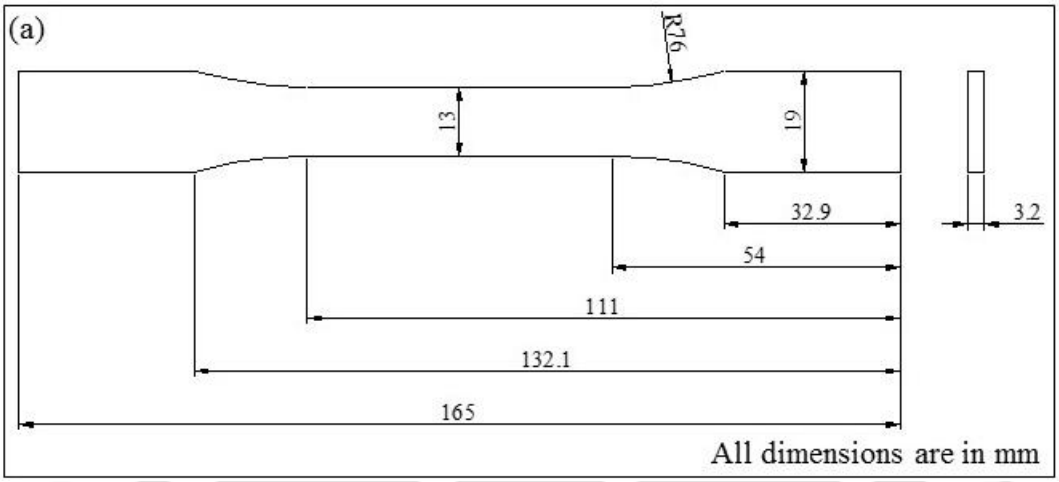

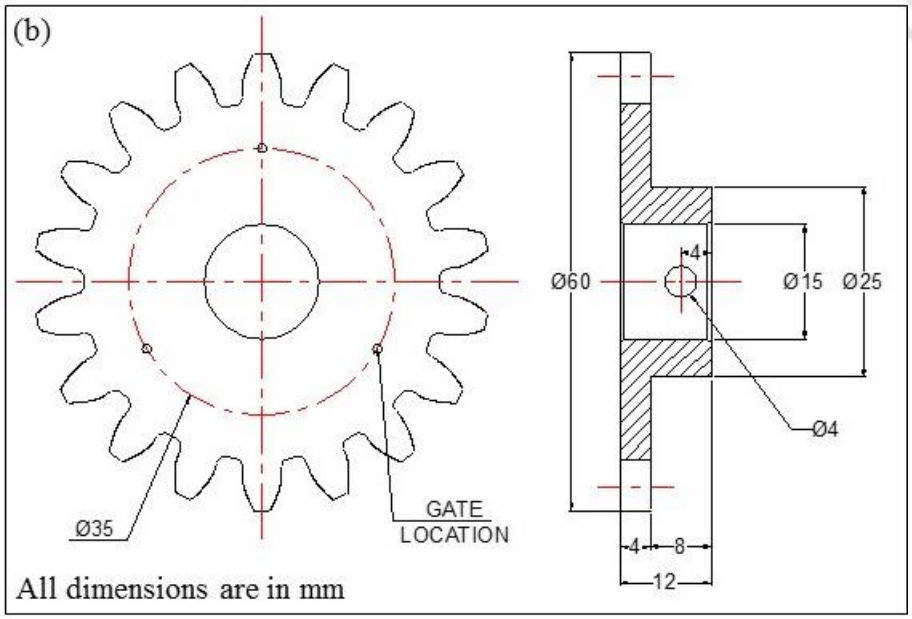

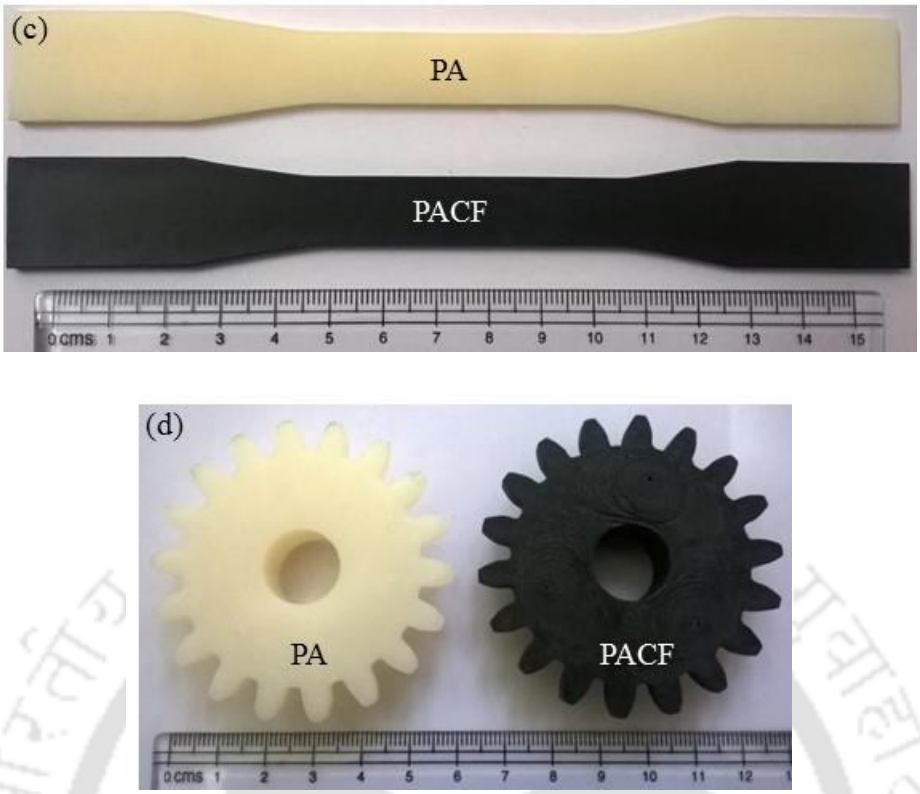

Figure 3.4 Geometry of (a) tensile specimen (ASTM D638-10), (b) test gear and injection molded (c) tensile specimens and (d) test gears

Table 3.1 Gear parameters for driver/driven (1:1 gear ratio)

Parameter	Driver	Driven
Material	AISI 316 Stainless steel	PA and PACF
Type	Spur gear	
Profile	Involute	
Pressure angle (°)	20	
Module (mm)	3	
Number of teeth	18	

Pitch circle diameter (mm)	54	
Addendum diameter (mm)	60	
Root diameter (mm)	46.5	
Face width (mm)	8	4
Root radius (mm)	1.14	
Hub inner diameter (mm)	15	

3.3 INSPECTION OF GEARS

Comprehensive metrological inspections were carried out on the (a) ground stainless steel gears, injection molded (b) unreinforced polyamide and (c) carbon fiber reinforced polyamide gears using NILES gear measuring system. The (i) profile, (ii) lead and (iii) pitch deviations were measured and reported as per DIN 3962. For profile and lead measurements, both the left and right flanks were measured in three/four teeth, which are equally spaced in the gear. For pitch measurement, both left and right flanks were considered. The total involute profile deviation was measured along the involute of the gear tooth between the base circle diameter and tip circle diameter. The lead of gear is the angle of tooth relative to axis of gear. In spur gears, lead is the straight line measured along the face width of gear at mid-height of the gear tooth. The algebraic difference between the actual pitch and the corresponding theoretical pitch in the transverse plane defined on a circle concentric with the gear axis is the pitch/tooth-to-tooth spacing deviation.

3.3.1 Gear tooth profile deviations

Profile plot of a gear tooth indicates a deviation of total involute profile (Fa), profile slope deviation (fha), and deviation of involute profile form (ffa) from the design

values. Gear tooth profile deviations were measured on three to four teeth, which are equally spaced. Figures 3.5, 3.6 and 3.7 show the involute profile deviation of the ground stainless steel, unreinforced and carbon fiber reinforced polyamide gears respectively.

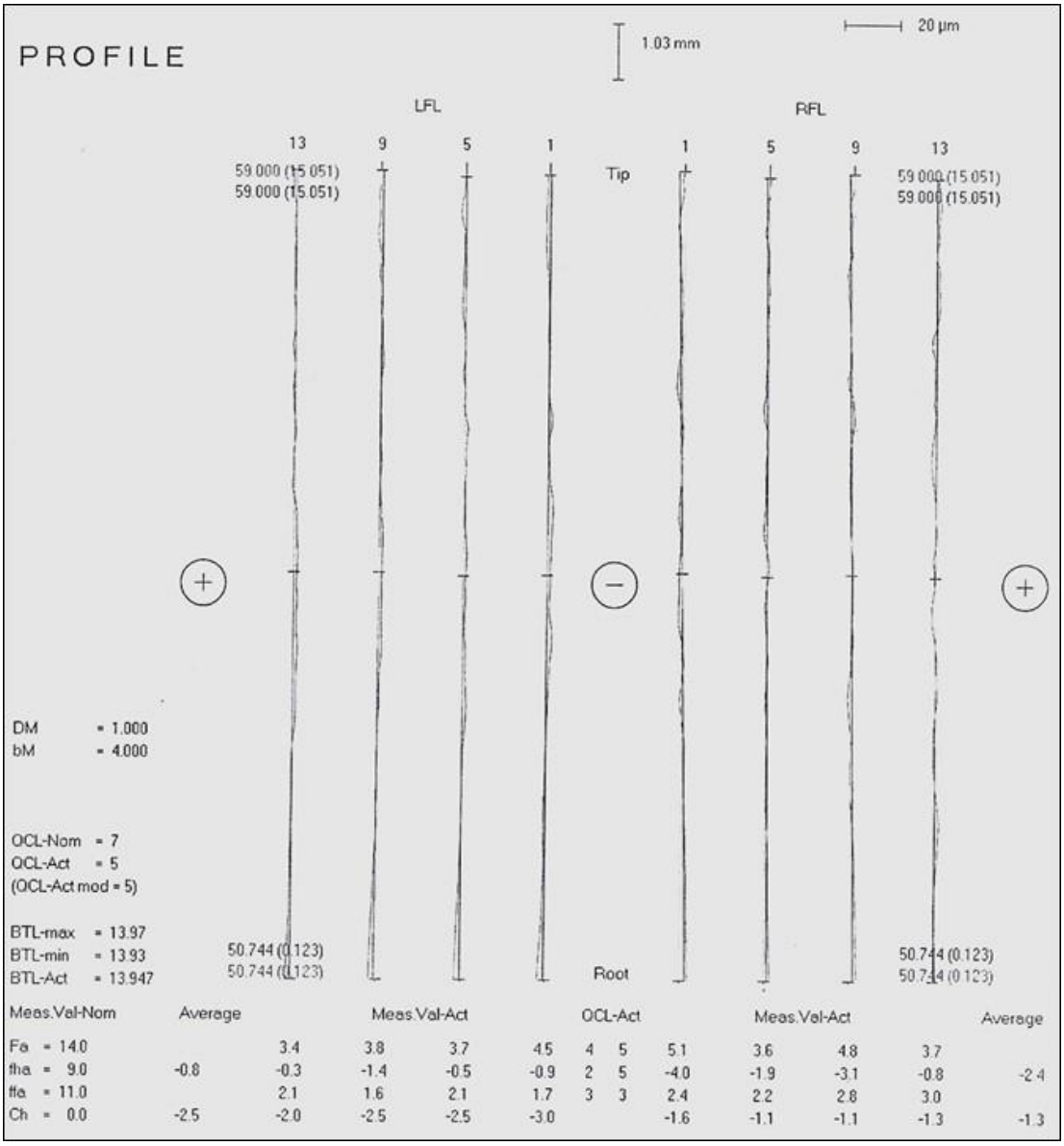

Figure 3.5 Involute profile deviation of ground stainless steel gear

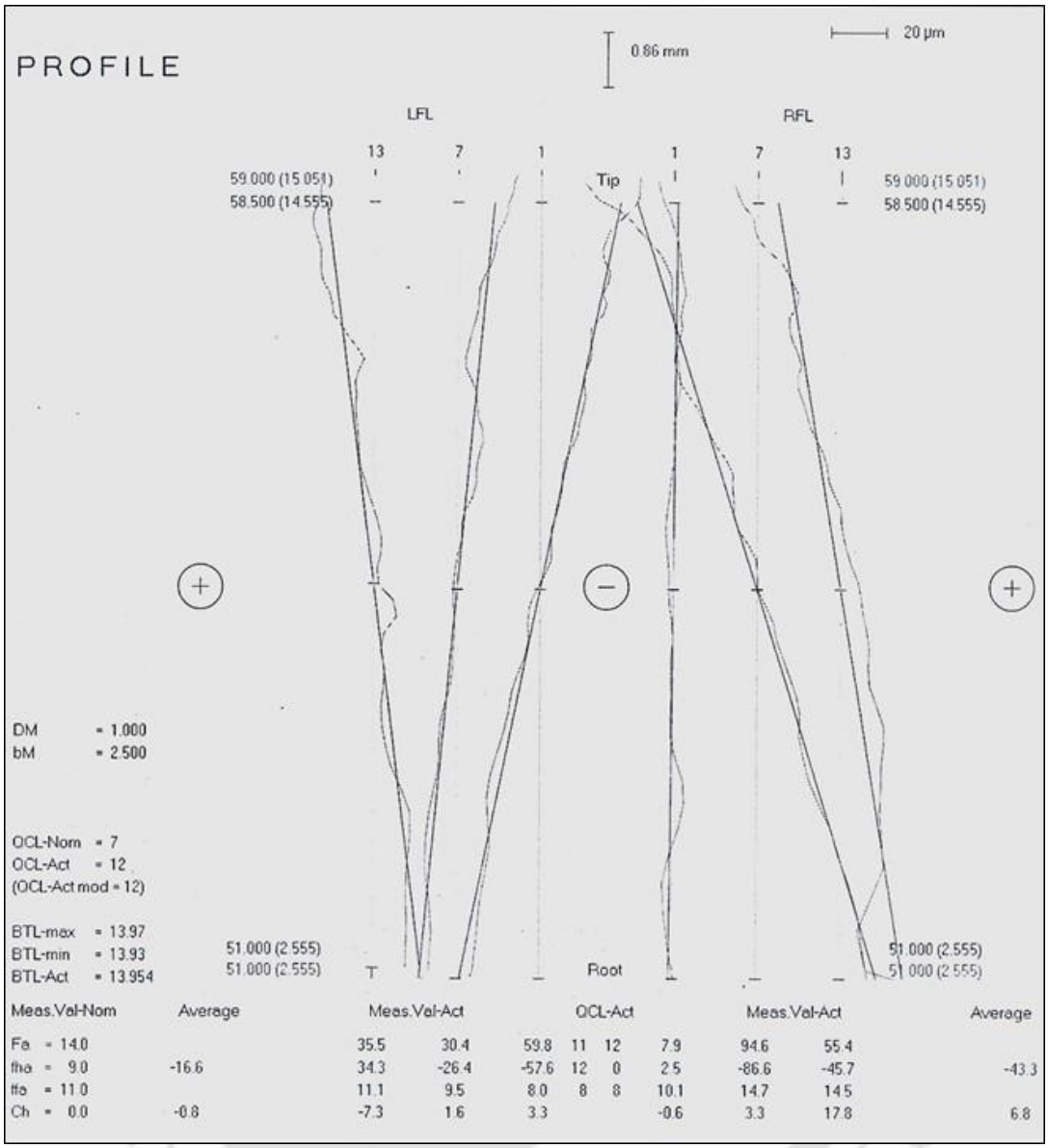

Figure 3.6 Involute profile deviation of unreinforced polyamide gear

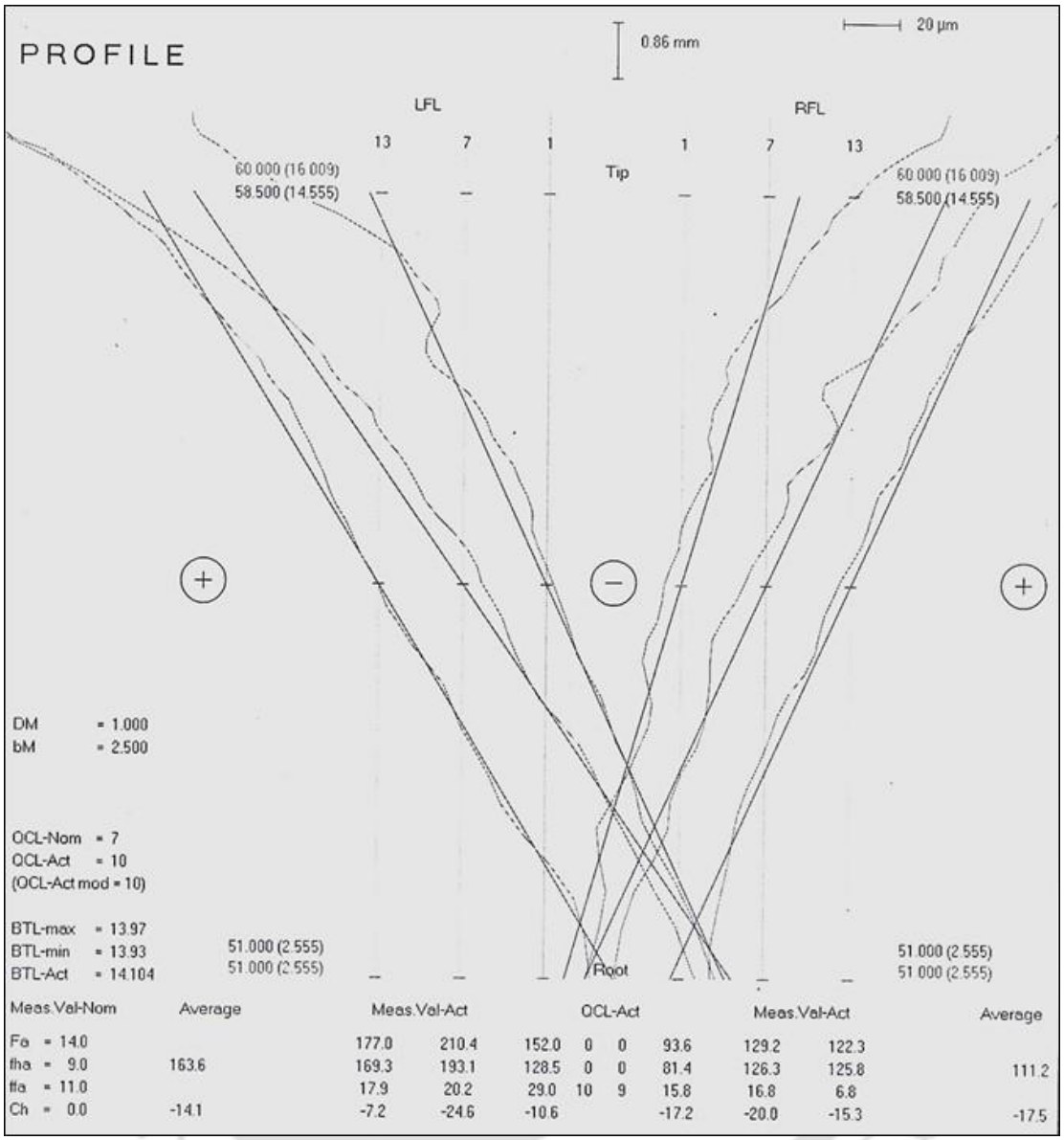

Figure 3.7 Involute profile deviation of carbon fiber reinforced polyamide gear

The involute profile deviations of left and right flank surfaces of four teeth (tooth no. 1, 5, 9 and 13) for the stainless steel gears / three teeth (tooth no. 1, 7 and 13) for the unreinforced and carbon fiber reinforced polyamide gears and are shown in a single plot. No appreciable profile deviation was observed among teeth as well as between left and right flank surfaces and hence average value is taken for further discussion. In the profile plot, position of tip and root of the gear tooth as well as chosen horizontal and vertical scales are also shown. The involute profile deviation (Fa) for the ground

stainless steel, unreinforced and carbon fiber reinforced polyamide gears conform to DIN 5, DIN 12 and DIN >> 12 quality respectively. Similarly average profile slope deviation (fha) were –2.4 μm (DIN 5), –43.3 μm (DIN > 12) and 163.6 μm (DIN >> 12) for the ground stainless steel, unreinforced and carbon fiber reinforced polyamide gears respectively. The higher deviation (DIN >> 12) observed in the reinforced polyamide gears were due to the anisotropic shrinkage exhibited by carbon fiber reinforcement. The involute profile form deviation (ffa) conform to DIN 3 (2.1 μm) for ground stainless steel gear. It was 14.7 μm (DIN 8) for the unreinforced gears due to the homogenous nature of the unreinforced polyamide melt. However, in the carbon fiber reinforced polyamide gears, random orientation of the fibers embedded in the skin surfaces of gears (Figure 3.8) deteriorate the smoothness of test gear profile and increase the involute profile form deviation (20.2 μm correspond to DIN 10 quality). The profile deviations on the glass fiber reinforced nylon 6/6 gears were reported by Senthilvelan and Gnanamoorthy (2006c, 2008).

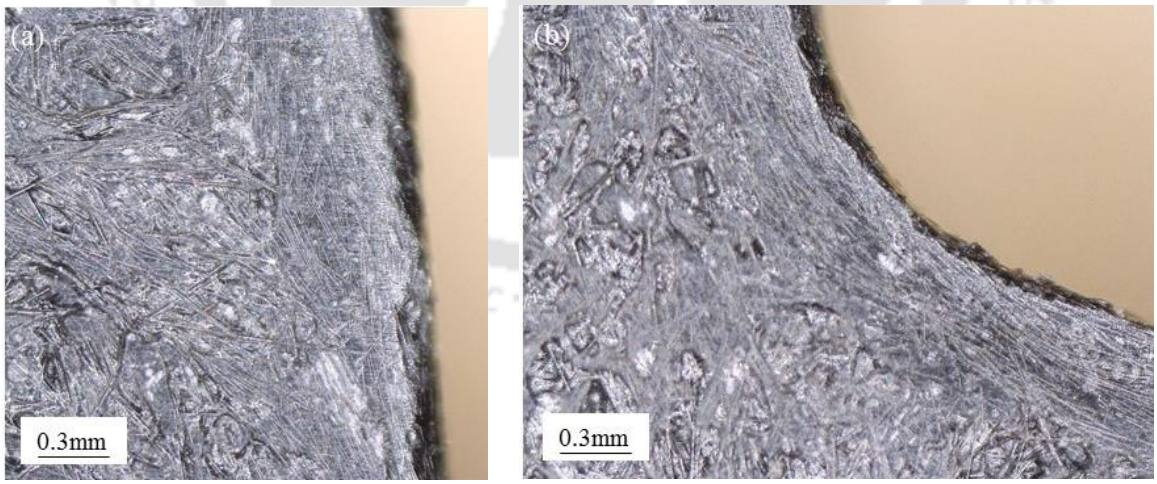

Figure 3.8 Micrographs showing the random orientation of carbon fibers in the molded reinforced gear (a) profile region and (b) root region

3.3.2 Gear tooth lead deviations

The lead plot of the investigated gears indicate the total lead deviation (Fβ), lead slope deviation (fhβ) and lead form deviation (ffβ). Figures 3.9, 3.10 and 3.11 show the lead deviation of the ground stainless steel, unreinforced and carbon fiber reinforced polyamide gears respectively. The lead deviations of the left and right flank surfaces of four teeth (tooth no. 1, 5, 9 and 13) for the stainless steel gears and three teeth (tooth no. 1, 7 and 13) for the unreinforced and carbon fiber reinforced polyamide gears, are shown in the plots. No appreciable deviation was observed among the measured three teeth as well as between the left and right flank surfaces of an investigated gear tooth and hence the average value is taken for further discussion. In the lead plot, position of top and bottom face of the gear tooth as well as chosen horizontal and vertical scales are shown (Figures 3.9–3.11).

The carbon fiber reinforced gears exhibited a higher lead deviation (Fβ) than the unreinforced gears and ground stainless steel gears. Quality conforms to DIN 2 (3.0 μm), DIN 10 (42.5 μm) and DIN 11 (63.9 μm) for the ground stainless steel, unreinforced and reinforced gears respectively. Since the orientation of reinforced fibers does not coincide with lead direction, an appreciable anisotropic shrinkage was observed in the lead. Similarly average lead slope deviation (fhβ) decreased from +3.9 μm (DIN 11) to –24.3 μm (DIN 10) due to the anisotropic shrinkage. It was 2.2 μm (DIN 3) only for ground stainless steel gear.

In the reinforced gears, the lead form deviation (ffβ) increases due to the embedded fibers in the skin surface of polyamide resin similar to the involute profile form deviation. The maximum lead form deviation of the ground steel, unreinforced and

reinforced polyamide gears were 1.7 µm (DIN 4), 13.6 µm (DIN 9) and 22.6 µm (DIN 10) respectively.

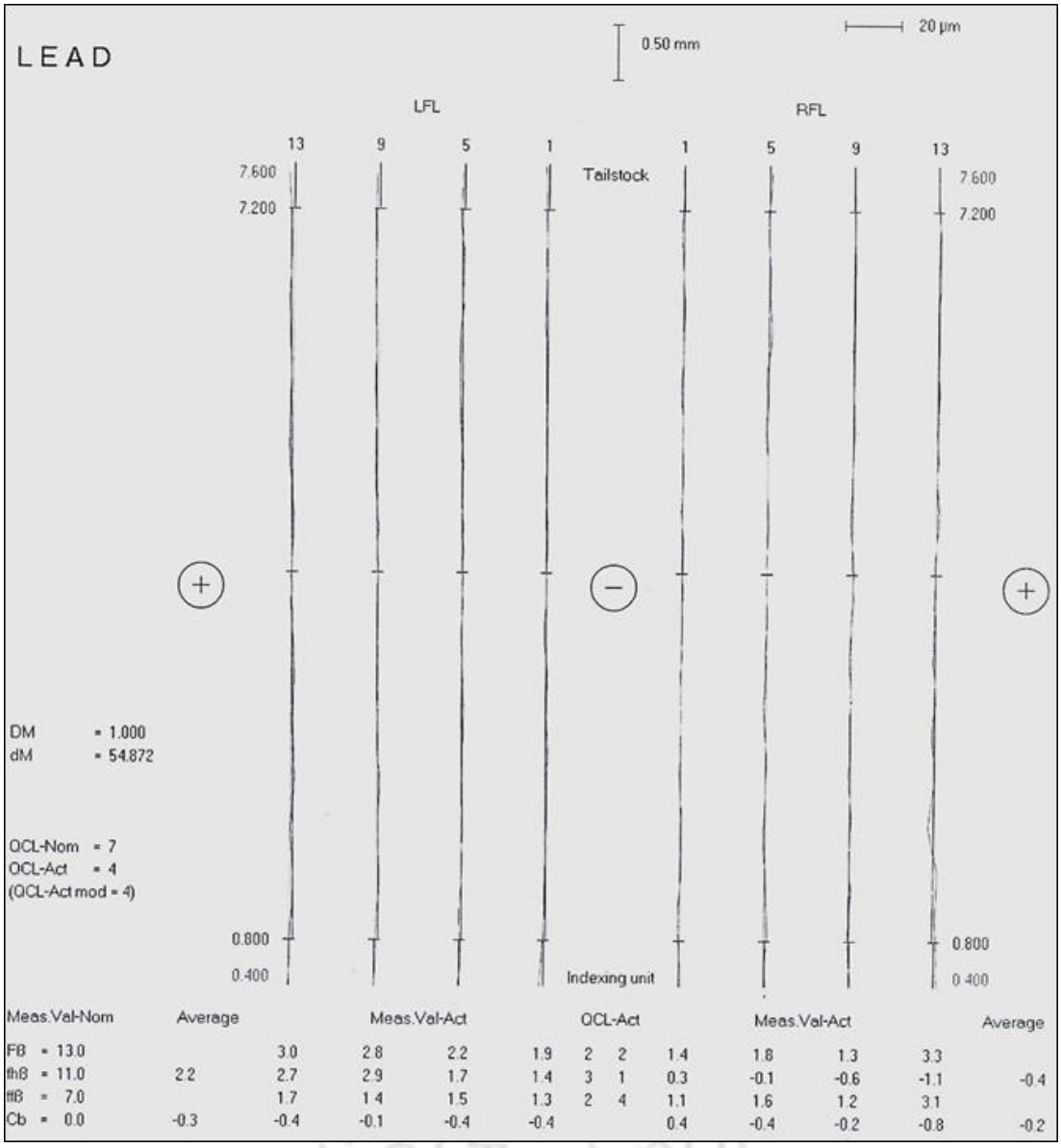

Figure 3.9 Lead deviation of ground stainless steel gear

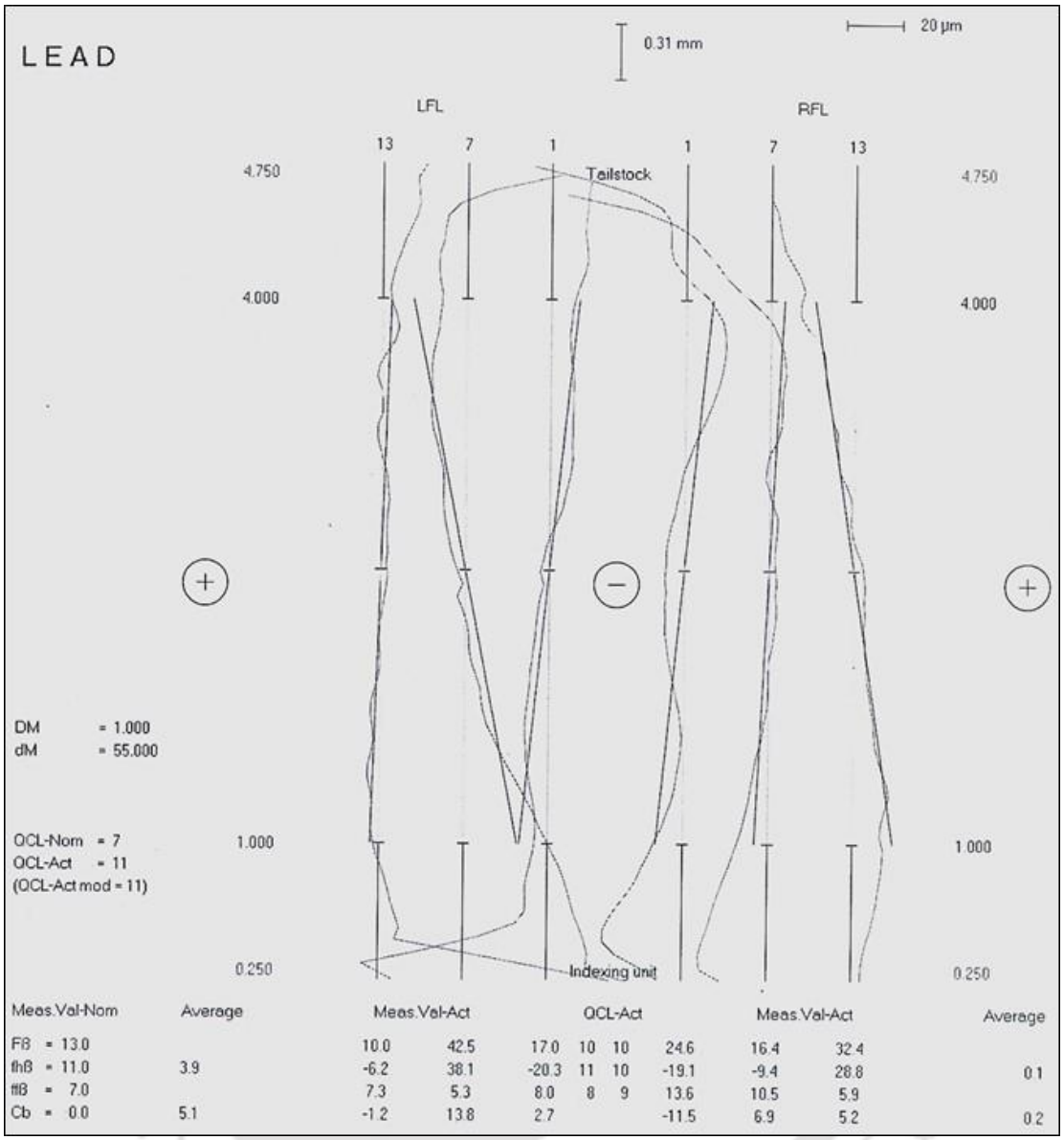

Figure 3.10 Lead deviation of unreinforced polyamide gear

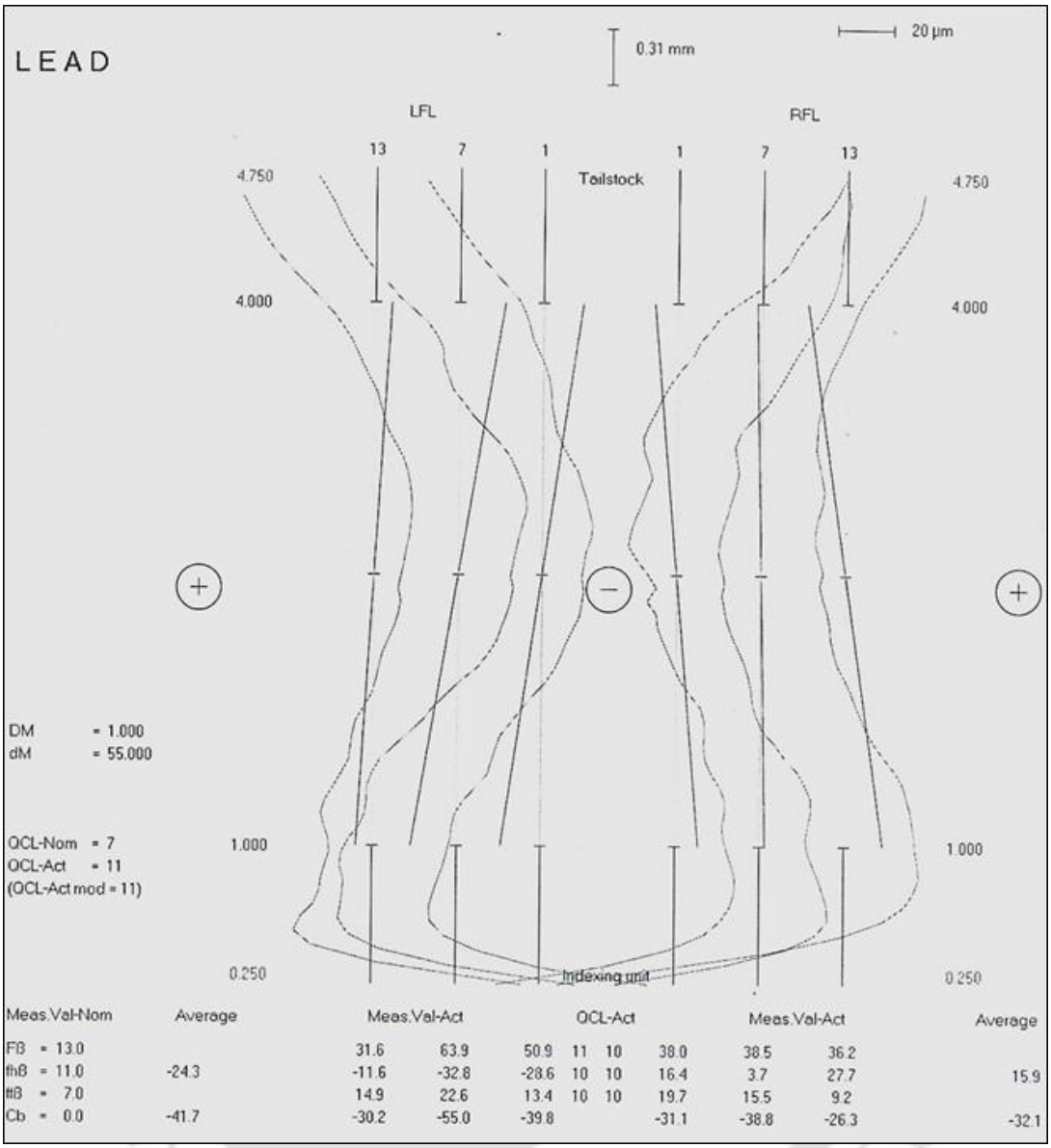

Figure 3.11 Lead deviation of carbon fiber reinforced polyamide gear

3.3.3 Gear tooth pitch deviations and radial runout variations

The ground stainless steel, unreinforced and carbon fiber reinforced polyamide gears were inspected for tooth-to-tooth spacing / pitch deviation (fp) and radial runout variations (Fr) and are shown in Figures 3.12, 3.13 and 3.14, respectively. The tooth-to-tooth spacing deviations of left and right flank of test gears are reported in the plots. This plot indicates the deviation of tooth-to-tooth spacing for all the 18 teeth present in

the gears. Tooth-to-tooth spacing conforms to DIN 1 (1.3 μm), DIN >> 12 (116.8 μm) and DIN > 12 (98.9 μm) for the ground stainless steel, unreinforced and carbon fiber reinforced gears respectively. Reinforced gear exhibits lesser deviation of tooth-to-tooth spacing than unreinforced gear due to lower shrinkage effect. For the gears, minimizing the pitch error reduces the noise and vibration levels in the transmission system. Senthilvelan and Gnanamoorthy (2006b) reported the increased noise levels for the glass fiber and carbon fiber reinforced nylon 6/6 gears than that of unreinforced nylon 6/6 gears.

Ground stainless steel, unreinforced and carbon fiber reinforced gears were inspected for radial run out (Fr) and are also shown in Figures 3.12, 3.13 and 3.14, respectively. The plots indicate the deviation of radial runout of all the 18 teeth present in the gears. Radial runout conforms to DIN 2 (3.8 μm), DIN > 12 (232.8 μm) and DIN >> 12 (275.9 μm) for the ground stainless steel, unreinforced and carbon fiber reinforced gears respectively. Presence of carbon fibers contribute to the anisotropic shrinkage which resulted in higher radial runout for reinforced gears.

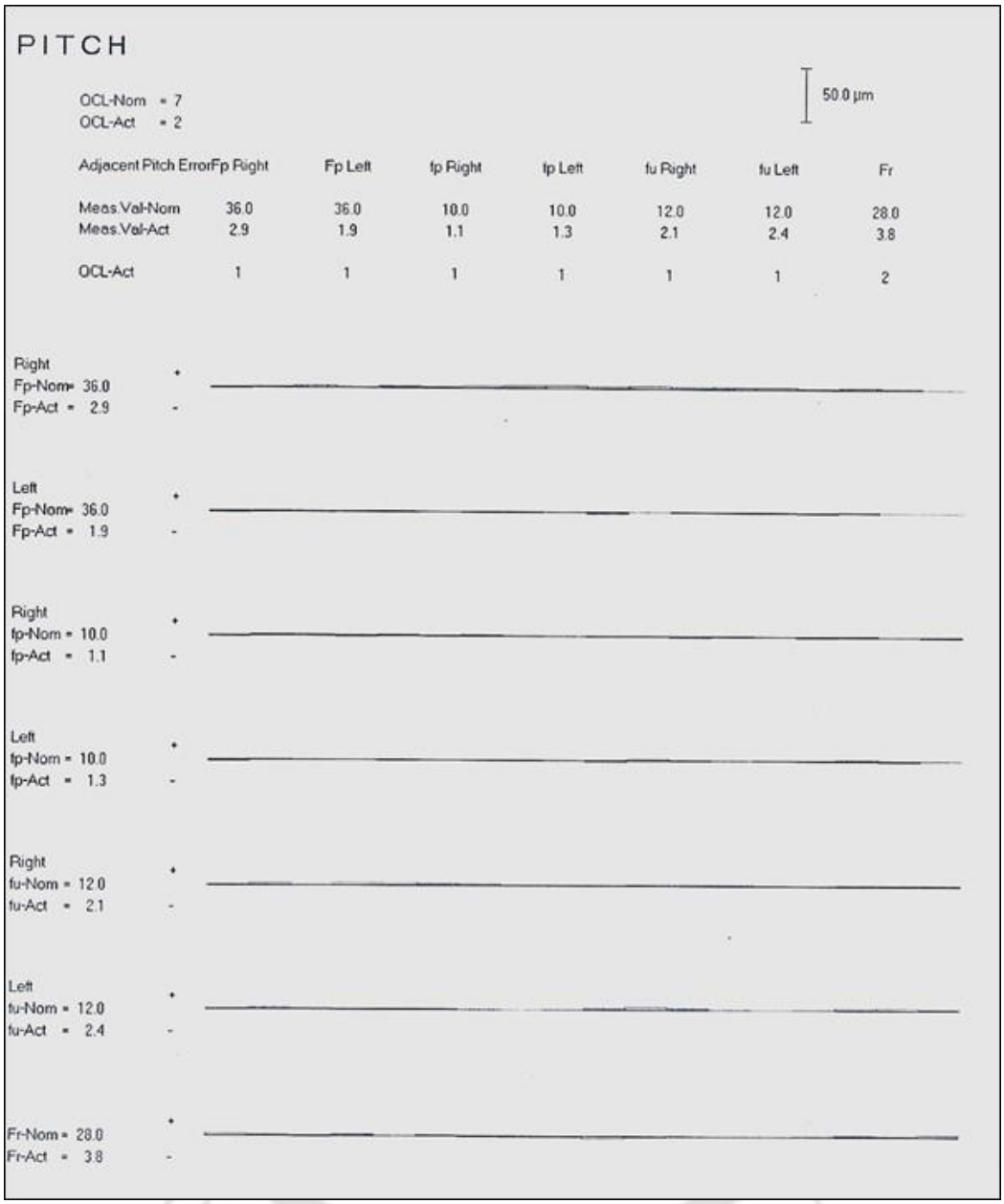

Figure 3.12 Pitch deviation and radial runout variation of ground stainless steel gear

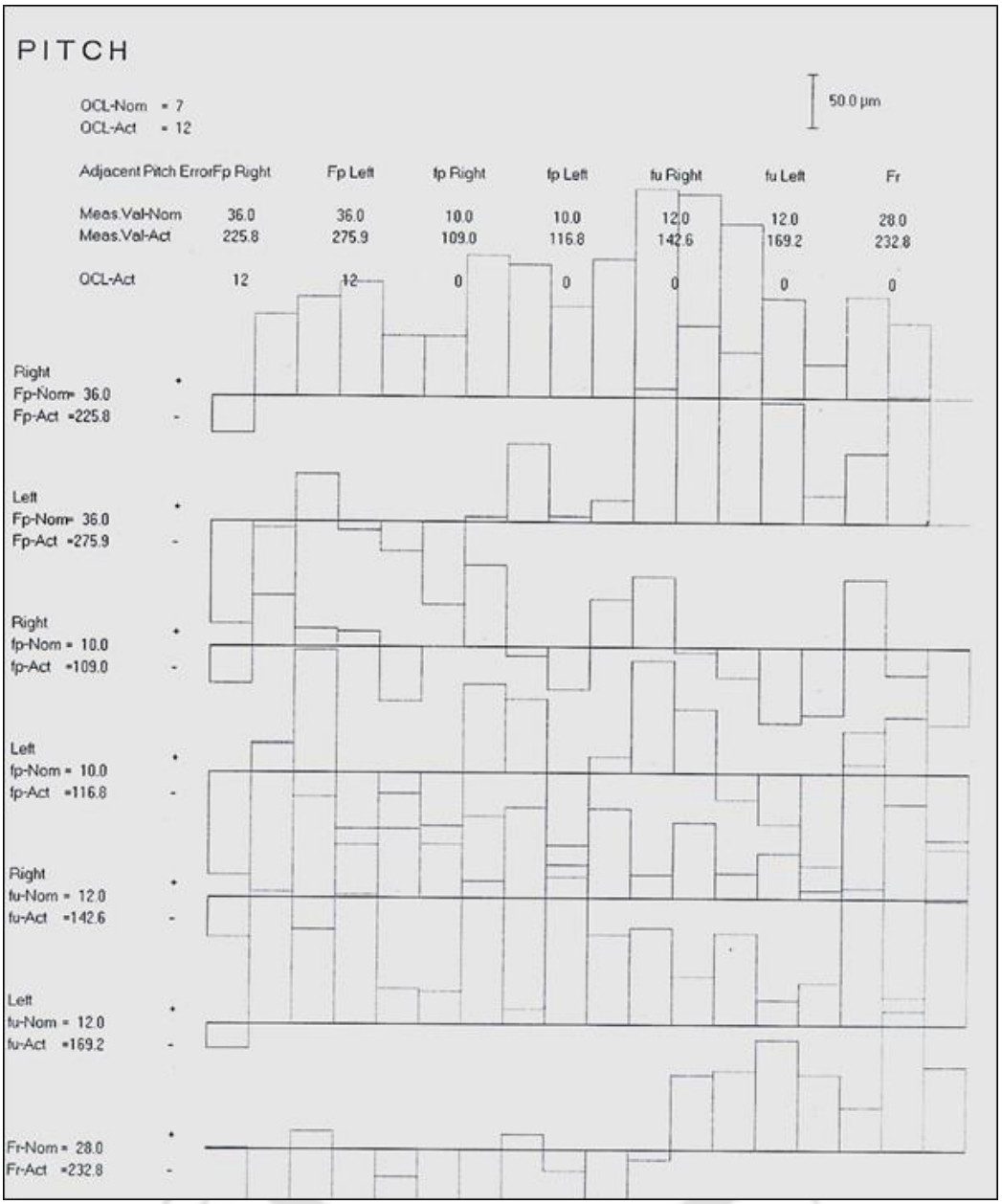

Figure 3.13 Pitch deviation and radial runout variation of unreinforced polyamide gear

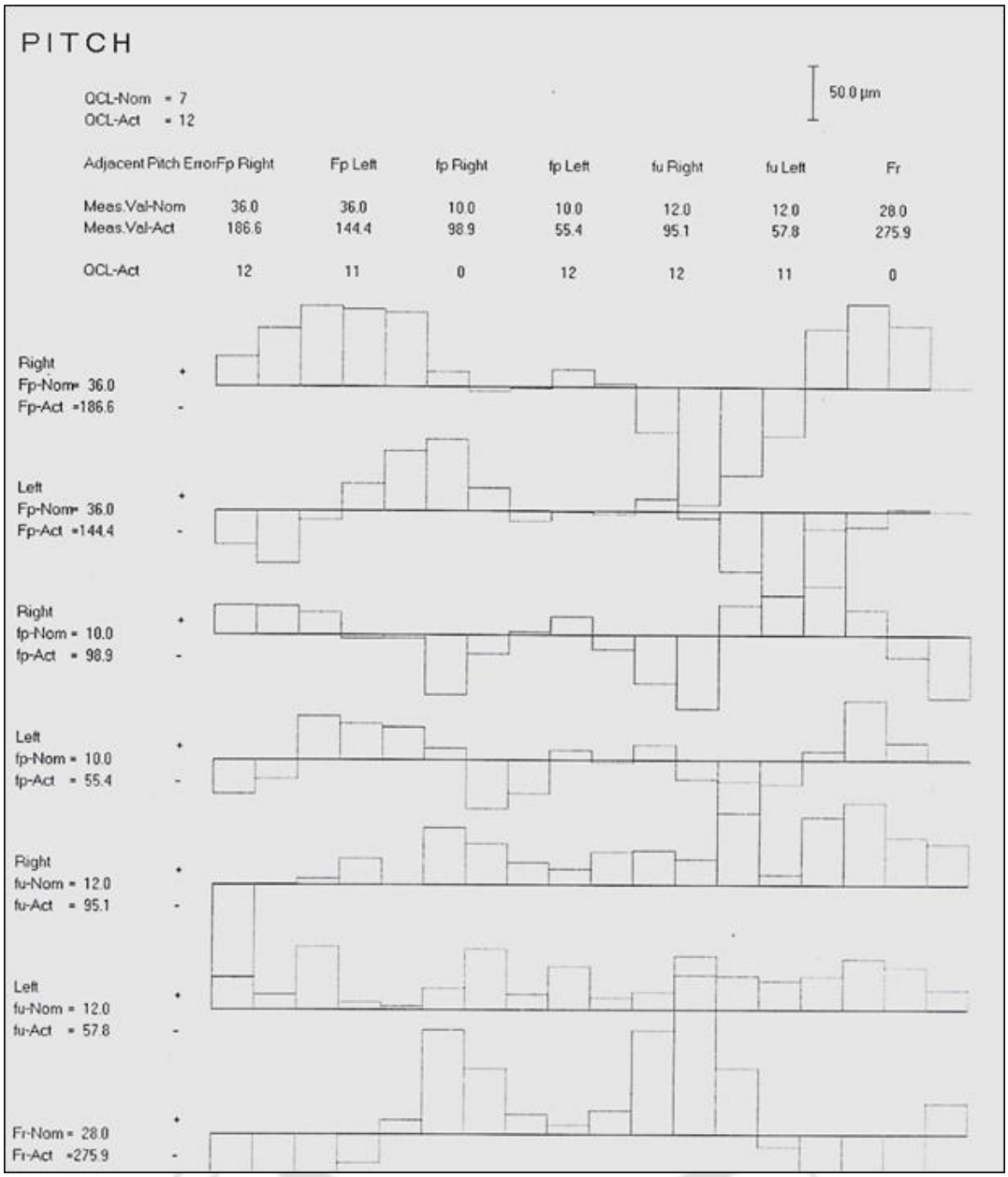

Figure 3.14 Pitch deviation and radial runout variation of carbon fiber reinforced polyamide gear

3.4 MECHANICAL PERFORMANCE OF GEAR MATERIALS

The tensile properties of the unreinforced (PA) and carbon fiber reinforced polyamide (PACF) specimens as per ASTM D638-10 standard, were evaluated at laboratory temperature (296±5 K) at the rate of 1 mm/min, using servo hydraulic testing machine, INSTRON 8801 (Figure 3.15(a)). Three numbers of PA and PACF specimens were used for the evaluation tests. From each test data, material properties such as Young's modulus, ultimate tensile strength and % elongation were calculated. The average and deviation from average were calculated from the three sets of data. The stress-strain plots and evaluated mechanical properties of PA and PACF specimens are given in Figure 3.15(b) and Table 3.2 respectively (1.74 indicates an average and 0.18 indicates the deviation from an average).

Table 3.2 Mechanical properties of test gear materials

Parameter / Material	PA	PACF
Young's modulus (GPa)	1.74±0.18	7.88±0.46
Ultimate tensile strength (MPa)	*49±1.62	104±1.46
Elongation (%)	*72±1.66	4±0.38

*specimens were not tested upto rupture (extension of 40 mm observed at 1.8 kN)

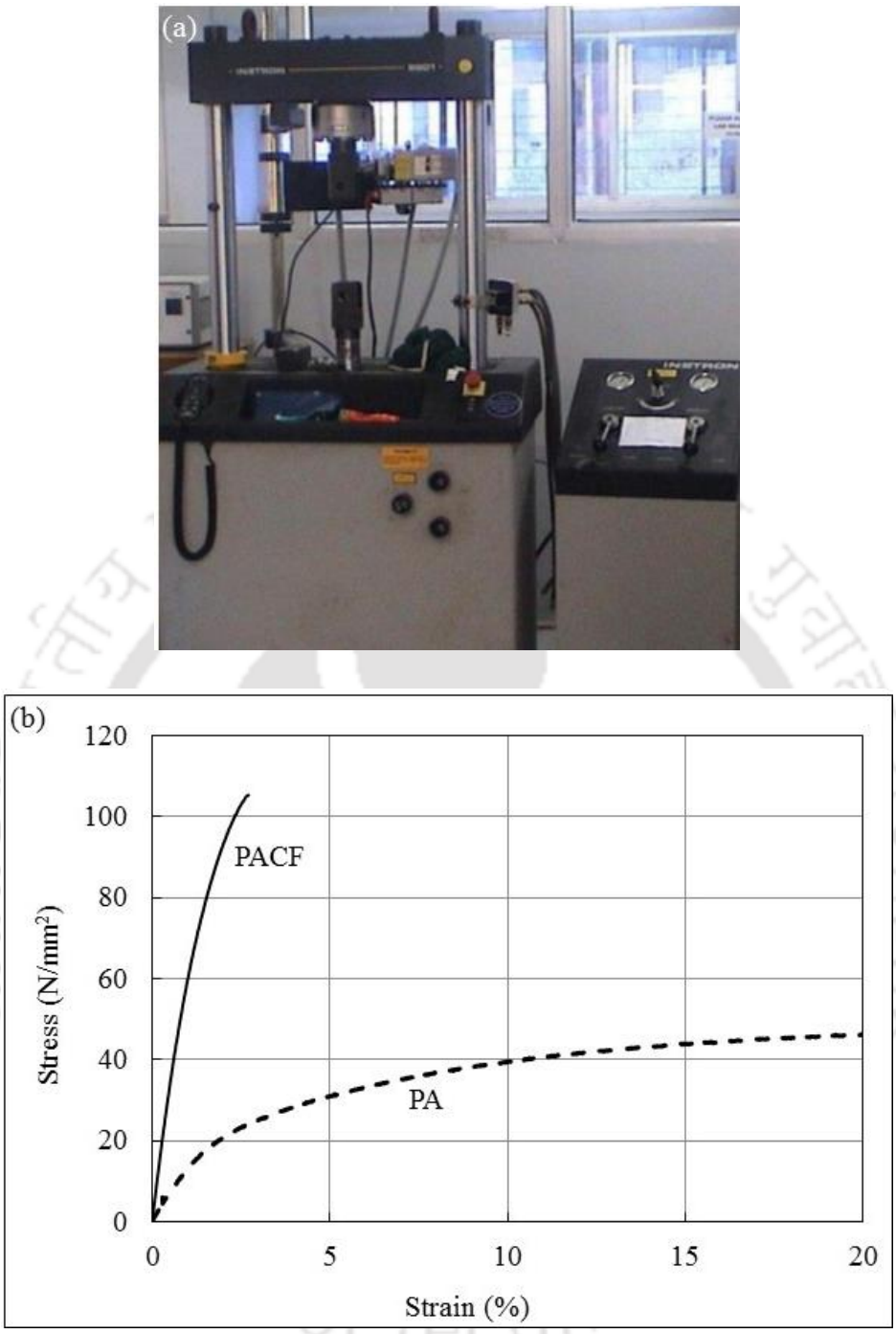

Figure 3.15 Tensile strength evaluation (a) servo hydraulic testing machine and (b) stress-strain plots of test gear materials

Failure morphology on the crack surface of PACF tensile test specimens were analyzed using scanning electron microscope (Zeiss, Sigma). Figures 3.16(a) and 3.16(b) show the scanning electron microscope (SEM) images of PACF crack, confirming the

random orientation of fibers, fiber fracture, fiber pull-out and matrix cracking including brittle fracture morphology of base polymer.

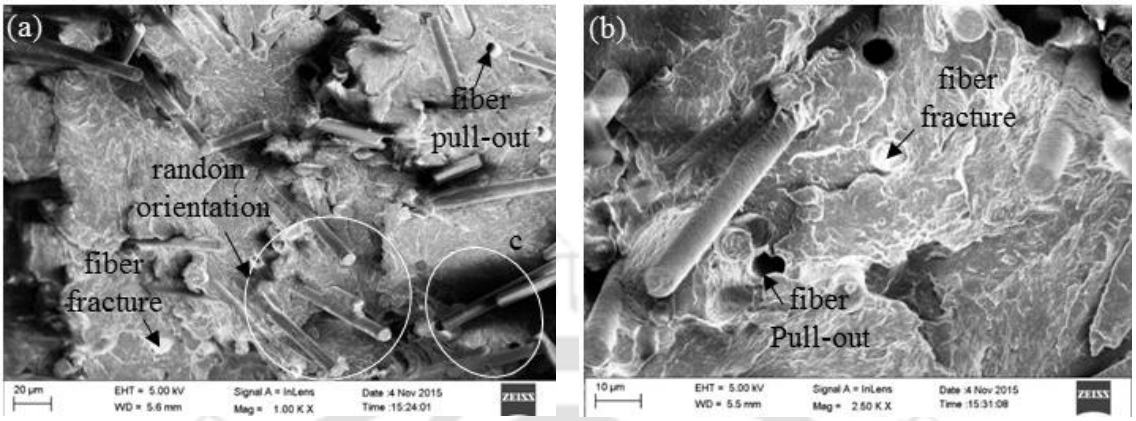

Figure 3.16 Crack surface of specimen failed during tensile test (a) showing fiber pull-out, fiber fracture and random orientation of fibers and (b) close-up view of region marked as c in Figure 3.16(a)

The hardness of the injection molded samples were measured as per ASTM D-2240 using Shore-D-Durometer. The measured hardness of PA and PACF samples were 78±2.03 and 84.4±2.36.

3.5 GEAR BENDING FATIGUE TEST RIG AND METHODOLGY

Unreinforced polyamide 66 and 20 wt. % long carbon fiber reinforced polyamide 66 were considered for injection molding the test gears. Ground stainless steel gear (AISI 316) was used as driver gear. A servo motor driven gear test rig simulating actual gear mesh condition was developed in-house and was used to evaluate the bending fatigue performance of polymer composite gears. The entire system consisting of loading system, control panel, thermal camera and data acquisition, is shown in Figure 3.17(a). As shown in Figures 3.17(b)–3.17(c), test rig consists of driving and driven shafts which were suitably supported between bearings at a desired center distance. Stainless

steel gear was mounted on the driving shaft and inline torque sensor (HBM, T100WN) was connected through bellow couplings (KBK, KB4C). Test gear mounted on the driven shaft can be firmly locked at any desired roll angle/contact position with a stainless steel gear using shaft locking plate.

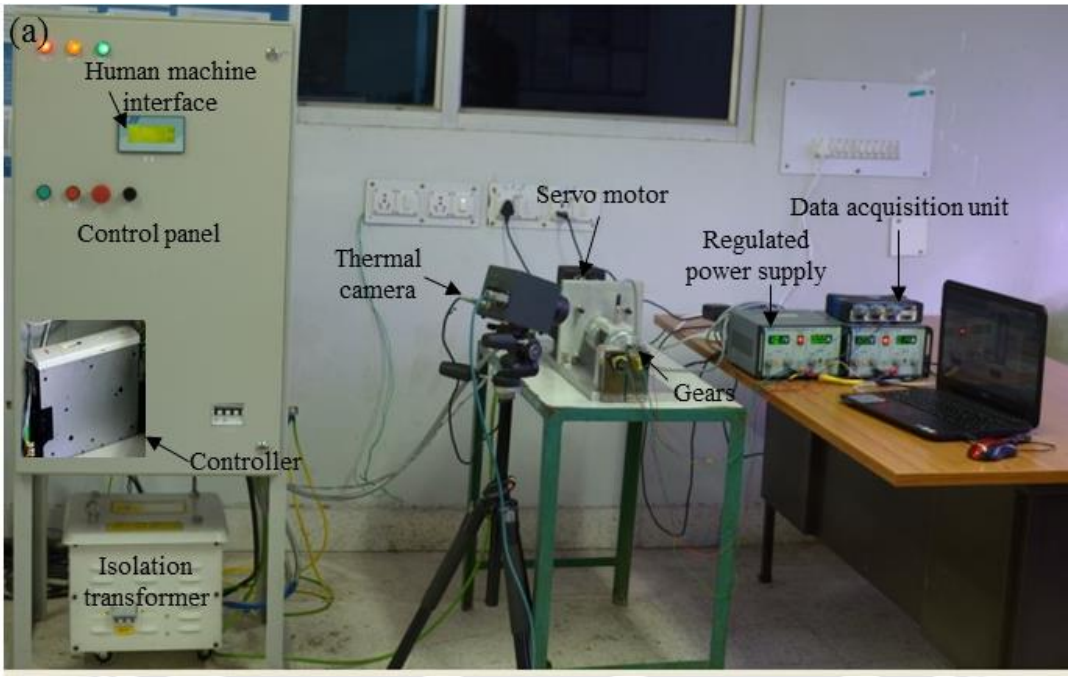

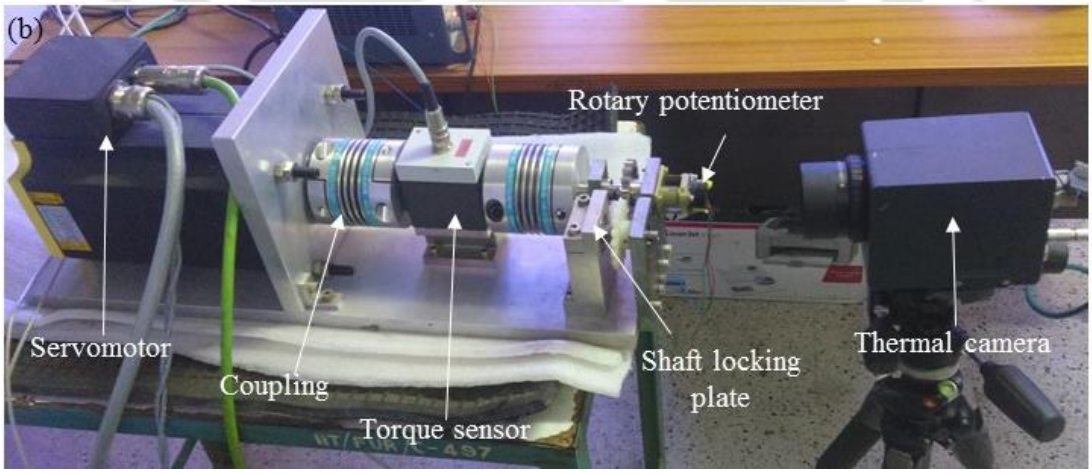

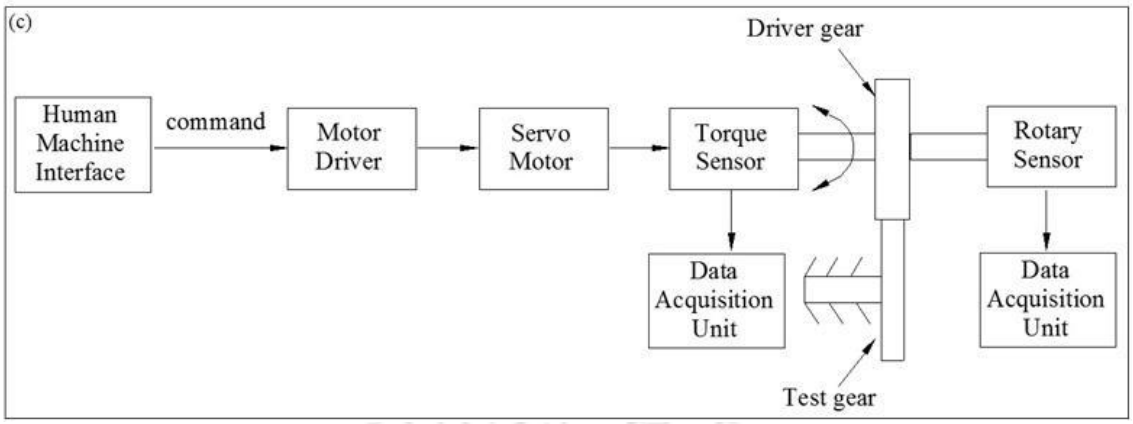

Figure 3.17 In-house developed test rig (a) gear bending fatigue test rig, (b) close-up view of gear test rig and (c) motion flow in test rig

The assembly and the fabrication drawings drawn in third angle projection, of in-house developed gear test rig are shown in Figure 3.18. A servo motor (BALDOR, BSM-100C-3250) was coupled to one end of the driving shaft through bellow coupling. Servo motor is capable of exerting torque upto 14 Nm at frequency upto 20 Hz on the gear mesh. Human machine interface was used to feed input to the controller (BALDOR, MotiFlex e100) of the servo motor. The motor controller was programmed to make the motor to develop the required torque loading pattern by controlling motor current accordingly. A dedicated control panel was developed which houses human machine interface, motor controller, regenerative resistor, and isolation transformer. Rotary position sensor, potentiometer (MCB, PR27M) was connected at the other end of the driver gear shaft to measure angle turned during test (Figure 3.17(c), Figure 3.18(a)).

Infrared thermal camera (InfraTec, VarioCAM hr head 600) was used to monitor the temperature rise of the test gear in mesh. Data acquisition (HBM, QuantumX-MX840A) was used to continuously record the torque exerted and angular

displacement of gear mesh during tests at a rate of 300 Hz. Bi-directional cyclic and uni-directional repeated torque load tests were performed at R-ratios (ratio of minimum to maximum stresses) of –1 and 0 respectively using the gear test rig.

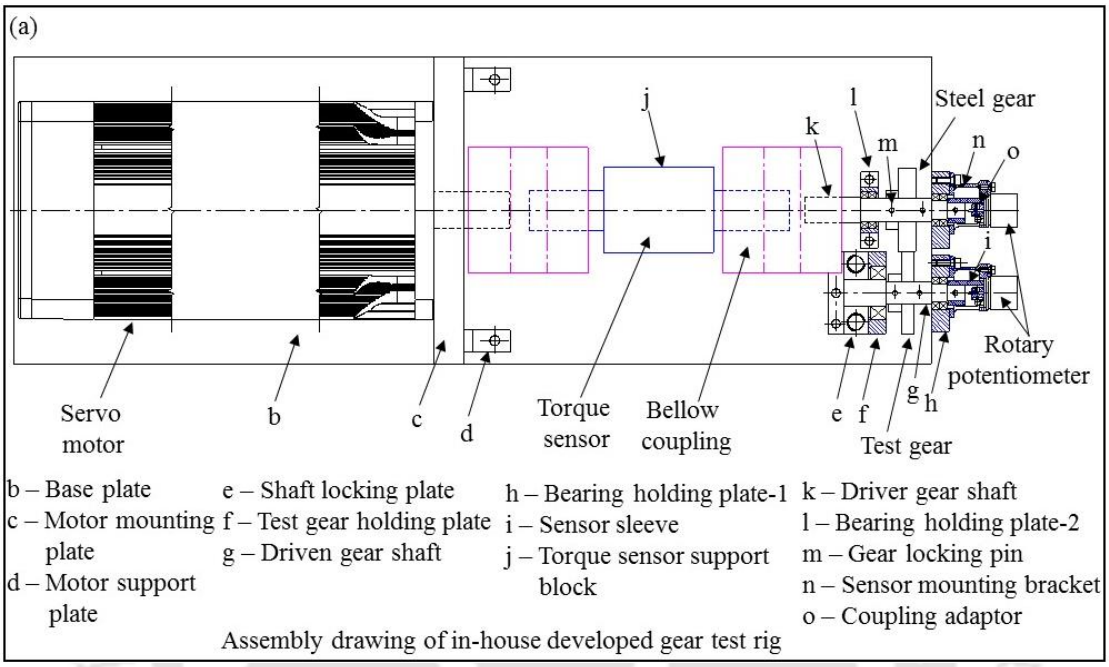

Assembly drawing of in-house developed gear test rig

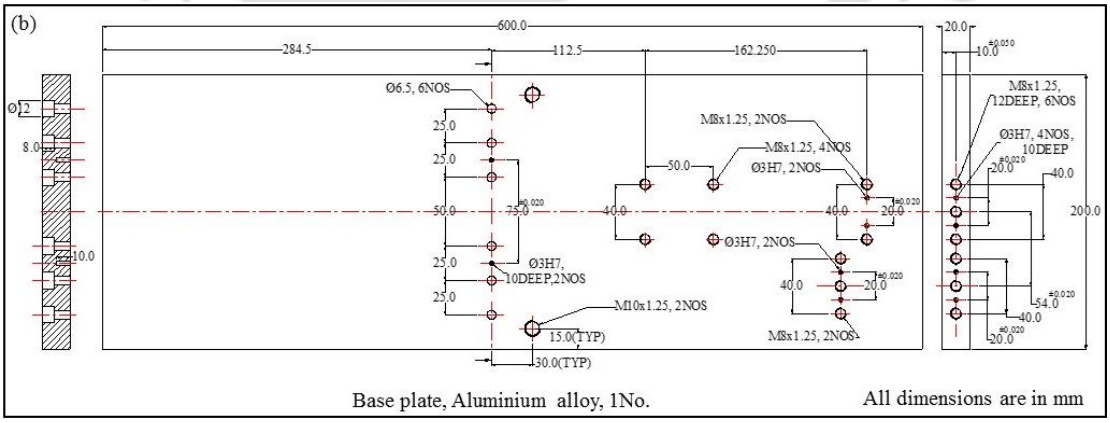

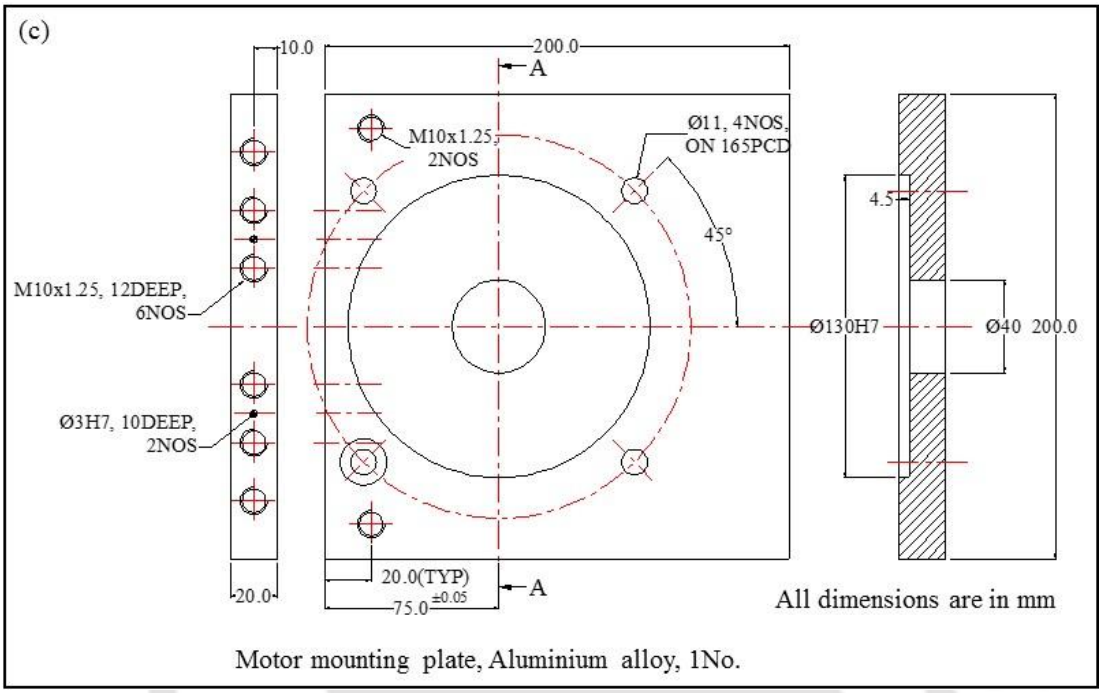

Motor mounting plate, Aluminium alloy, 1No.

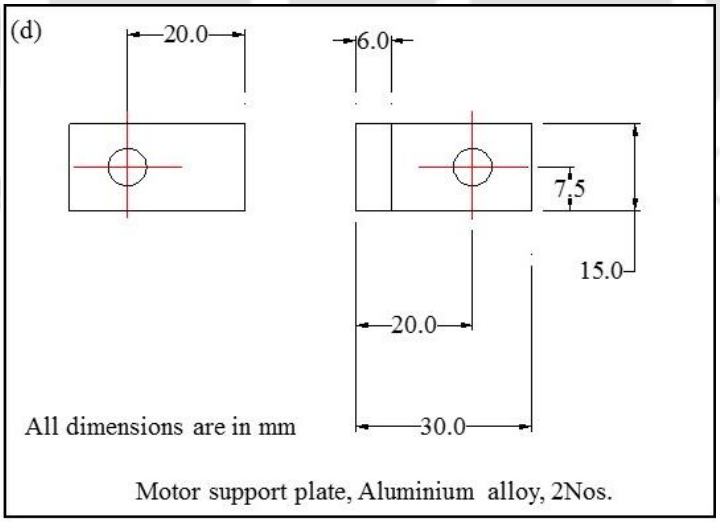

Motor support plate, Aluminium alloy, 2Nos.

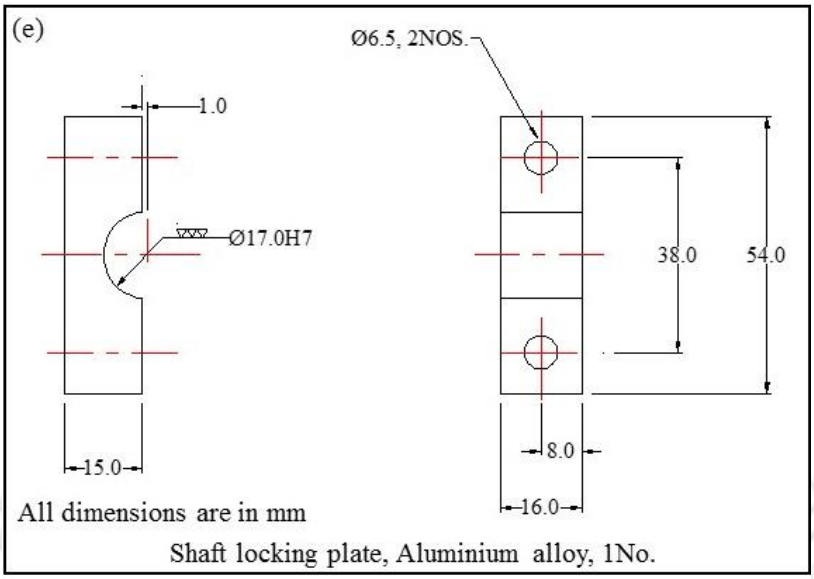

Shaft locking plate, Aluminium alloy, 1No.

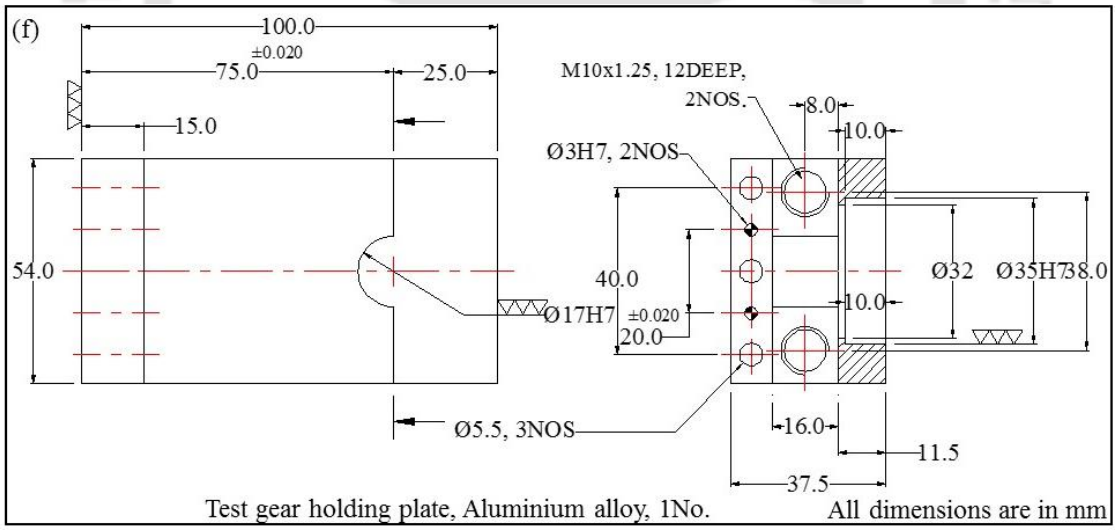

(g)

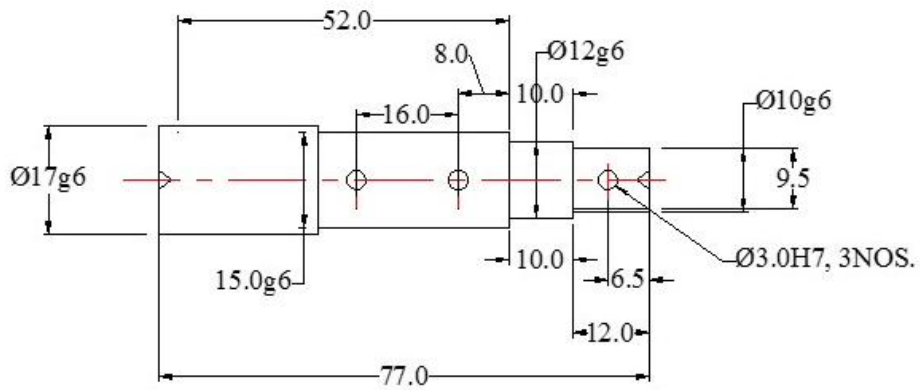

Dimensions with H7 and g6 tolerances are to be ∇∇∇ finished

Driven gear shaft, EN24 steel, 1No. All dimensions are in mm

(h)

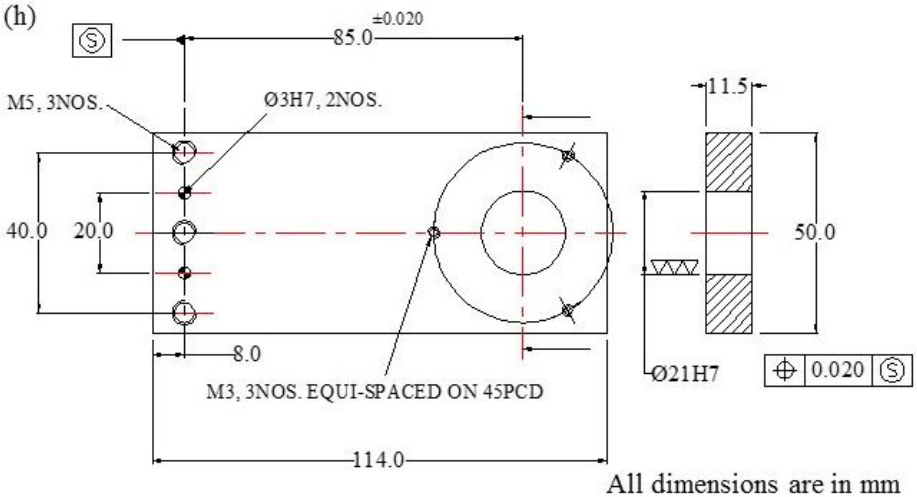

All dimensions are in mm

Bearing holding plate-1, EN24 steel, 2Nos.

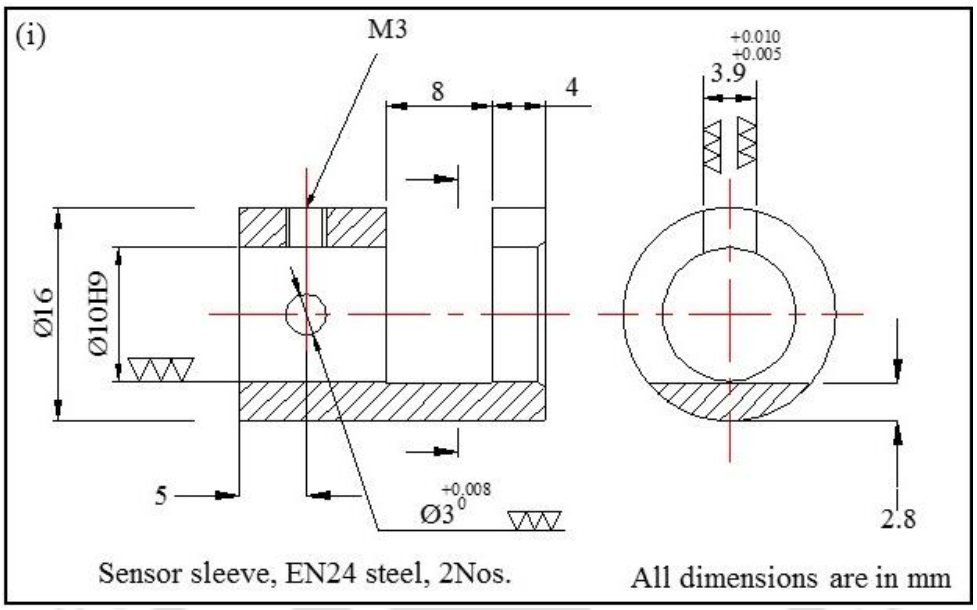

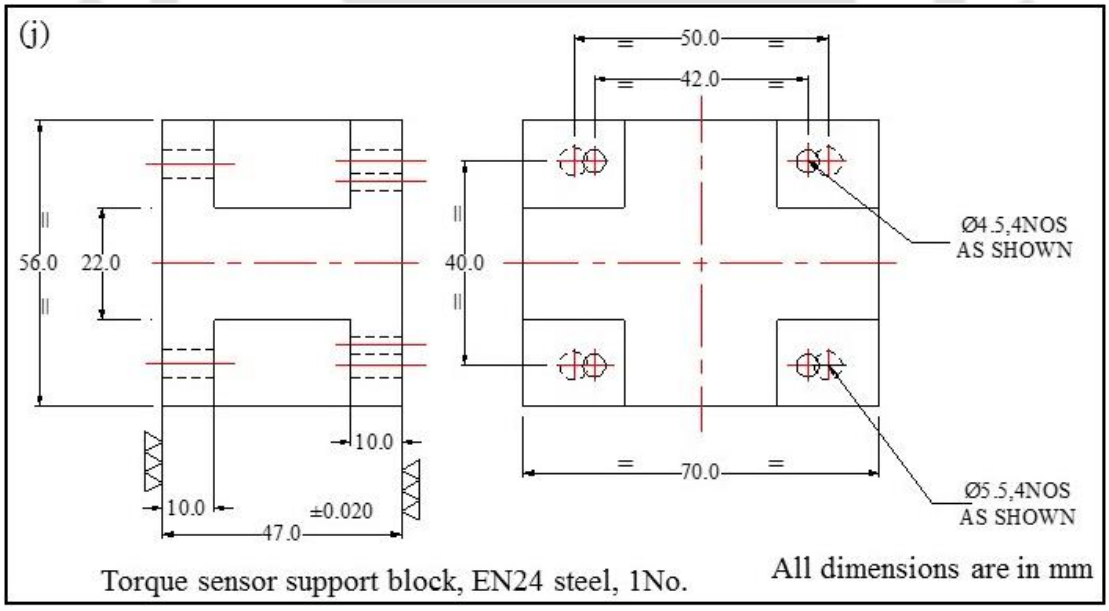

(k)

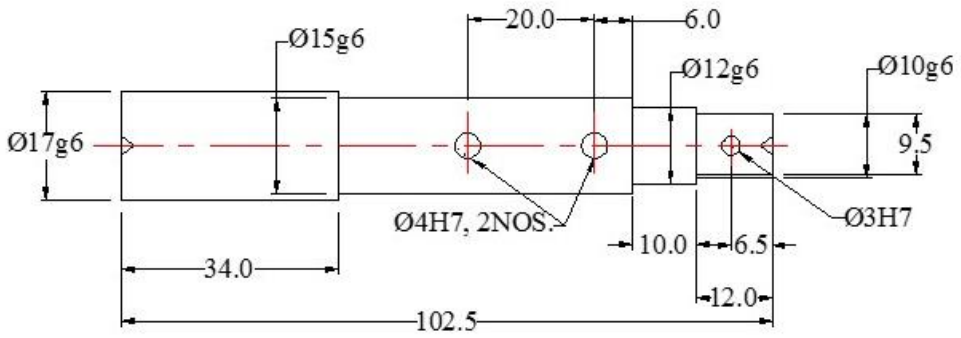

Dimensions with H7 and g6 tolerances are to be ∇∇∇ finished

Driver gear shaft, EN24 steel, 1No. All dimensions are in mm

(l)

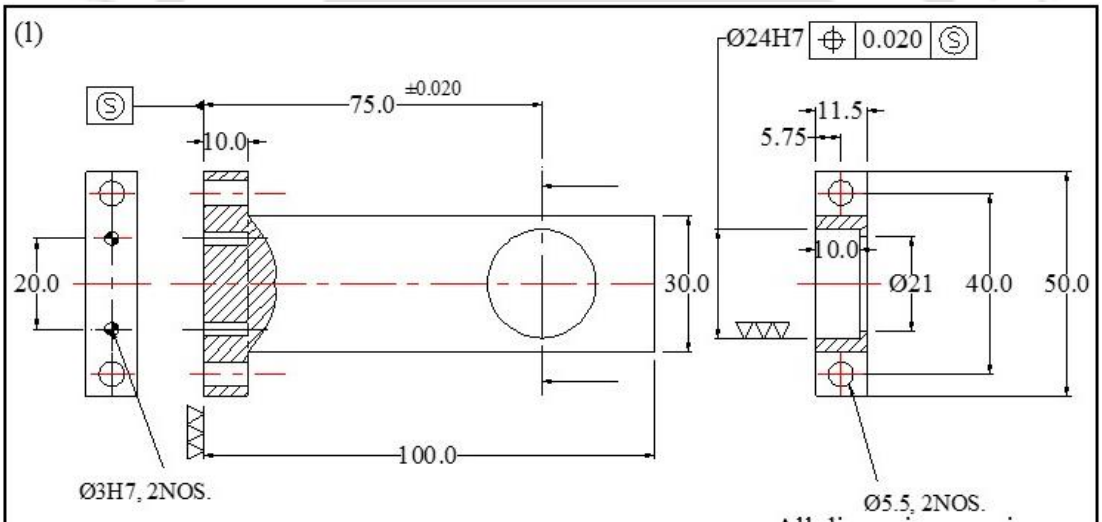

All dimensions are in mm

Bearing holding plate-2, EN24 steel, 1No.

(m)

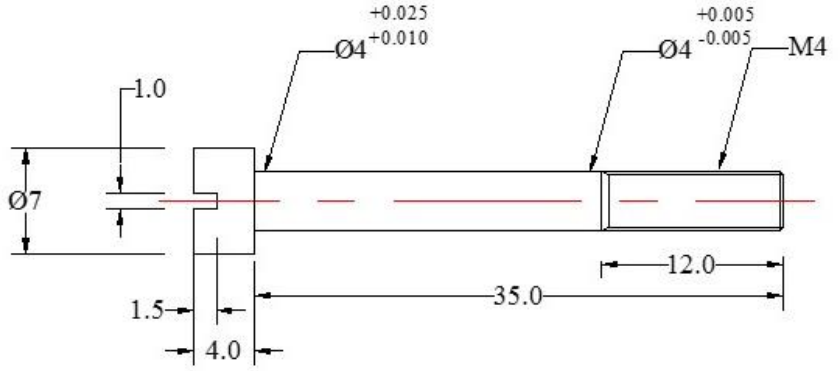

All dimensions are in mm

Gear locking pin, EN24 steel, 2Nos.

(n)

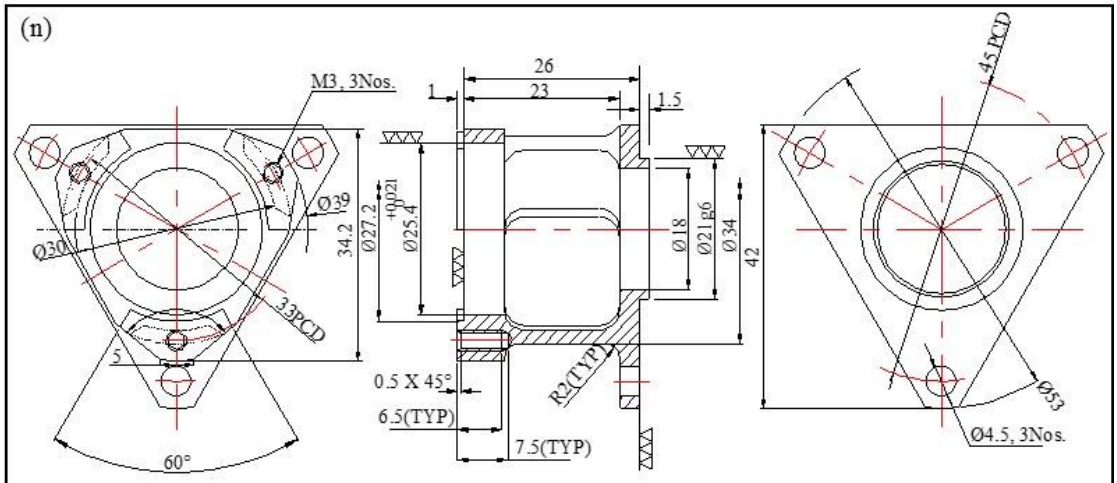

Sensor mounting bracket, Aluminium alloy, 1No.

All dimensions are in mm

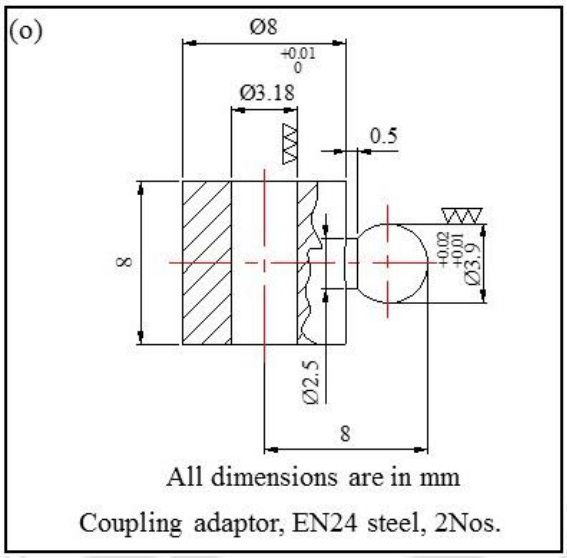

Figure 3.18 In-house developed test rig (a) Assembly drawing and fabrication drawings of (b) Base plate, (c) Motor mounting plate, (d) Motor support plate, (e) Shaft locking plate, (f) Test gear holding plate, (g) Driven gear shaft, (h) Bearing holding plate-1, (i) Sensor sleeve, (j) Torque sensor support block, (k) Driver gear shaft, (l) Bearing holding plate-2, (m) Gear locking pin, (n) Sensor mounting bracket and (o) Coupling adaptor

The variation of torque with time for bi-directional load is schematically represented in Figure. 3.19(a). It can be seen from the figure that test gear was subjected to constant cyclic frequency of 5 Hz with torque amplitude of 7.5 Nm. Similarly, uni-directional repeated load tests were carried out at 10 Hz frequency, as shown in Figure 3.19(b). These frequencies were selected in such a way that the load experienced by the test gears in one-half cycle of the bi-directional loading is equal to the one-cycle of the uni-directional loading. Tests were carried out in the torque range of 7–12 Nm. Minimum three gears were tested in every loading condition. Gear mesh test position was selected in such a way that tooth experiences almost equal load on its either sides during bi-directional loading as shown in Figure 3.20. Torque variations represented by

continuous and dashed lines in Figure 3.19 develop tensile stress on root locations marked as ‘x’ and ‘y’ respectively for driven gear (Figure 3.20). Each test was performed till the gear tooth fracture or 5×10^6 cycles, whichever was earlier. The unreinforced and reinforced gears were tested at lower and higher torque levels, respectively. Failed gear tooth was observed under scanning electron microscope to determine the failure mechanism.

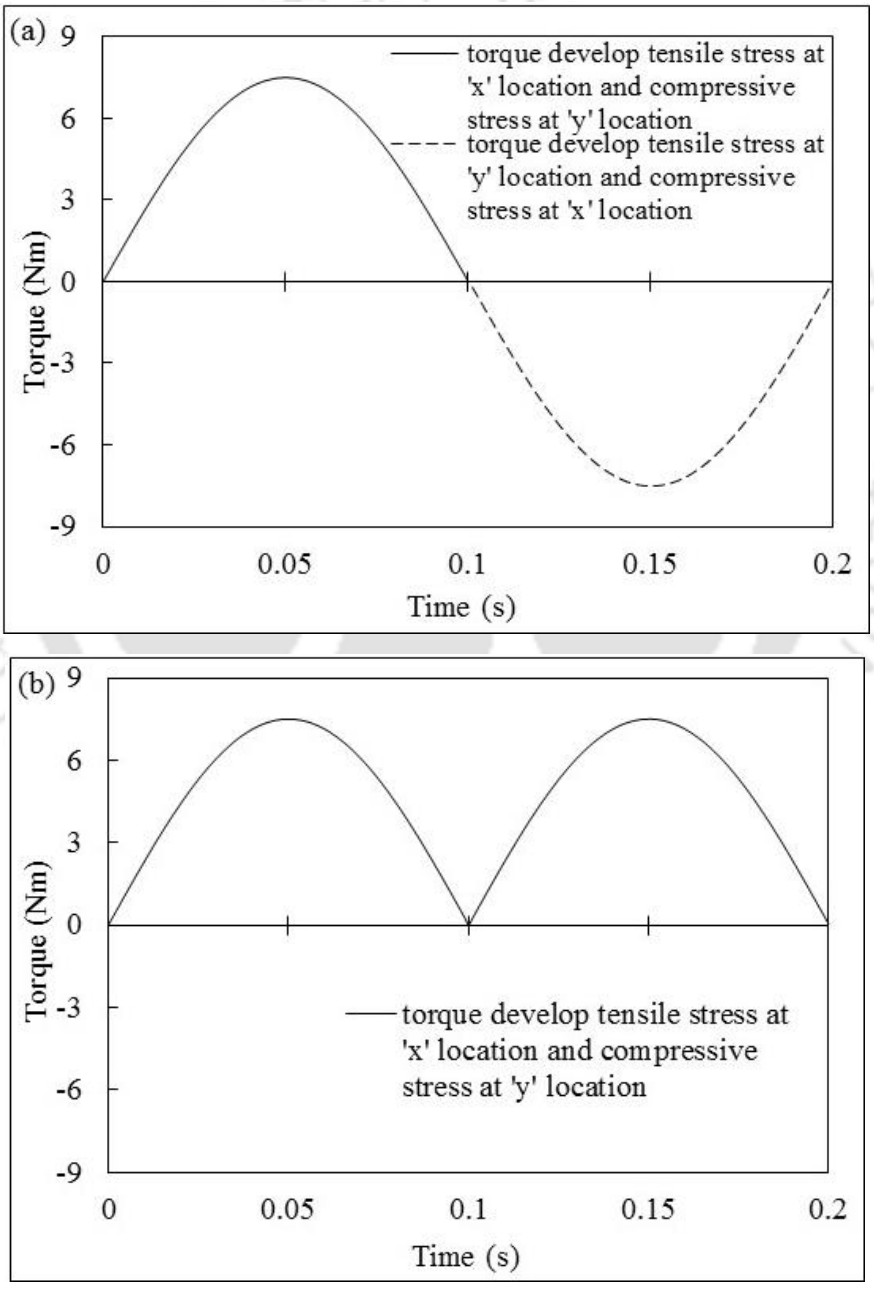

Figure 3.19 Torque pattern in (a) bi-directional loading and (b) uni-directional loading

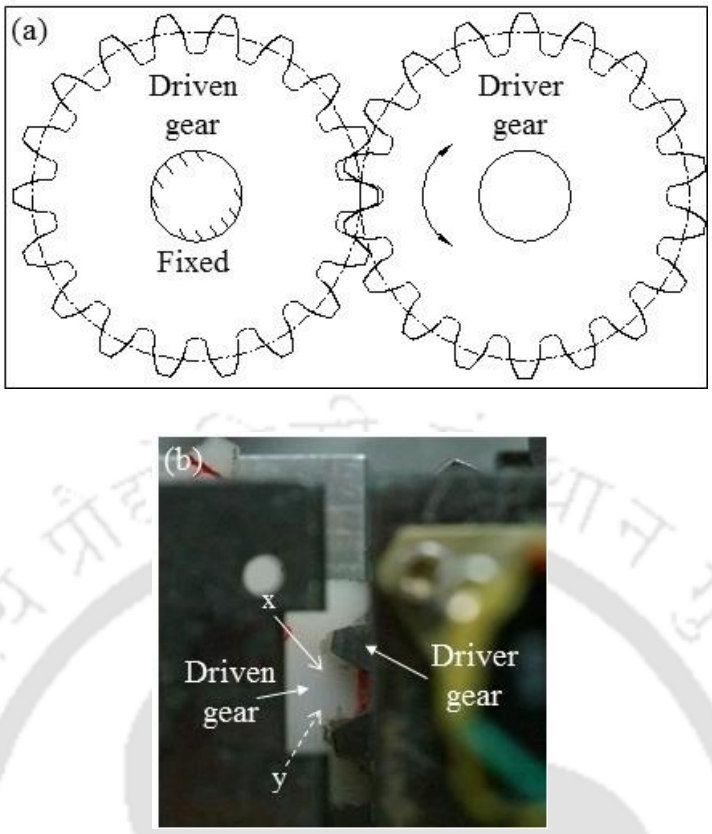

Figure 3.20 Gear mesh (a) schematic of gear tooth contact position in test and (b) close-up view of gear mesh

Tests were conducted on the unreinforced polyamide 66 spur gears to assess the effects of loading frequency on the hysteretic heating and fatigue life. The tests were conducted in a torque range of 6–13.5 Nm at different frequencies (2, 5, and 7.5 Hz for bi-directional loads, stress ratio R = −1; 4, 10, and 15 Hz for uni-directional loads, R = 0) using an in-house developed servo motor operated gear test rig. The test was run for 3600 s to stabilise the surface temperature of the gear, which is required to assess the hysteretic heating. An infrared thermal camera (InfraTec, VarioCAM hr head 600) was used to monitor and acquire the surface temperature of the gear. To evaluate the fatigue life, each test was performed until the gear tooth fractured or when the number of cycles reached 5×10^6, whichever was earlier. For every load condition, the tests were repeated for the three gears. Torque exerted and angular displacement of gear mesh

obtained from torque sensor and rotary position sensor, respectively, were used for plotting hysteresis loop. The hysteresis loop area is a measure of hysteretic heating and was computed for both the bi-directional and uni-directional loads at different torques with the help of commercial technical computing tool, MATLAB®.

3.6 STATIC TRANSMISSION ERROR TEST RIG AND METHODOLOGY

Transmission error is the difference between theoretical position of the output gear with perfect geometric accuracy and rigid drive and actual output position. In the gear metrology, tooth-to-tooth transmission error and total transmission error represent composite error which can be measured by rotating test gear against master gear in the single flank gear roll testing equipment. In the composite error, all the individual errors (profile error, pitch error, tooth alignment error, tooth thickness error, radial and axial runout) are included.

In this work, polyamide test gears were fabricated using injection molding process following the identical process parameters as the tensile specimens. Ground stainless steel gear made of AISI 316 material was considered as driver gear. A test rig (Figure 3.21) was developed in-house for measuring the transmission error using an optical encoder (BEI, DHM5_10//PG59//80000//G3R020). The resolution of sensor is 80000 cpt (counts per turn), implying that it can measure the minimum angle of 0.0045º (360º/80000) corresponding to one count. The polyamide gear was rotated to the required contact position with the help of an optical encoder and firmly locked using shaft locking plate. Static torque was applied on polymer gear tooth by stainless steel gear using dead weights and a pulley. The torque applied was measured using an in-line torque sensor (HBM, T100WN). The tests were carried out at different torques (1 to 2.5 Nm) under laboratory condition maintained at the temperature of 296±5 K and relative

humidity of 60±5 %. The tests were conducted only on single tooth for the two different teeth of three different gears at single tooth contact (STC) positions (pitch–1º, pitch, pitch+1º) and double teeth contacts (DTC) positions at the addendum side (pitch+9º, pitch+10º, pitch+11º), near ending of contact and at the dedendum side (pitch–9º, pitch–10º, pitch–11º), near beginning of contact. Hence, transmission error due to both the geometric inaccuracies and rigidity variation of polymer gear was measured in this work and reported as static transmission error. For each test, a holding time of approximately 3 s was allowed after applying torque to obtain a steady state measurement. Intervals of approximately 5 min elapsed between the successive tests to regain the elastic tooth deformation of the previous loading. The optical encoder output was measured within 0.01º before and after loading to ensure no creep/relaxation of polymer gear.

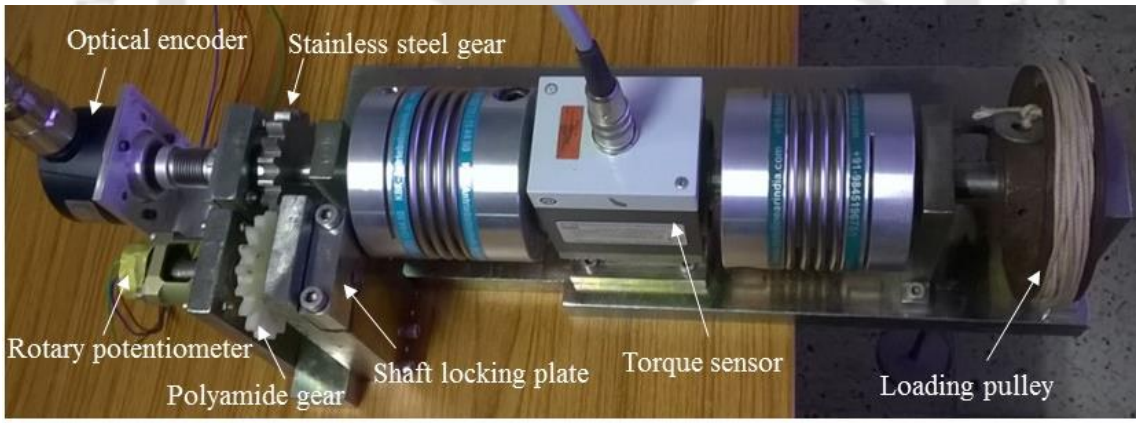

Figure 3.21 Gear transmission error test rig

3.7 NUMERICAL EVALUATION OF GEAR TRANSMISSION ERROR

Finite element model of a gear pair is shown in Figure 3.22. In order to reduce the computational time of the simulation, only disc and five meshing teeth were modeled. Wang and Howard (2004) and Karimpour *et al.* (2010) also used ten and five teeth,

respectively, in their models. Geometric nonlinear analysis was carried out using commercial tool ABAQUS®. After systematic comprehensive and convergence study, the elements of 8 µm size at root region, 55 µm size at contact region and coarse elements at the disc portion were used. Evaluated properties of gear materials at 296±5 K as per ASTM D638 were used for the study. Isotropic linear material and nonlinear material models and plain stress linear quadrilateral elements (CPS4R) were considered. All degrees of freedom of driven gear at the hub portion were constrained as it was rigidly fixed in the driven shaft using locking pin and driven shaft was firmly fixed using shaft locking plate. For driver gear, a reference node at hub center was created for the application of torque and its degrees of freedom in x and y directions were constrained. Kinematic coupling was established between hub center/reference node and hub inner diameter of driver gear as it was rigidly fixed in the driver shaft using locking pin. Simulation was carried out for different torques (0.5–2.5 Nm at 0.5 Nm steps). It can be noted that torque is applied at a reference node of driver gear. Frictional contact was provided for the driver and driven gears.

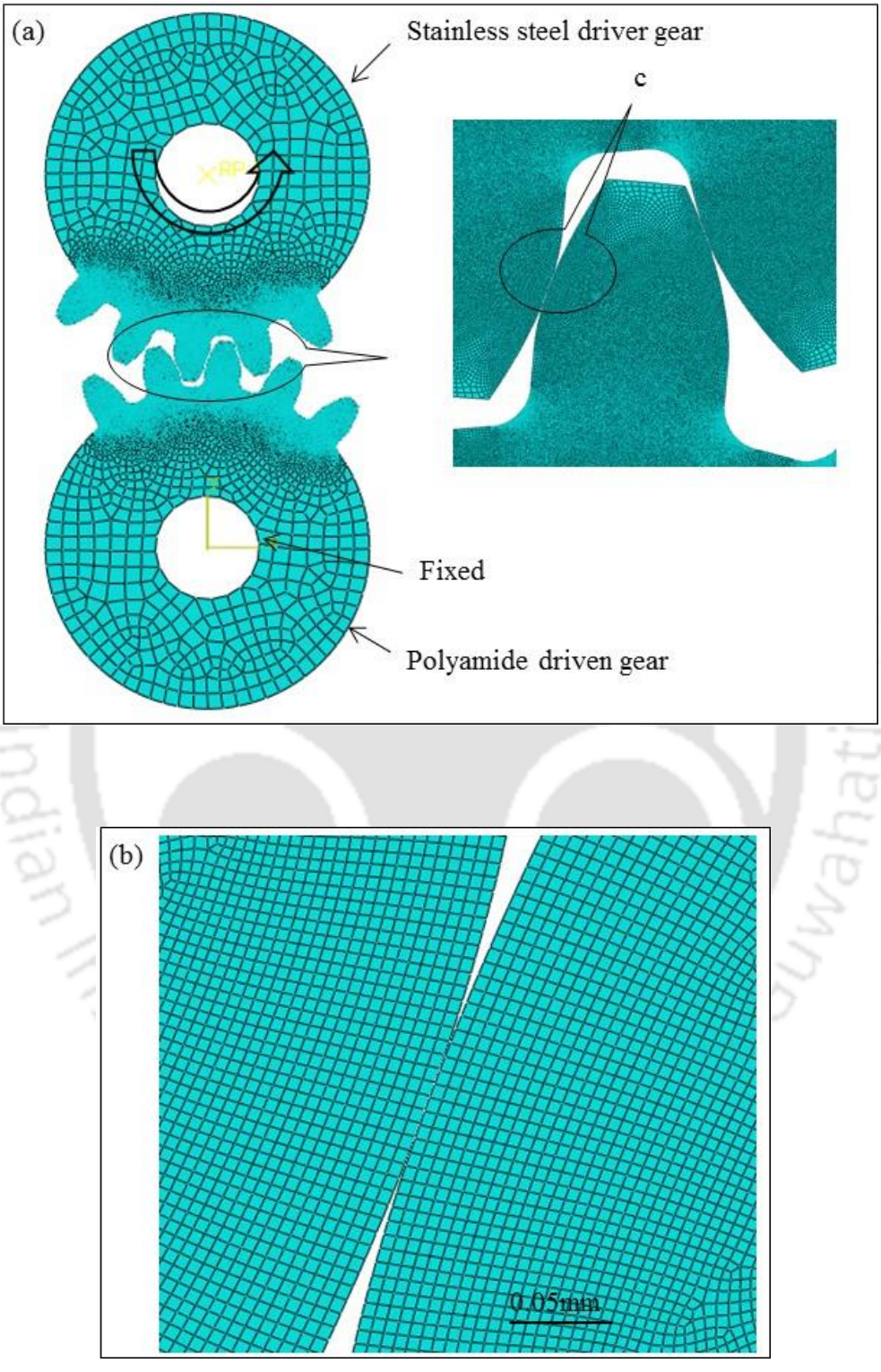

Figure 3.22 Finite element model of (a) stainless steel-polyamide gear pair and (b) close-up view of contact region marked as c in Figure 3.22(a)

3.7.1 Numerical simulation methodology

Geometric nonlinear analysis was repeated for each roll angle position by rotating the gear by 1º. In order to cover the roll angle from −20º to +20º, total 41 simulations were carried out for each torque value, where 0º, −20º and +20º correspond to contact at pitch, near beginning of contact and near ending of contact of driven gear, respectively. The simulation time was typically 27 min in VAIO laptop having Intel(R) Core(TM) i5-4200 CPU @ 1.60 GHz, 4.00GB RAM and 64-bit operating system. From each simulation, coordinate of surface node of driven gear tooth experiencing maximum contact normal force, maximum principal stress and angular rotation of driver gear were extracted. The path/line of contact was plotted using the coordinates of contact surface nodes of driven gear. The maximum principal stress and angular rotation of driver gear are the measure of root bending stress and static transmission error, respectively. The gear mesh stiffness is defined as ratio of torque applied to the static transmission error and was calculated from the results.

3.8 SUMMARY

The gear materials and injection molding process conditions used for preparing the test specimens and gears were discussed. The gear inspection methodology for profile, lead and pitch deviations were highlighted. The methods for evaluating the tensile properties and hardness were explained. The details of the gear test rigs used for assessing bending fatigue performance and static transmission error including the failure criteria were reported. The numerical evaluation methodology for predicting the static transmission error, bending stress and path of contact were also discussed.

CHAPTER 4

BI-DIRECTIONAL AND UNI-DIRECTIONAL BENDING FATIGUE PERFORMANCE OF UNREINFORCED AND CARBON FIBER REINFORCED POLYAMIDE 66 SPUR GEARS

4.1 INTRODUCTION

Polymer and polymer composite gears are nowadays considered for medium torque applications. Bending fatigue of polymer composite gears become important in bi-direction applications such as robotics, actuators of satellite launchers, etc., due to their lower mechanical and inferior thermal properties. Extensive investigations have been carried out to understand the fatigue and wear performance of polymer composite gears under uni-directional cyclic bending and contact loads (Kurokawa *et al.* (1999, 2003), Senthilvelan and Gnanamoorthy (2006a, 2006b), Mao *et al.* (2007, 2010), Imrek (2009), Duzcukoglu (2009a, 2009b), Kirupasankar *et al.* (2012), Hoskins *et al.* (2014), Pogacnik and Tavcar (2015)) and fatigue behaviour of polymer composites subjected to uni-directional / bi-directional loads (Goel *et al.* (2009), Mortazavian *et al.* (2015c), Mortazavian and Fatemi (2016)). Mohan and Senthilvelan (2014)) evaluated the preliminary bending fatigue performance of polymer composite gears under bi-directional constant deflection mode.

This chapter investigates the bending fatigue performance of unreinforced and carbon fiber (20 wt. %) reinforced polyamide 66 injection molded spur gears under bi-

directional and uni-directional loads. The fatigue life obtained in bi-directional loads were compared with that of uni-directional loads for both the unreinforced and carbon fiber reinforced gears.

4.2 METHODOLOGY

The unreinforced polyamide 66 (PA) and 20 wt. % long carbon fiber reinforced polyamide 66 (PACF) were injection molded into spur gears using injection molding machine. The gear processing, molding conditions, test gear details, parameters and inspection are explained in Sections 3.2 and 3.3. (CHAPTER 3). The bending fatigue performance tests were carried out using in-house developed servo motor operated gear test rig. The details of test rig are explained in Section 3.5 (CHAPTER 3). The tests were conducted at various torques (7, 7.5, 8.5, 10, 11, and 12 Nm) under bi-directional loading at a frequency of 5 Hz and uni-directional loadings at a frequency of 10 Hz. These frequencies were selected in such a way that the load experienced by the test gears in one-half cycle of the bi-directional loading is equal to the one-cycle of the uni-directional loading. Minimum three gears were tested in every loading condition. Gear mesh test position was selected in such a way that tooth experiences almost equal load on its either sides during bi-directional loading as highlighted in Section 3.5 (CHAPTER 3). Each test was performed till the gear tooth fracture or 5×10^6 cycles, whichever was earlier. Torque exerted on gear mesh and angular displacement of gear mesh measured at driver gear end, were continuously measured and acquired at a rate of 300 Hz.

4.3 MECHANICAL PROPERTIES OF TEST GEAR MATERIALS

The mechanical properties of unreinforced and carbon fiber reinforced polyamide 66 were evaluated as per ASTM D638 standard. The evaluated properties at 296±5 K are given in Table 3.2 (reported in Section 3.4, CHAPTER 3). The carbon reinforcement enhanced the Young's modulus and yield strength and reduced the elongation of polyamide composite.

4.4 GEAR TOOTH BENDING STRESS

Schematic view of the gear tooth is shown in Figure 4.1. Induced tooth root bending stress for different torques was computed using the Lewis equation (4.1)

$$\sigma_b = \frac{F_t}{m\, b\, Y} \qquad (4.1)$$

where F_t, m and b are the tangential load acting on the gear tooth, module and face width respectively. Important gear parameters used for computation is provided in Table 3.1. The Lewis form factor (Y) of 0.736 was computed using equation (4.2)

$$Y = \frac{S_q^2}{6\, m\, h_q} \qquad (4.2)$$

where S_q and h_q are critical section thickness and height at which the applied force acts from the critical section respectively. The computed bending stress at the different torques is shown in Table 4.1.

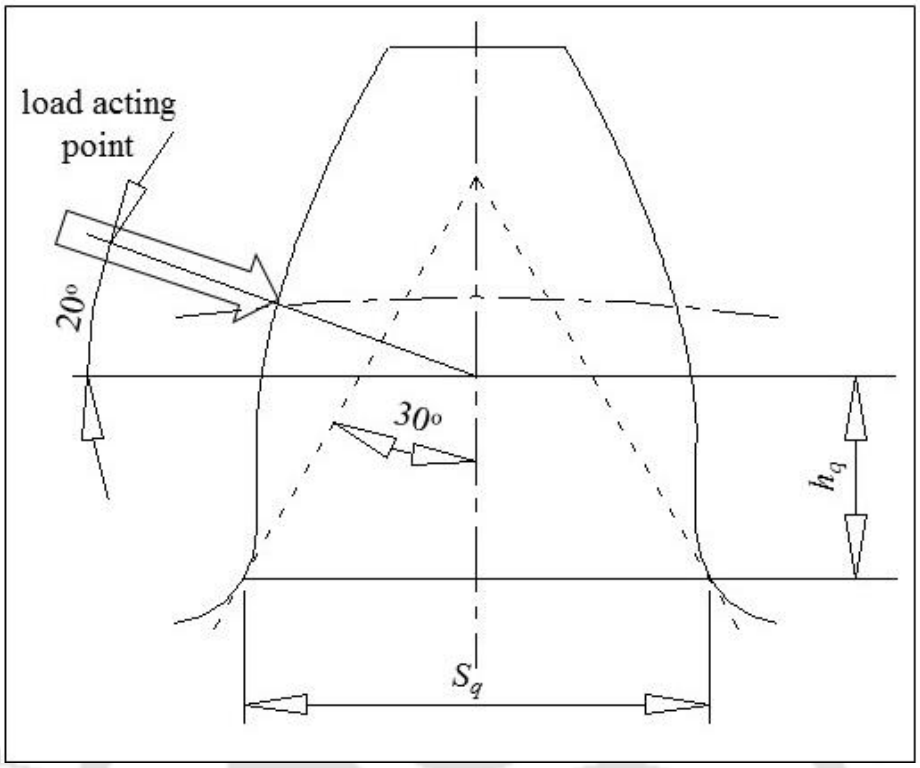

Figure 4.1 Schematic view of gear tooth

Table 4.1 Bending stress at gear tooth root

Torque (Nm)	7	7.5	8.5	10	11	12
Bending stress (MPa)	29	31	36	42	46	50

The bending stress variation across the root section A–A is shown schematically in Figure 4.2. It can be observed that the gear tooth root is subjected to tensile stresses in drive (loading) side and compressive stresses in coast side.

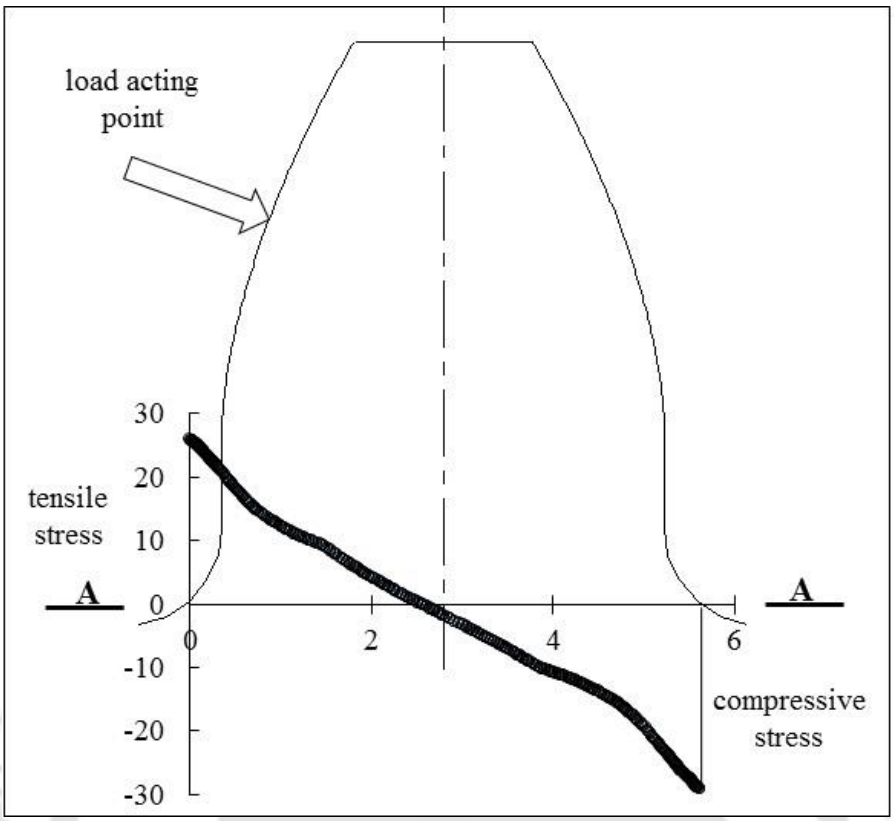

Figure 4.2 Bending stress variation across the root section (A-A)

4.5 FATIGUE LIFE

Testing for the entire range of torque for unreinforced and reinforced gears under bi-directional and uni-directional loading would be more time consuming. It is well known fact that life experienced by unreinforced gears will be less as compared to reinforced gears. Hence, unreinforced and reinforced gears were tested at lower and higher torque levels, respectively. The fatigue life plots of PA and PACF gears subjected to bi-directional and uni-directional loads are shown in Figure 4.3. It was observed that the fatigue life of gears subjected to bi-directional loads (R = –1) exhibited decreased fatigue life when compared to uni-directional loads (R = 0). In uni-directional loading, the gear tooth root is subjected only to tensile stresses at driving side and compressive stresses at coast side, whereas, gear tooth root experience tensile

and compressive stresses alternatively in bi-directional loading. Additionally, viscoelastic nature of the base polymer matrix and low stiffness of gear tooth of polymer gear generate heat under cyclic bending load due to the gear material hysteresis loss. Both PA and PACF gears exhibited temperature rise during fatigue loading. The net surface temperature of polymer gear tooth after dissipating to the environment was measured by the infrared thermal camera.

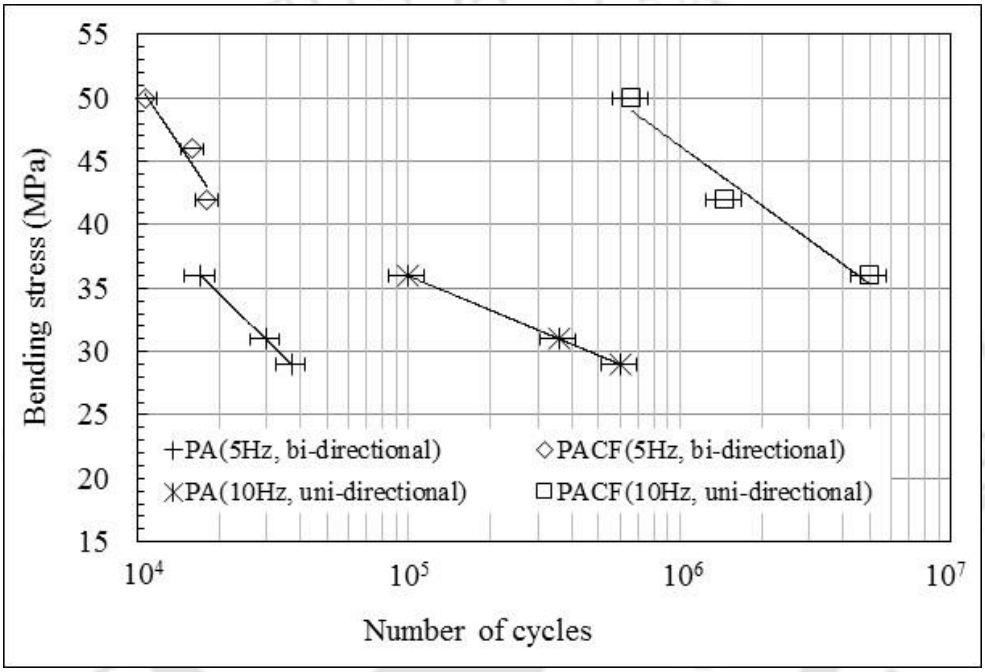

Figure 4.3 Fatigue life of PA and PACF gears

For the considered load range, PA gears subjected to bi-directional loads exhibited 83–94 % fatigue life reduction compared to that of uni-directional loads. Under bi-directional loading, PA gear generated significant heat due to the hysteresis effect, resulted in the deterioration of strength and modulus. However, generation of heat due to uni-directional loading was relatively less. The thermographs of PA gears subjected to bi-directional and uni-directional 7 Nm loadings (after 2000 s test duration) are shown Figures 4.4(a) and 4.4(b) respectively. The maximum temperature of 43 ºC at

the middle of tooth base during bi-directional loading was observed and it was only 36 ºC for uni-directional loading. It was observed that the temperature rise controlled the PA gears life. Mortazavian *et al.* (2015c) also observed a temperature rise of 10 ºC when the stress ratio was −1 and 3 ºC rise when the stress ratio was 0.1 at 1 Hz frequency for PP specimens. Figure 4.4(c) shows the thermograph of PACF gear (after 2000 s test duration) subjected to bi-directional load, where the maximum temperature of 37 ºC only was observed even for higher torque level of 12 Nm. Due to superior material modulus (5 times) and thermal conductivity (140 times), the net surface temperature of PACF gear was very small as compared to PA gears.

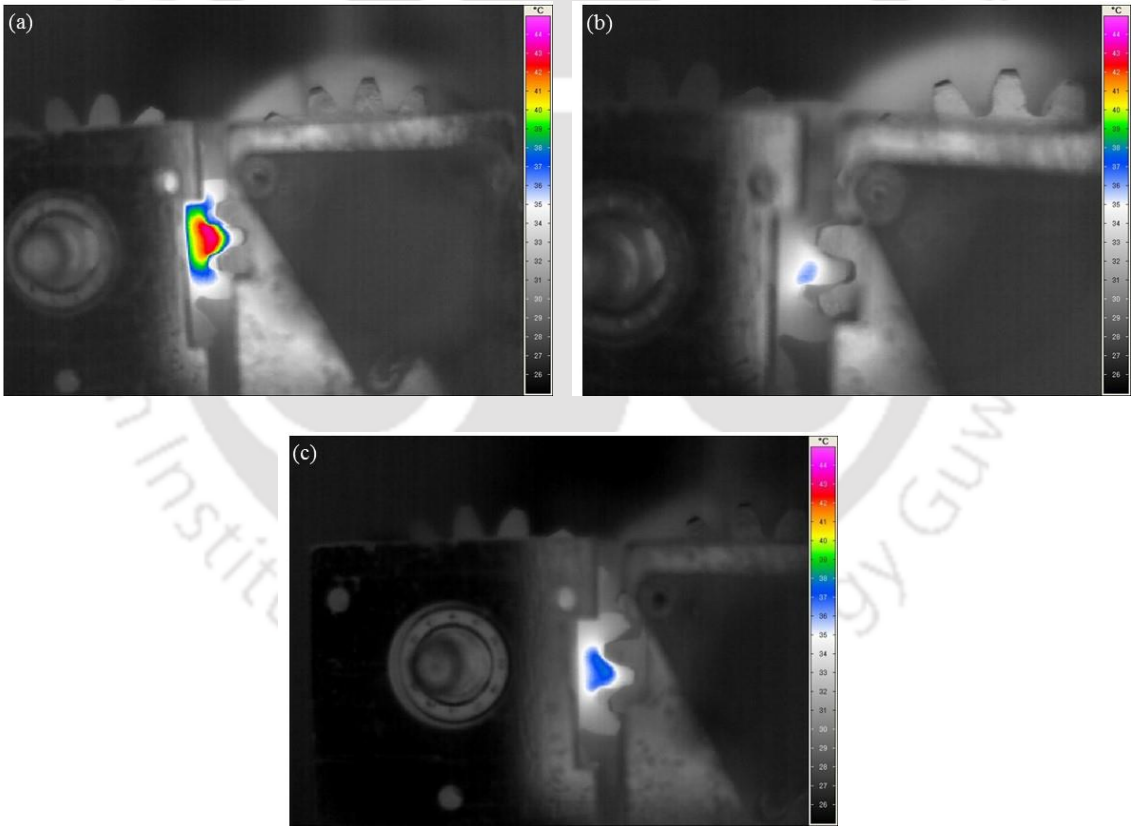

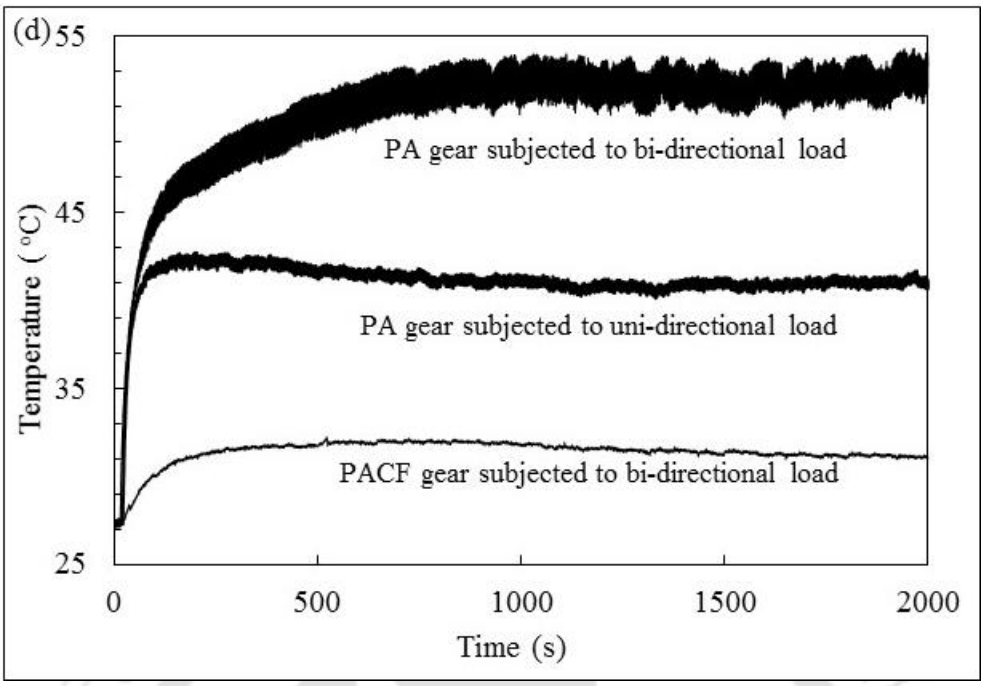

Figure 4.4 Surface temperature (a) thermograph of PA gear subjected to bi-directional 7 Nm load, (b) thermograph of PA gear subjected to uni-directional 7 Nm load, (c) thermograph of PACF gear subjected to bi-directional 12 Nm load and (d) net surface temperature of PA and PACF gears at 8.5 Nm load

Figure 4.4(d) shows the net surface temperature of PA and PACF gears subjected to 8.5 Nm load. Temperature rise of PACF gears was about 84 % lesser than that of PA gears subjected to bi-directional loads. It can also be seen that temperature rise in PA gear under bi-directional load was higher than uni-directional load. This is due to the fact that higher hysteresis loss seen from the torque-angular displacement curve (acquired hysteresis loop after 2000 s test duration) for PA gear under bi-directional load compared to uni-directional load as shown in Figures 4.5(a) and 4.5(b). It can further be noted that though the hysteresis loss for PACF was comparable with PA gear under bi-directional load, by virtue of its superior thermal conductivity, temperature rise was minimum for PACF gears. Thus PACF gears have not exhibited any thermal induced failures even at higher magnitude bi-directional loads.

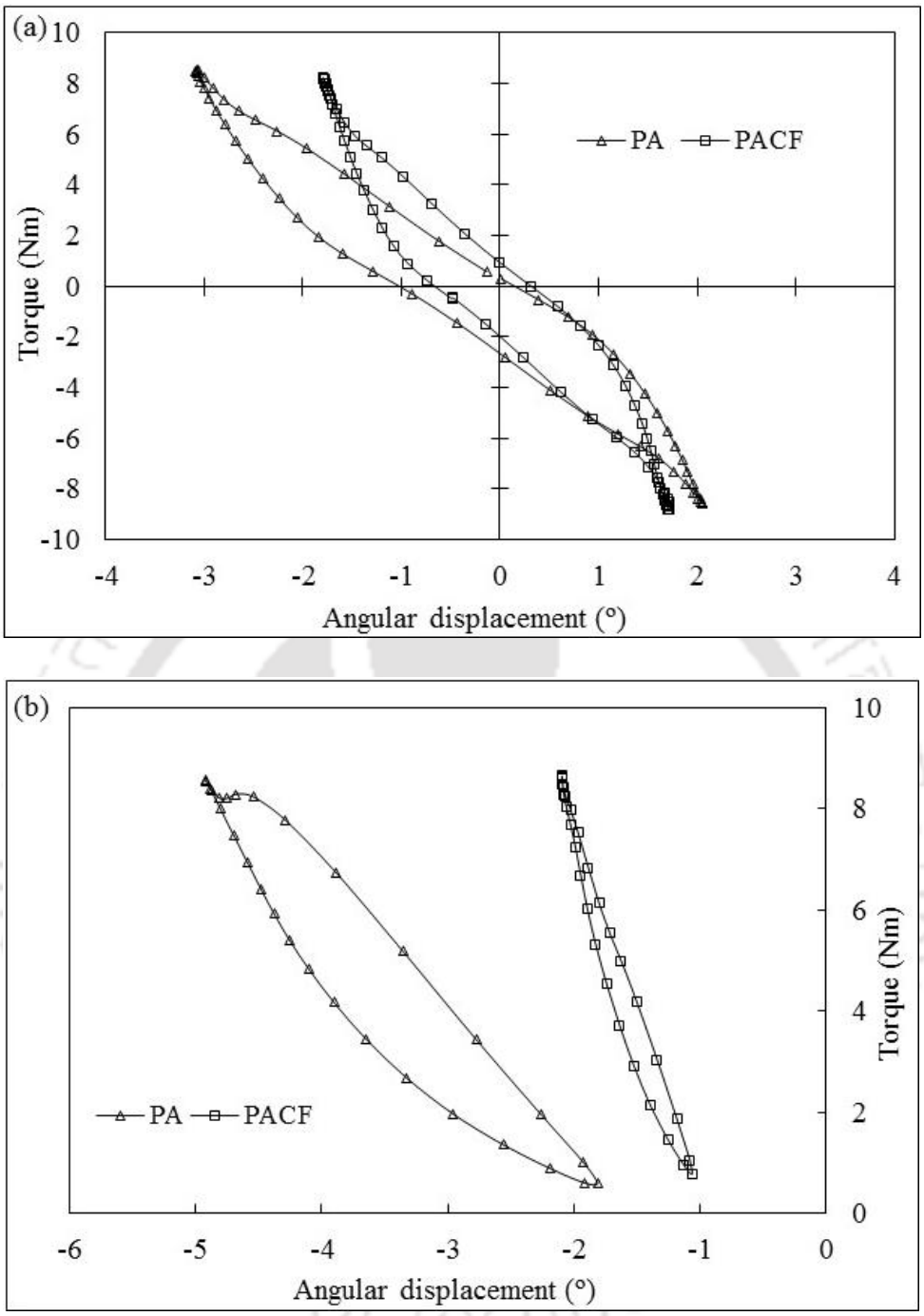

Figure 4.5 Hysteresis loops of PA and PACF gears subjected to

(a) bi-directional 8.5 Nm load and (b) uni-directional 8.5 Nm load

Goel *et al.* (2009) also observed a temperature rise of 5 and 3 ºC in unreinforced polypropylene (PP) and long glass fiber reinforced PP specimens respectively when tested at 15 MPa and 20 Hz frequency. For the considered load range, PACF gears

subjected to bi-directional loads exhibited 98–99% fatigue life reduction compared to that of uni-directional loads. It was observed that the life of both the PA and PACF gears was load pattern dependent. Zhou *et al.* (1994) also observed similar behaviour while investigating the flexural fatigue strength of polyphenylene ether ketone (PEK-C) and polyphenylene sulfide (PPS) with the aid of four point bending test at various stress ratios (0.1–0.5) and observed decreased fatigue life with less stress ratio. Similar finding was inferred from the investigation of Mortazavian and Fatemi (2016), where tensile fatigue performance of short glass fiber reinforced polybutylene terephthalate (PBT), PA6 at various stress ratios (–1. 0.1, 0.3) was studied. Fatigue life was more at 0.1 stress ratio than at –1 stress ratio for the same magnitude of alternating stress.

Due to the superior modulus, strength (2 times) and thermal conductivity, PACF gears exhibited superior bending fatigue performance (51 times) when compared to that of PA gears, which is in-line with the earlier investigations. Kurokawa *et al.* (1999, 2003) also observed the increased surface and bending durability for the carbon fibre reinforced PEEK and carbon fiber reinforced PA gears. Senthilvelan and Gnanmoorthy (2006b, 2007) observed the improved surface and bending durability for the glass and carbon fiber reinforced nylon gears. It is to be noted that the present investigation evaluates only bending fatigue.

4.6 FAILURE MODES

Unreinforced polyamide gears exhibited both thermal induced tooth deformation and root crack failures, whereas carbon fiber reinforced polyamide gears exhibited only root crack failures. Unreinforced polyamide gear subjected to higher load (8.5 Nm) exhibited thermo mechanical fatigue failure which is confirmed by tooth deformation

and is shown in Figure 4.6(a). This behaviour was due to the higher material hysteretic heating because of bi-directional loading beside poor thermal conductivity of polyamide, which resulted in temperature rise to the level of glass transition temperature of material (50 ºC).

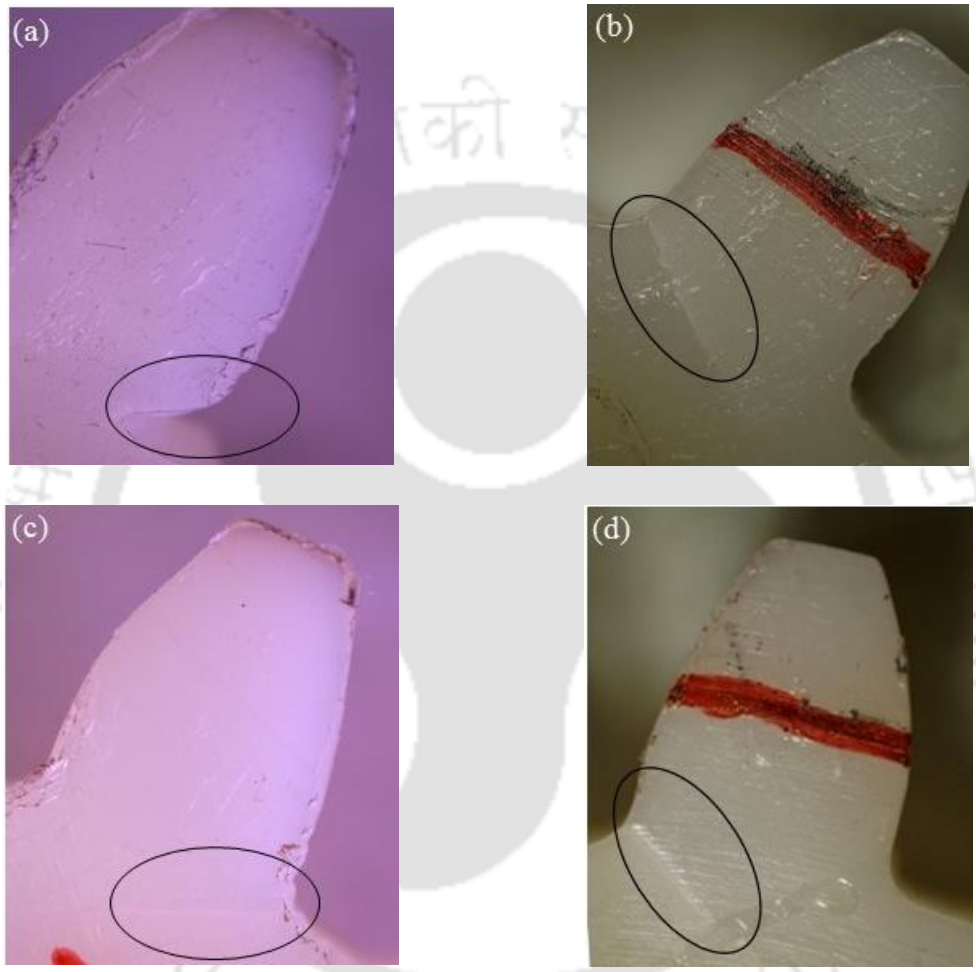

Figure 4.6 Tooth failure of PA gears (a) thermo mechanical failure: bi-directional 8.5 Nm, 1.7 × 10^4 cycles and root crack failures: (b) uni-directional 8.5 Nm load, 9.9 × 10^4 cycles, (c) bi-directional 7.5 Nm load, 3.0 × 10^4 cycles and (d) uni-directional 7.5 Nm, 36 × 10^4 cycles

Pogacnik and Tavcar (2015) reported the similar thermal induced gear tooth deformation in the PA gear subjected unidirectional bending and contact fatigue at 0.42

Nm at 1176 rpm. Senthilvelan and Gnanamoorthy (2004b) also observed both root crack and tooth deformation due to thermal effect in the unreinforced polyamide gears subjected to bending stress of 25 MPa alongwith contact stress. When the heat generated due to the cyclic bending load is not sufficient to soften the considered gear material, then the gear tooth exhibited fatigue failure confirmed by the tooth root crack. Figures 4.6(b)–4.7(d) show the root crack observed in the PA gears at various test conditions. Figure 4.6(b) shows the root crack observed in the PA gear subjected to 8.5 Nm uni-directional load. The heat generated due to the repeated uni-directional load at 8.5 Nm was not sufficient to soften the gear material hence deformation was not observed. However, when the gear was subjected to 8.5 Nm but bi-directional load exhibited thermo mechanical failure (Figure 4.6(a)). Figures 4.6(c) and 4.6(d) show the root cracks observed in the PA gears subjected to 7.5 Nm bi-directional and uni-directional loads respectively. Thus PA gear subjected to 7 Nm load and above, exhibited only mechanical fatigue failure for both uni-directional and bi-directional loads. From the observations, it is confirmed that failure modes of unreinforced polyamide gears depend on the temperature rise due to material hysteretic heating. Further, these gear tooth root crack failures were observed under scanning electron microscope and shown in Figures 4.7(a) and 4.7(b).

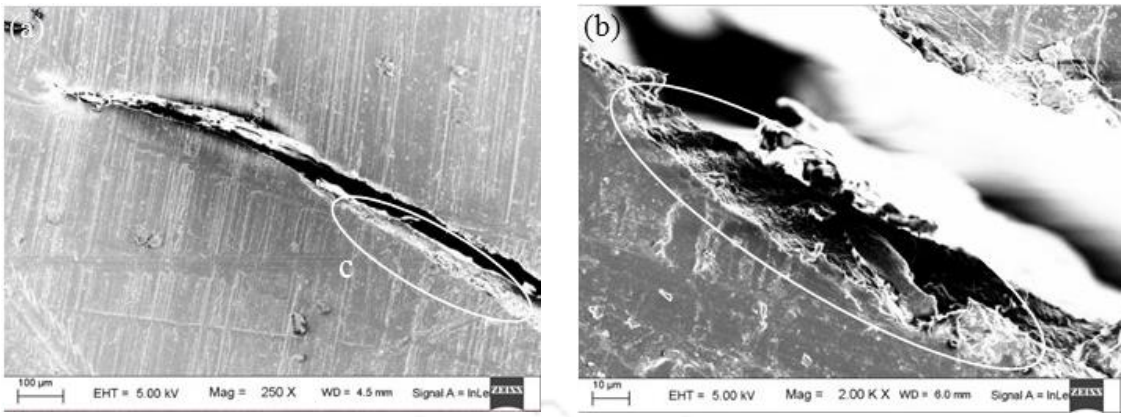

Figure 4.7 Root crack of PA gear (a) showing straight crack: bi-directional 7.5 Nm load and (b) close-up view of region marked as c in Figure 4.7(a) showing molten material

This failure morphology confirmed straight crack with some traces of molten surface on the fracture. Figure 4.8 represents the schematic of crack direction in the PA gears. During cyclic loading, crack is initiated at the root radius where maximum tensile stresses are developed. Crack propagates from the crack tip in the plane perpendicular to the direction of maximum tangential tensile stress and is almost perpendicular to the root fillet radius. Lower stiffness of PA, encourage the initiated crack of tooth to grow inward towards the gear center. Mohan and Senthilvelan (2014) reported similar root cracks on the unreinforced PP gears subjected to 2, 2.5 and 3 mm displacements at 1 Hz frequency, where gears were subjected to bending fatigue.

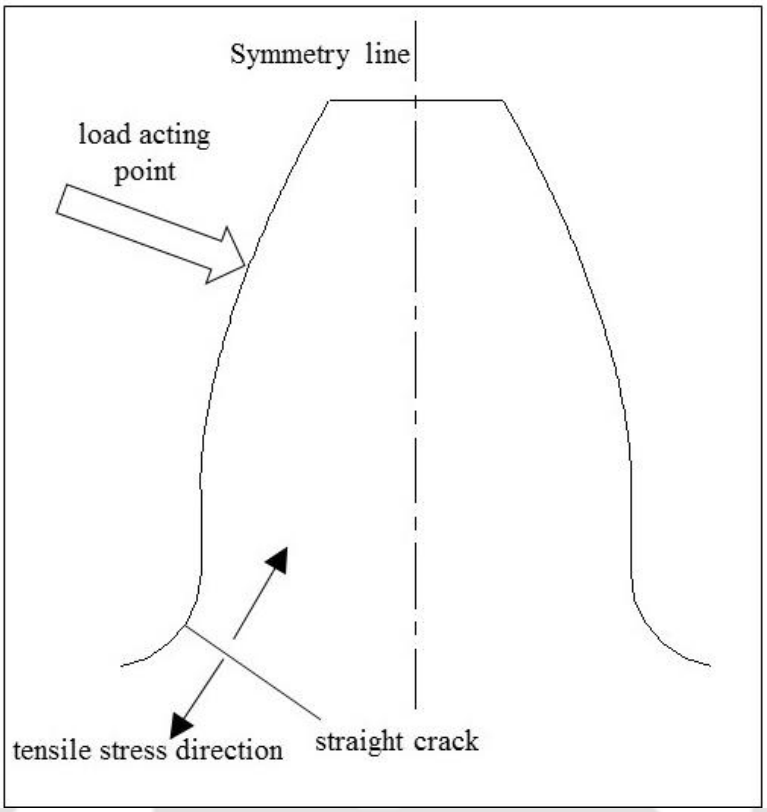

Figure 4.8 Schematic sketch showing crack direction in PA gear

PACF gears subjected to 8.5 Nm uni-directional load has not exhibited any failure upto 5×10^6 cycles. At higher loads (10–12 Nm) PACF gears exhibited root crack when subjected to both bi-directional and uni-directional loads as shown in Figures 4.9(a)–4.9(d). Similar to PA gear, crack initiate at the root of PACF gear tooth, however direction of growth is deflected by the presence of reinforced fibers near the gear tooth region. The orientation of reinforcing fibers near the root region of gear tooth are shown in Figure 4.10(a) and 4.10(b). Reinforced fibers are generally orient along the melt flow and boundary of the cavity. Due to the presence of reinforced fibers in the direction of crack growth, tortuous nature of path was observed on PACF gear tooth (Figures 4.9(a)–4.9(d)) when subjected to both uni-directional and bi-directional loads. Figures 4.9(a) and 4.9(b) show the failure of PACF gear tooth subjected to 10 Nm bi-directional and uni-directional loads respectively. Figures 4.9(c) and 4.9(d)

shows the failure of PACF gear tooth subjected to 12 Nm bi-directional and uni-directional loads respectively.

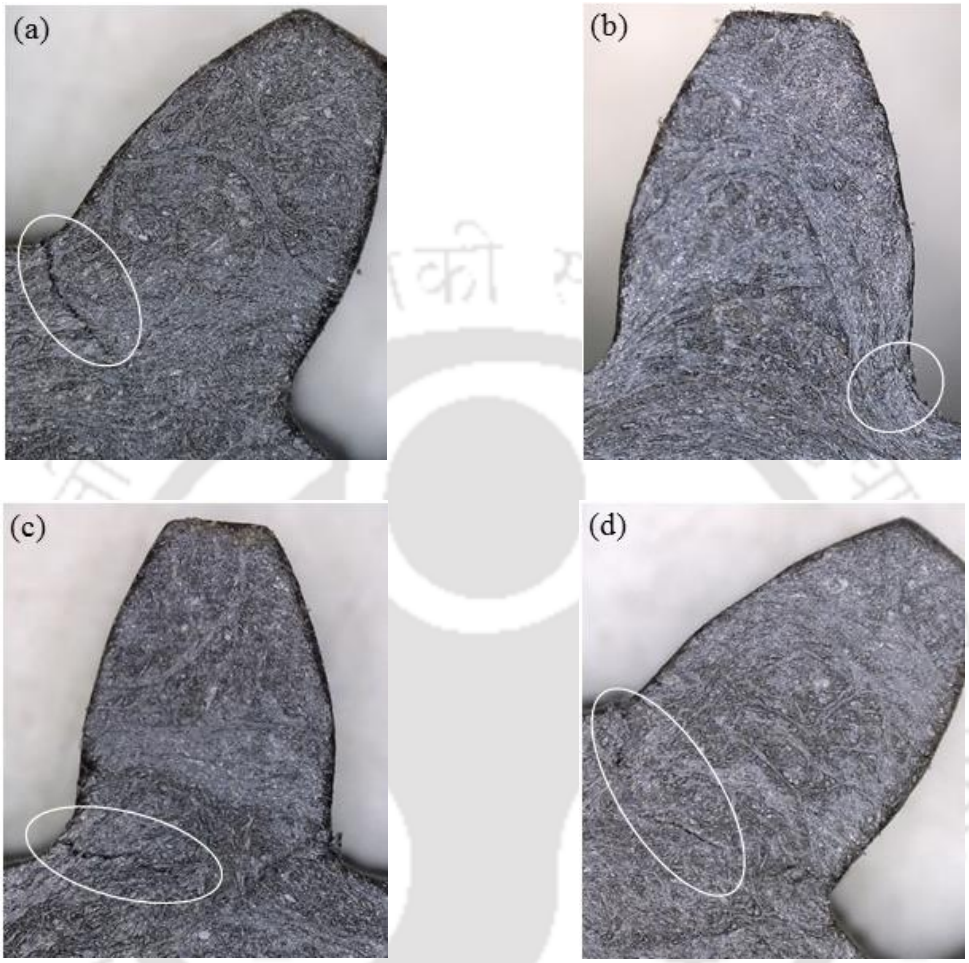

Figure 4.9 Root crack of PACF gear tooth: (a) bi-directional 10 Nm load, 1.8 × 10^4 cycles, (b) uni-directional 10 Nm load, 147 × 10^4 cycles, (c) bi-directional 12 Nm load, 1.1 × 10^4 cycles and (d) uni-directional 12 Nm load, 66.2 × 10^4 cycles

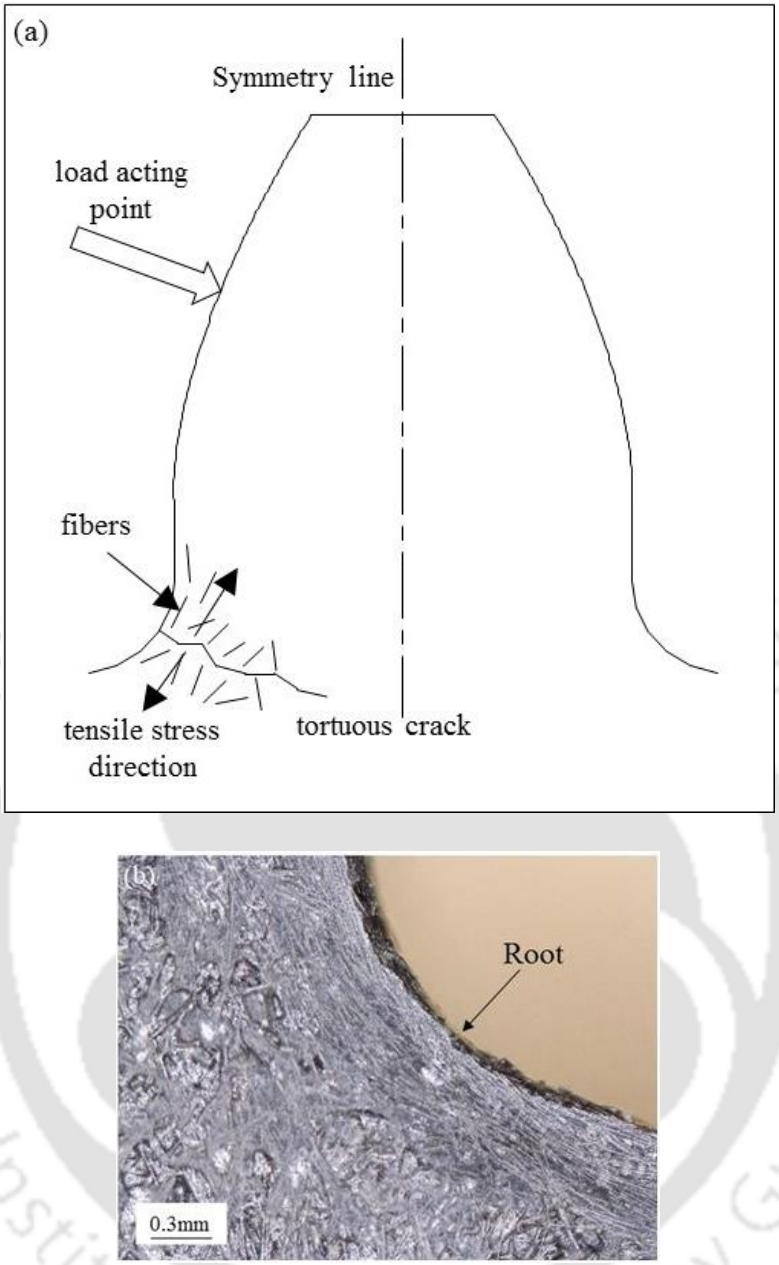

Figure 4.10 Orientation of reinforcing fibers and tortuous crack path in PACF gear (a) schematic gear tooth and (b) micrograph

These root cracks were observed under scanning electron microscope. Figures 4.11(a) and 4.11(b) show the failure of PACF gear tooth 12 Nm uni-directional load showing tortuous crack path, fiber pull-out and matrix separation. Similarly, Figures 4.12(a) and 4.12(b) show the root cracks observed in the PACF gear tooth 12 Nm bi-directional load under scanning electron microscope shown the tortuous crack path, fiber pull-out

and matrix separation. Thus, both bi-directional and uni-directional loads generated similar failure in the PACF gear.

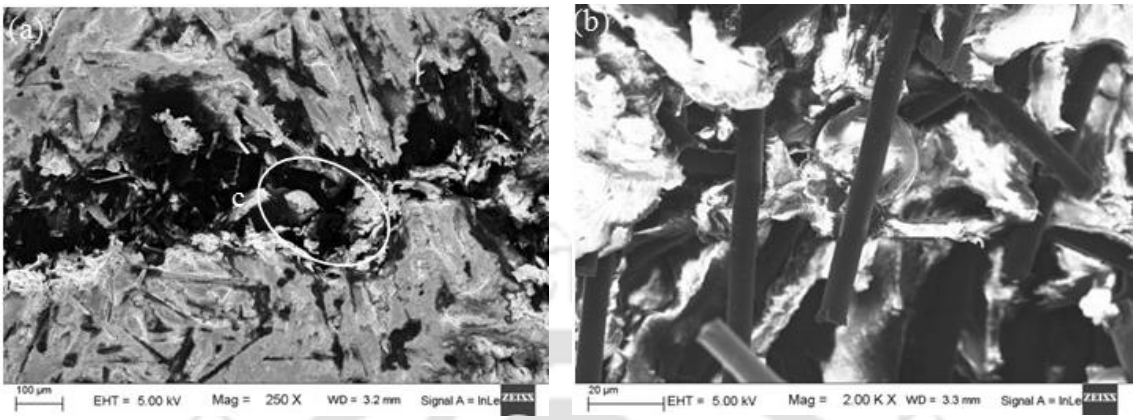

Figure 4.11 Root crack of PACF gear tooth (a) showing tortuous crack path: uni-directional 12 Nm load and (b) Close-up view of region marked as c in Figure 4.11(a) showing fiber pull-out and matrix separation

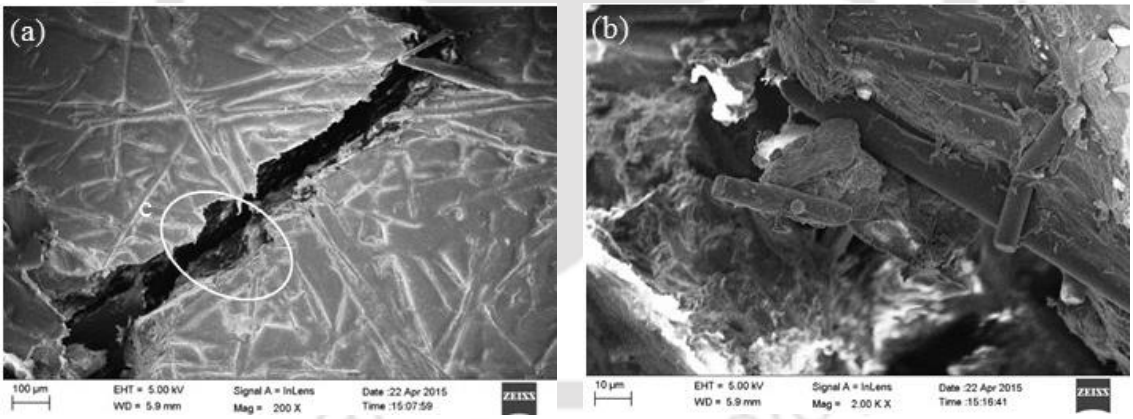

Figure 4.12 Root crack of PACF gear tooth (a) showing tortuous crack path: bi-directional 12 Nm load and (b) Close-up view of region marked as c in Figure 4.12(a) showing fiber pull-out and matrix separation

Similar tortuous crack behaviour in the reinforced gear was also observed in the earlier investigations where carbon fiber reinforced nylon 66 gears were subjected to 20 MPa uni-directional bending stress alongwith contact stress (Senthilvelan and

Gnanamoorthy, (2004)). Glass fiber reinforced PP gears subjected to bending load also exhibited similar tortuous crack behaviour (Mohan and Senthilvelan, (2014)).

4.7 SUMMARY

Bi-directional (R = −1) and uni-directional (R = 0) bending fatigue performance of injection molded unreinforced polyamide 66 (PA) and carbon fiber reinforced polyamide 66 (PACF) gears were evaluated using a servo motor driven test rig developed in-house. The following are the major conclusions arrived

- Test gears exhibited decreased fatigue life in bi-directional loads (R = −1) when compared to uni-directional loads (R = 0).
- PA gears exhibited thermo mechanical failure under bi-directional higher torque loading due to hysteretic heating. PA gears showed mechanical fatigue failures at lower torque levels which was mainly due to the heat generated under these bending loads was not sufficient to soften the gear material. However, PACF gears exhibited mechanical fatigue failures only.
- PACF gears exhibited higher bending load carrying capability and fatigue life than PA gears due to superior mechanical and thermal properties.
- In PA gears, due to their lower stiffness, crack direction was almost perpendicular to the root fillet radius. Orientation of reinforcing fibers and their failures were responsible for the tortuous crack path in the case of PACF gear tooth failure.
- Failure morphology studied using scanning electron microscope confirmed the straight root cracks and tortuous cracks for PA and PACF gears respectively.

CHAPTER 5

EFFECTS OF FREQUENCY ON HYSTERETIC HEATING AND FATIGUE LIFE OF UNREINFORCED INJECTION MOLDED POLYAMIDE 66 SPUR GEARS

5.1 INTRODUCTION

Gears are subjected to different rotational speeds/frequencies during their service life. The effect of the rotational speed on the performance of a metal gear is insignificant; however, it affects the thickness of the lubricant film. Polymer gears generate hysteretic self-heating because of the viscoelastic behaviour of the material, thereby limiting their performance and usage in applications. Investigations for the effects of frequency and stress magnitude on hysteretic self heating and fatigue life were carried out on the polymer specimens for both bi-directional (stress ratio, R = –1) and uni-directional (R ≥ 0) loads ((Goel *et al.* (2009), Mortazavian *et al.* (2015), Peyrac *et al.* (2015), Boccardi *et al.* (2015), Mortazavian and Fatemi (2016)).

The effects of frequency on hysteretic heating and fatigue life of unreinforced injection molded polyamide 66 spur gears are discussed in this chapter. Tests were carried out for bi-directional (R = –1) and uni-directional (R = 0) loads at different frequencies using a servo motor driven gear test rig developed in-house. Hysteretic heating and surface temperature rise of the gears were correlated to hysteresis loops. Failure modes and morphology of failed gears are also discussed in this chapter.

5.2 METHODOLOGY

The unreinforced polyamide 66 (PA) was injection molded into spur gears using injection molding machine. The gear processing, molding conditions, test gear details, parameters and inspection are explained in Section 3.2 and 3.3. (CHAPTER 3). The bending fatigue performance tests were carried out using in-house developed servo motor operated gear test rig. The details of test rig are explained in Section 3.5 (CHAPTER 3). The tests were conducted at various torques (5, 6, 7, 7.5, 8, 8.5, 10.5 and 12.5 Nm) at different frequencies (2, 5, and 7.5 Hz for bi-directional loads, stress ratio R = −1; 4, 10, and 15 Hz for uni-directional loads, R = 0) using an in-house developed servo motor operated gear test rig. Figures 5.1(a) and 5.1(b) show the variations in torque and angular displacement with respect to time, respectively which were acquired at a rate of 300 Hz. The angular displacement variation shown with blue colour markers (Figure 5.1(b)) correspond to an angular rotation of gear mesh measured at driver shaft for the torque variation shown with blue colour markers (Figure 5.1(a)). The test was run for 3600 s so that the generated temperature saturates, which is required to assess the hysteretic heating. An infrared thermal camera (InfraTec, VarioCAM hr head 600) was used to monitor and acquire the surface temperature of the gear. To evaluate the fatigue life, each test was performed until the gear tooth fractured or when the number of cycles reached 5×10^6, whichever was earlier. For every load condition, the tests were repeated for the three gears.

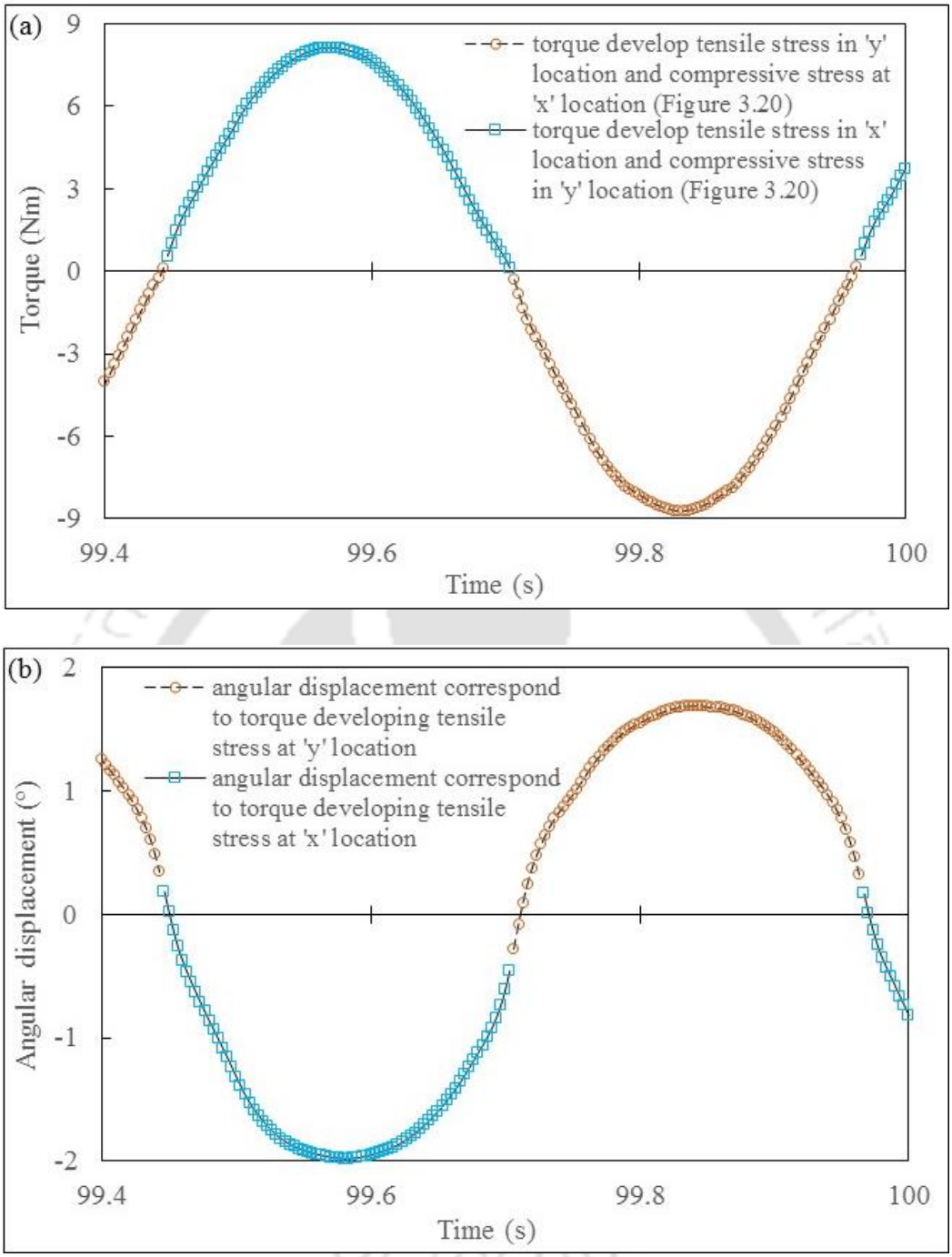

Figure 5.1 Measured parameters for bi-directional load at 2 Hz (a) torque and (b) angular displacement

5.3 MECHANICAL PROPERTIES OF TEST GEAR MATERIALS

The mechanical properties of unreinforced polyamide 66 were evaluated at 296±5 K as per ASTM D638 standard. The evaluated properties are given in Table 3.2 (reported in Section 3.4, CHAPTER 3).

5.4 GEAR TOOTH BENDING STRESS

Two-dimensional finite element analysis using commercial tool, ABAQUS®, for test condition was carried out on stainless steel-polyamide 66 gear pair to obtain induced stress at gear tooth root. The details of study are explained in Section 3.7 (CHAPTER 3). Young's modulus of 200 GPa, Poisson's ratio of 0.3 and density of 7850 kg/m^3 were used for the stainless steel driver gear. The stress-strain characteristic evaluated, with Young's modulus of 1.147 GPa, Poisson's ratio of 0.41 and density of 1140 kg/m^3 were considered for the polyamide driven gear for the material nonlinear analysis. All degree of freedoms of the nodes of driven polyamide gear at its hub were constrained. The rotational degree of freedom of reference node of driver stainless steel gear was alone kept unconstrained for the application of torque. Coefficient of friction of 0.3 was provided for the contacts between driver and driven gear surface nodes. The simulations were carried out for different loads (5–12.5 Nm). Maximum principal stress is a measure of tooth root bending stress. Figure 5.2 shows the bending stress distribution of polyamide gear for 6 Nm torque. Table 5.1 shows bending stress at gear tooth root for different torques. It was observed that bending stresses of polyamide gear were not linear with load increase because of nonlinear deflection and contact behaviour of polyamide gear material.

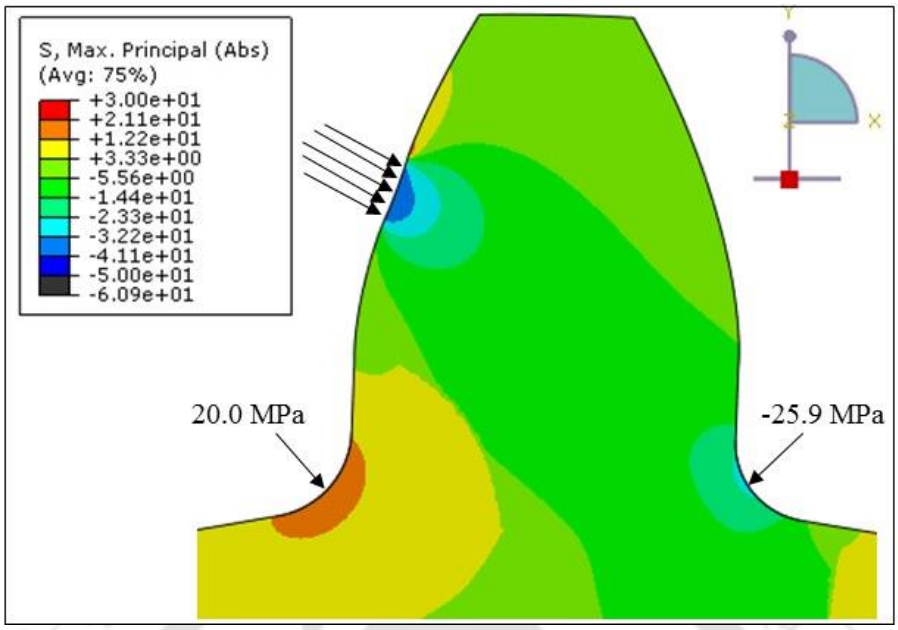

Figure 5.2 Bending stress distribution of polyamide gear for 6 Nm torque

Table 5.1 Bending stress at gear tooth root

Torque (Nm)	5	6	7	7.5	8	8.5	10.5	12.5
Bending stress (MPa)	17.0	20.0	22.7	24.1	25.4	26.6	32.0	37.1

5.5 EFFECT OF FREQUENCY ON HYSTERETIC HEATING

The bi-directional and uni-directional tests were conducted on polyamide gears at different loads and frequencies. The low stiffness viscoelastic nature of the polymer material leads to hysteretic heating under cyclic bending loads, thereby increasing the surface temperature of the gear. A hysteresis loop is a measure of the hysteretic heating and is plotted by combining the torque (Figure 5.1(a)) and angular displacement data (Figure 5.1(b)). Figures 5.3(a) and 5.3(b) show the hysteresis loops of the gears subjected to different bi-directional loads at 2 Hz and uni-directional loads at 4 Hz respectively. The figure shows that the angular displacement corresponding to a torque of 12.5 Nm varies from −3.03º to +3.24º for bi-directional loading compared to −3.24º

to −1.24º for uni-directional loading. No significant increase in the angular displacement due to gear tooth flank clearance (0.55º backlash) under bi-directional loads compared to that under uni-directional loads, was observed. Moreover, the angular displacement reduces with the decrease in the torque as expected. The hysteresis loop area is computed for both the bi-directional and uni-directional loads at different torques with the aid of commercial technical computing tool, MATLAB® (Figure 5.4). The hysteresis loop area increases with the increase in the torque and is more for the bi-directional loads. Figure 5.5 shows the net surface temperature of the gears subjected to different bi-directional and uni-directional loads. The temperature increases steadily during the initial phase of the testing and reaches steady state after attaining thermal equilibrium. Figure 5.5 shows that the temperature increases from 31.8 ºC at 8.5 Nm to 44.1 ºC at 12.5 Nm at the center of the tooth root for bi-directional loading at a frequency of 2 Hz. Similar to the hysteresis loop area, the surface temperature increases with the increase in the torque. Goel *et al.* (2009) reported an increase in temperature of 1 ºC, i.e. increase from 4 ºC at 10 MPa stress to 5 ºC at 15 MPa stress for PP specimens under tension–tension load control mode (R = 0.2). The temperature corresponding to uni-directional loads at 8.5 Nm and 12.5 Nm are 28.5 ºC and 34.2 ºC, respectively. The temperature corresponding to the uni-directional and bi-directional loads increases by 5.7 ºC and 12.3 ºC, respectively. This shows that the induced temperature is more in the case of the bi-directional loads compared to the unidirectional loads. Mortazavian *et al.* (2015) observed an increase in the temperature with the increase in the stress amplitude for PP specimens tested under load controlled mode at stress ratios R = −1 and R = 0.1; temperature rise of 10 ºC at R = −1; 3 ºC at R = 0.1 tested at 1 Hz frequency. Figures 5.6(a) and 5.6(b) show the thermographs of the gears subjected to 12.5 Nm bi-directional and uni-directional loads respectively at

the end of 3500 s. The higher tooth deflection from $-\theta^{o}$ to $+\theta^{o}$ leads to a higher localised mobility (stretching and compression) of the polymer chain in the gear material under the bi-directional load. Thus, the increase in temperature under the bi-directional load is more compared to that under the uni-directional load.

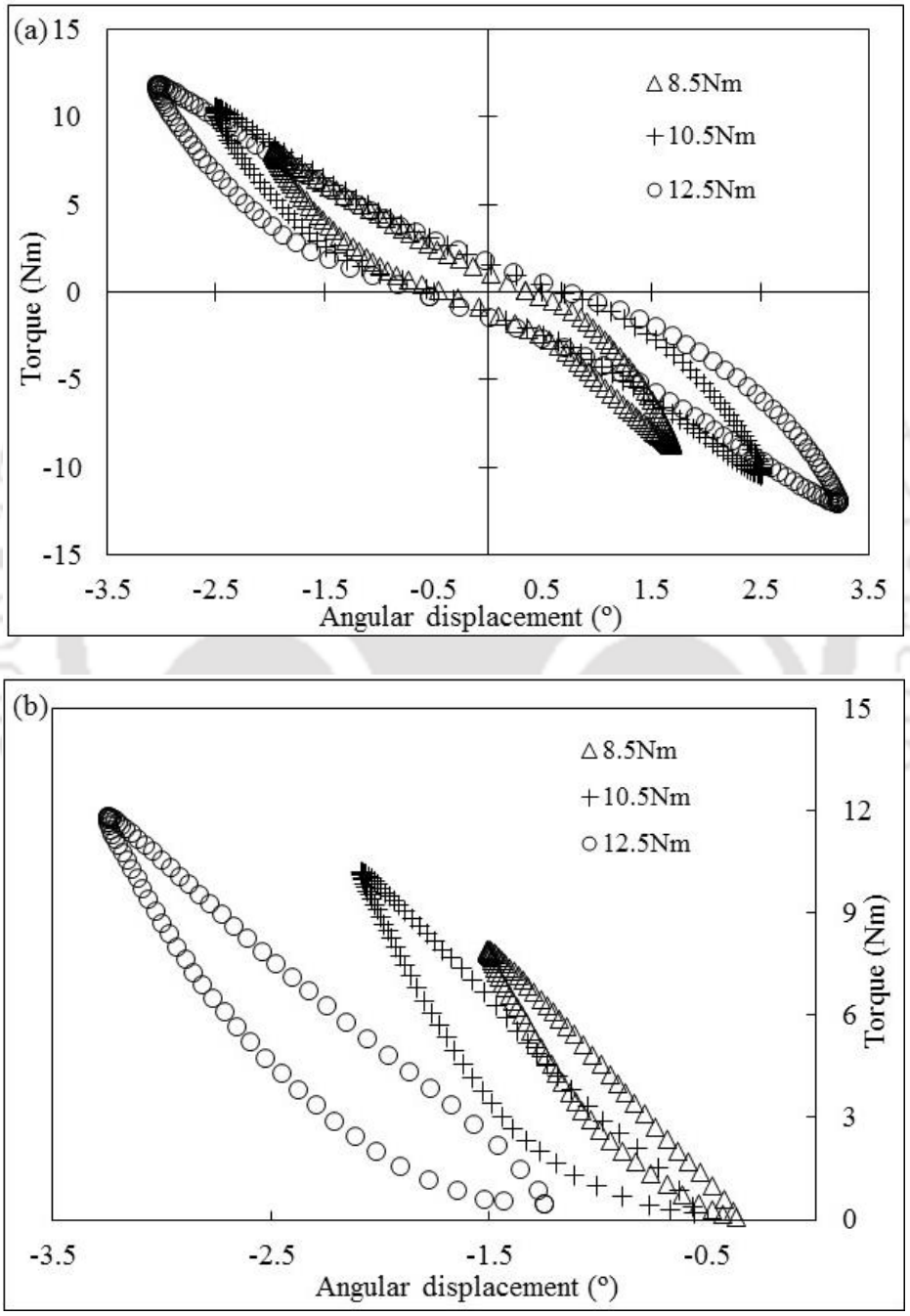

Figure 5.3 Hysteresis loops of gears subjected to different

(a) bi-directional loads at 2 Hz and (b) uni-directional loads at 4 Hz

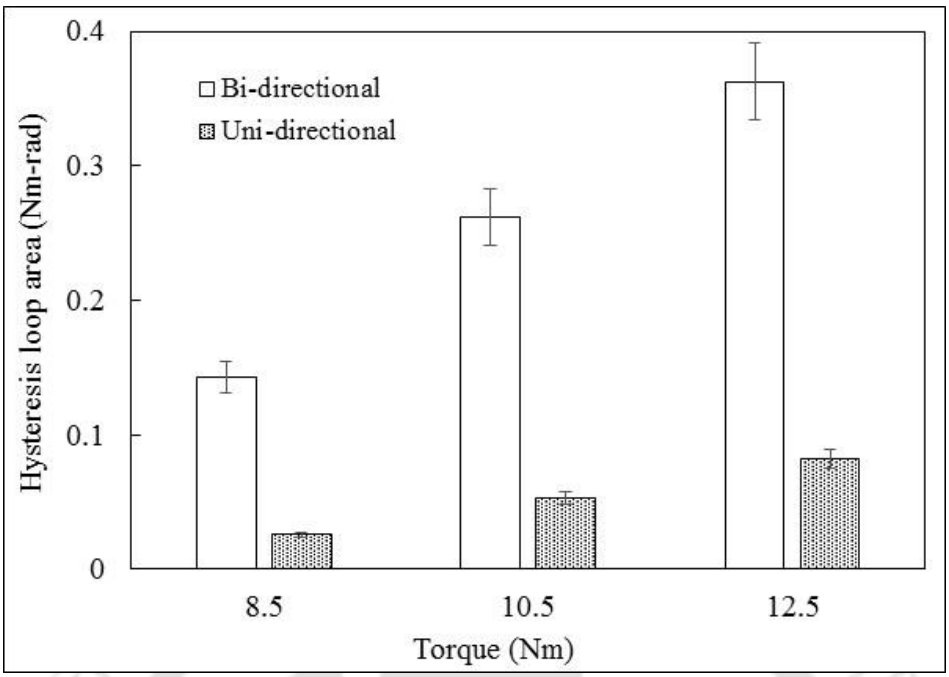

Figure 5.4 Hysteresis loop area of gears subjected to different bi-directional loads at 2 Hz and uni-directional loads at 4 Hz

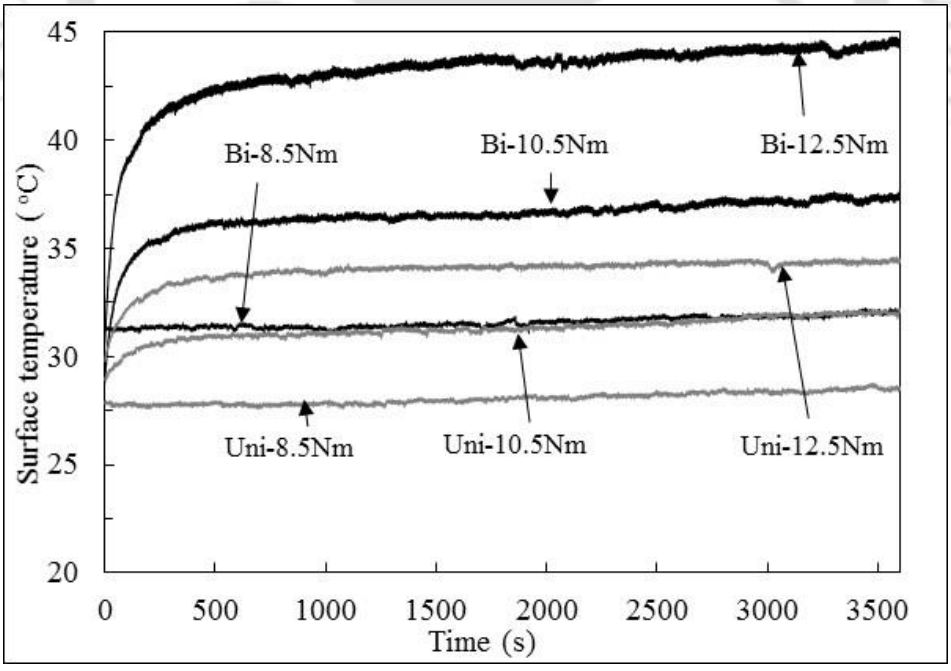

Figure 5.5 Temperature rise of gears subjected to different bi-directional loads at 2 Hz and uni-directional loads at 4 Hz

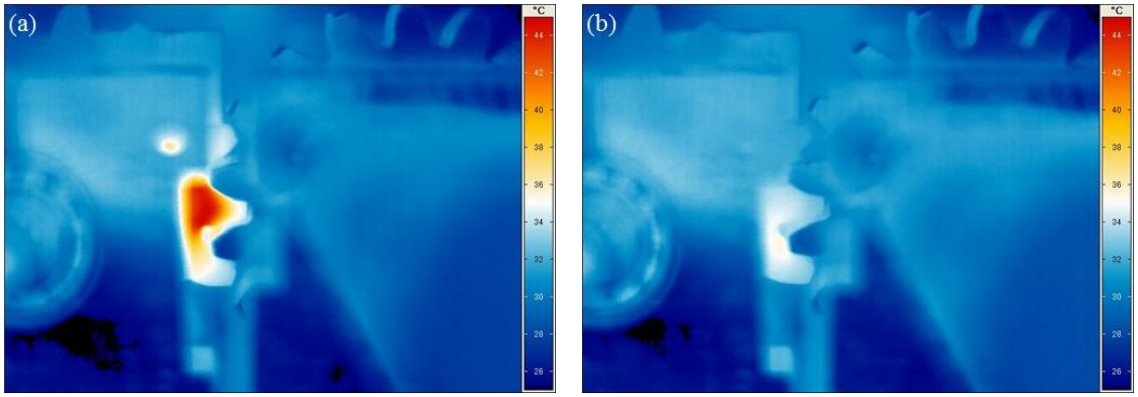

Figure 5.6 Thermographs of gears subjected to 12.5 Nm (a) bi-directional load at 2 Hz and (b) uni-directional load at 4 Hz

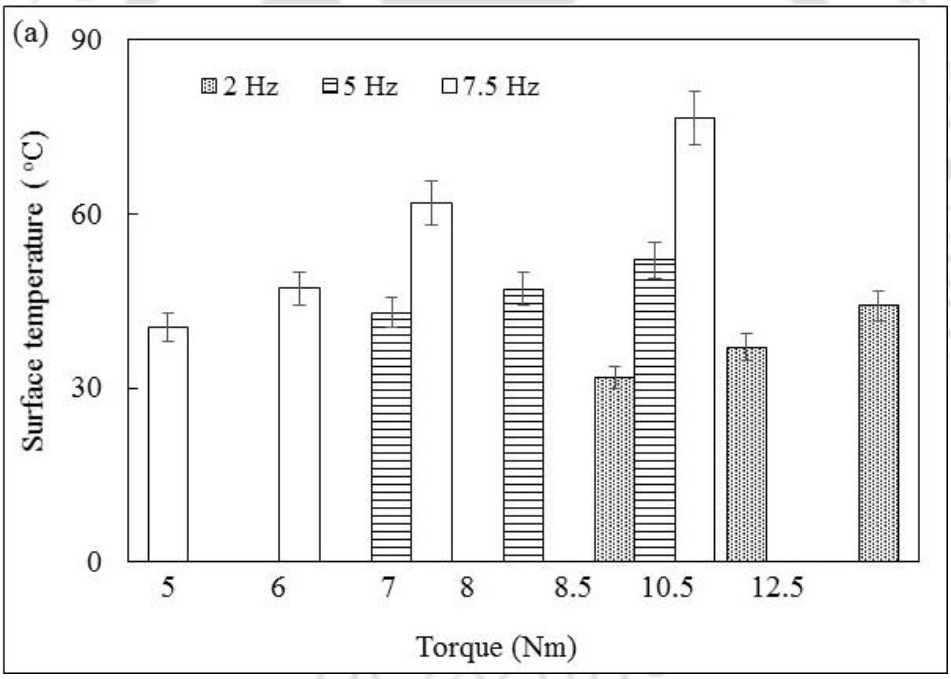

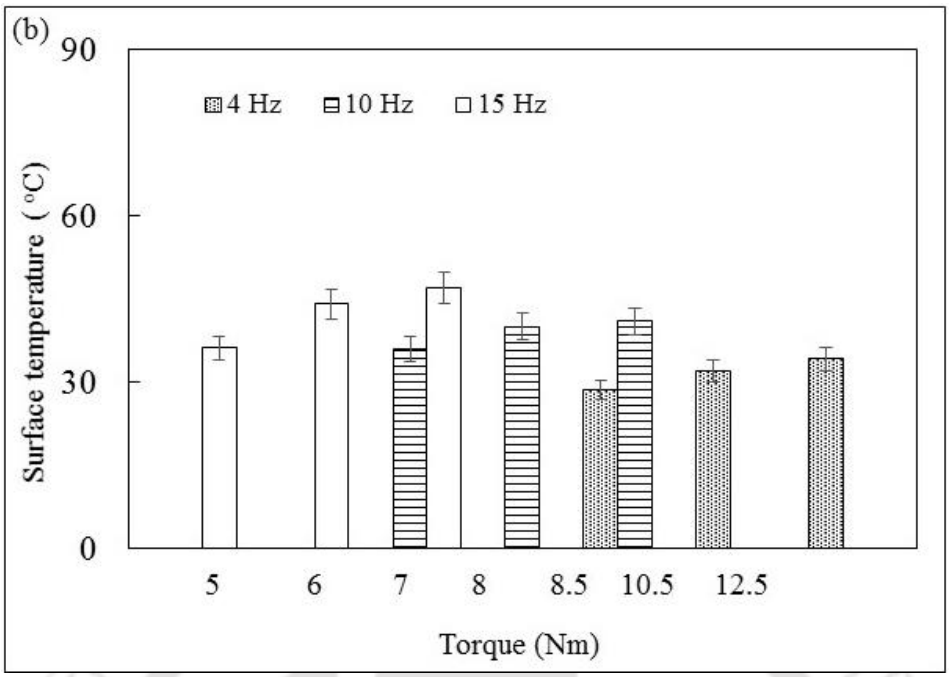

Figure 5.7 Surface temperature of gears subjected to

(a) bi-directional loads and (b) uni-directional loads at different frequencies

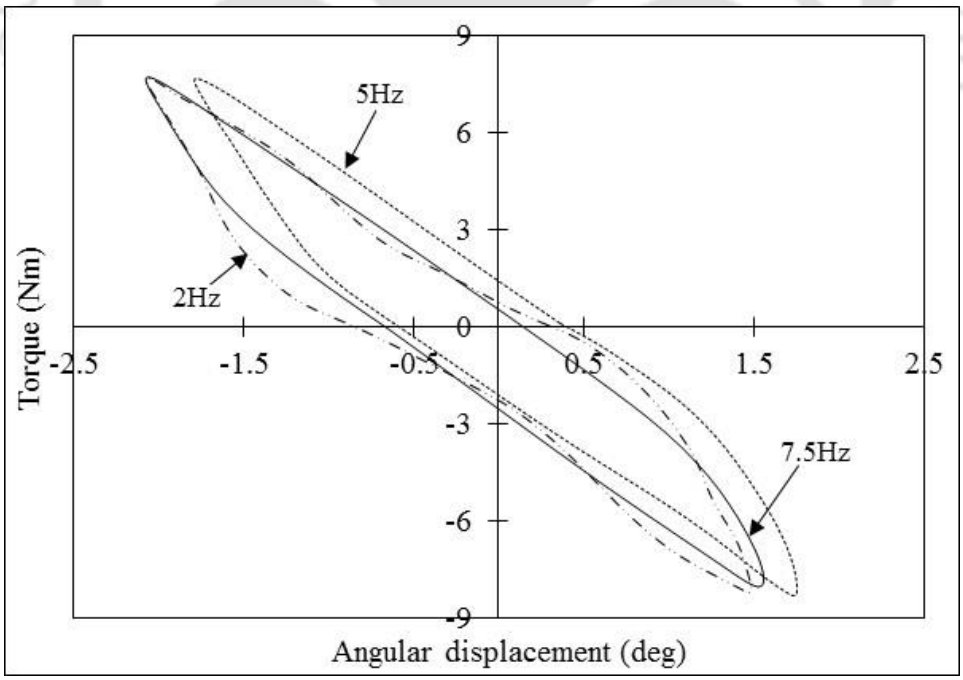

Figure 5.8 Hysteresis loops of gears for 8.5 Nm bi-directional loads at different frequencies

Figures 5.7(a) and 5.7(b) show the surface temperature of the gears subjected to different bi-directional and uni-directional loads at different frequencies, respectively. The figures show that the surface temperature of the gears increases with the increase in the frequency and is more for the bi-directional loads compared to the uni-directional loads. A similar observation was reported by Mortazavian *et al.* (2015); this increase in temperature was more when the PP specimens were tested at R = −1 compared to that at R = 0. Figure 5.8 shows the hysteresis loops for 8.5 Nm bi-directional loads at 2, 5, and 7.5 Hz frequencies. Although the hysteresis loop area increased marginally by 0.019 Nm-rad from 2 to 7.5 Hz (i.e. 0.143, 0.138, and 0.124 Nm-rad for 2, 5, and 7.5 Hz respectively), the temperature increases significantly by 44.7 ºC from 2 to 7.5 Hz (i.e. 31.8, 52.0, and 76.5 ºC for 2, 5, and 7.5 Hz, respectively). This is because of the increased mobility and sliding of the polymer chains at higher frequencies. Figure 5.9 shows the thermographs of the gears subjected to 7.5 Nm bi-directional loads at different frequencies.

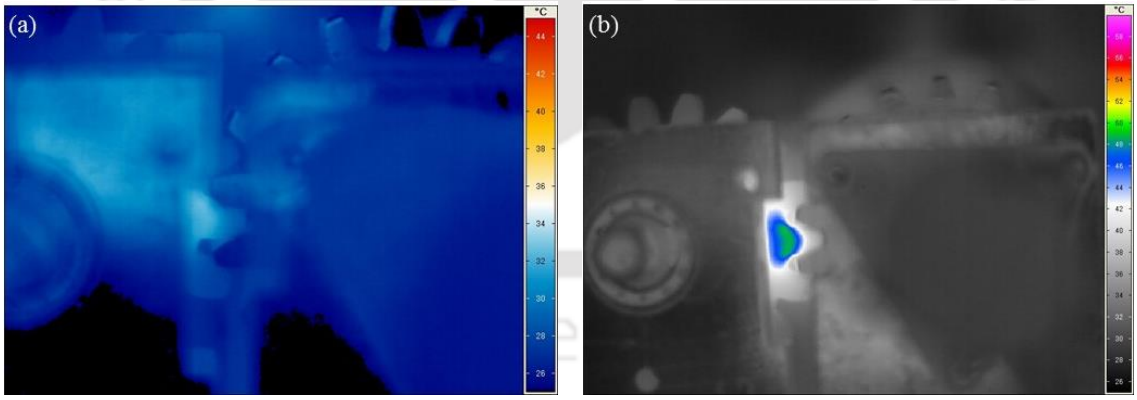

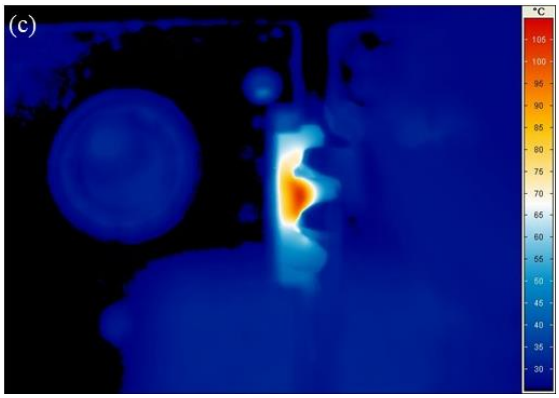

Figure 5.9 Thermographs of gears subjected to (a) 8.5 Nm bi-directional load at 2 Hz, (b) 8.5 Nm bi-directional load at 5 Hz and (c) 8.5 Nm bi-directional load at 7.5 Hz

5.6 EFFECTS OF FREQUENCY ON FATIGUE LIFE AND FAILURE MODES

The fatigue life of the gears subjected to bi-directional loads at 5 Hz and uni-directional loads at 10 Hz were reported in CHAPTER 4. To understand the effect of the frequency or rate of loading on the fatigue life of gears, the fatigue tests were extended for higher frequencies such as 7.5 and 15 Hz for bi-directional and uni-directional loads, respectively. The fatigue life obtained in the present tests is compared with that obtained in the previous tests. Figure 5.10 shows the comparison results.

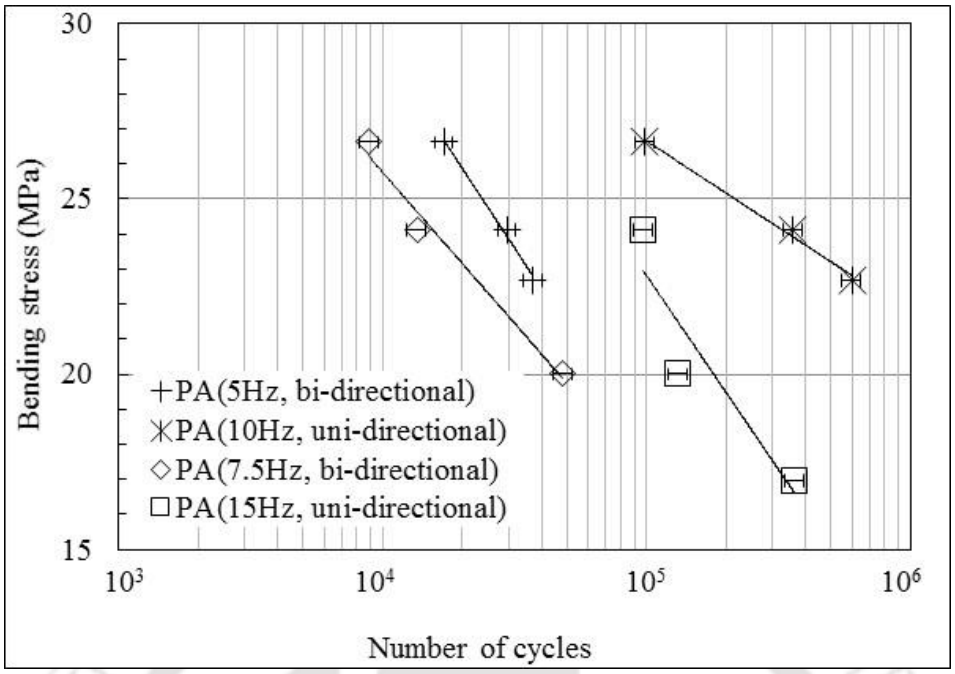

Figure 5.10 Fatigue life of gears at different frequencies

The fatigue life of the gears at 15 Hz uni-directional loads decreases with the increase in the torque/stress magnitude. The gears tested at 15 Hz uni-directional loads exhibited inferior fatigue life compared to those tested at 10 Hz uni-directional loads. The increase in the gear temperature at higher frequencies leads to the decrease in the fatigue life (36 ºC at 10 Hz and 47 ºC at 15 Hz for a torque of 7 Nm). Mortazavian *et al.* (2015) reported similar decrease in the fatigue life at a frequency of 4 Hz compared to that at 0.25 Hz for PA6 specimens tested at R = 0.1, load controlled mode.

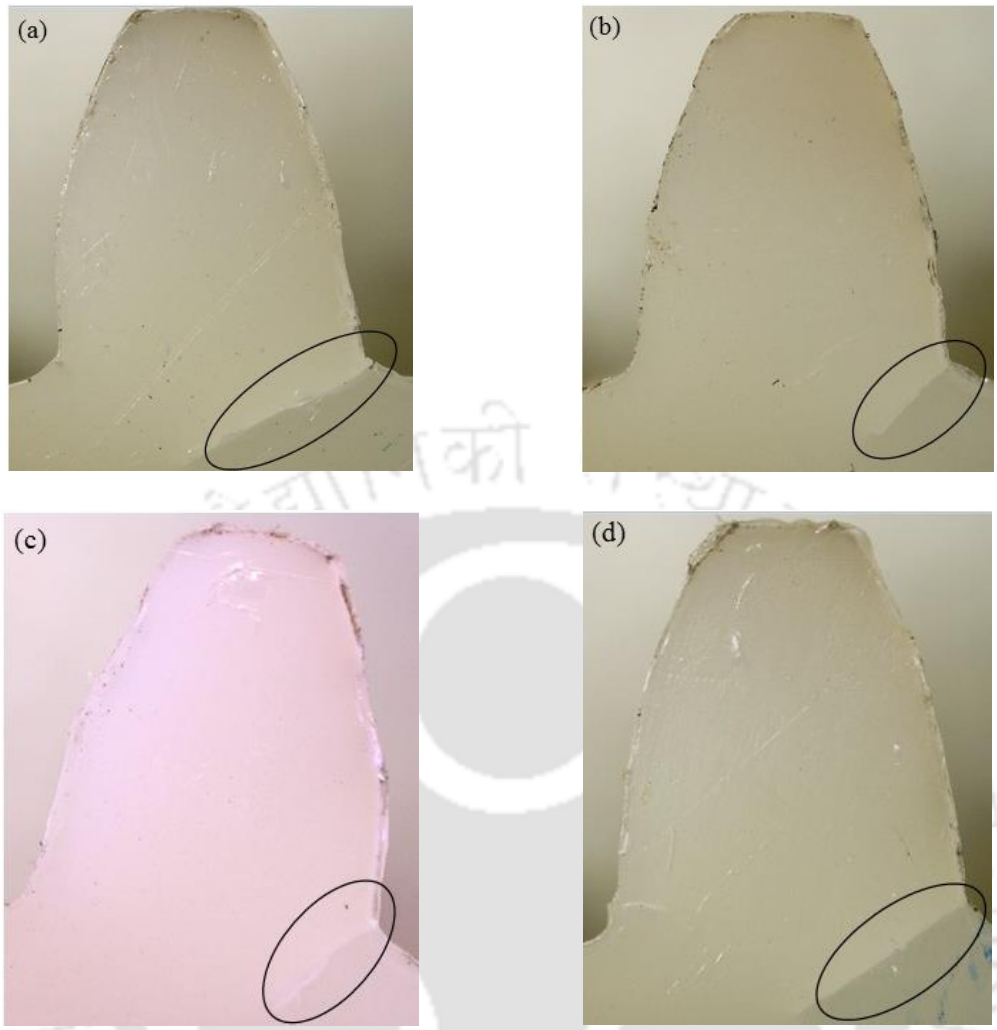

Figure 5.11 Failure morphology of test gears (a) thermo mechanical failure of gear: bi-directional 7.5 Nm, 13.5 × 10^3 cycles and root crack failure of gears: (b) uni-directional 7.5 Nm, 97.5 × 10^3 cycles, (c) bi-directional 6 Nm load, 48.2 × 10^3 cycles and (d) uni-directional 6 Nm, 131.2 × 10^3 cycles

In the bi-directional loads, the fatigue life of the gears decreases with the increase in the torque. The gears tested at a frequency of 7.5 Hz have also shown inferior fatigue life than the gears tested at 5 Hz because the degree of hysteretic self-heating was high (43 ºC at 5 Hz and 61.8 ºC at 7.5 Hz for a torque of 7 Nm). For the same torque of 7 Nm, the temperature increases by 43.7 % (18.8 ºC) when the frequency increases from 5 to 7.5 Hz under bi-directional load; however, the temperature increases by only

30.6 % (11 ºC) under the uni-directional load for the same frequency range. This is because the angular displacement is high under the bi-directional load, inducing localised polymer chain mobility, which in turn causes higher heat generation. Because of the low thermal conductivity of the polymer, the heat generated is not entirely dissipated to the surrounding. Therefore, the temperature increases, thereby changing the viscoelastic state, which subsequently softens the material. Mortazavian *et al.* (2015) also reported inferior fatigue life for PA6 specimens tested at 4 Hz as compared to those tested at a frequency of 2 Hz, because the increase in the temperature was considerable (87 ºC at 4 Hz and 7 ºC at 2 Hz) at R = −1.

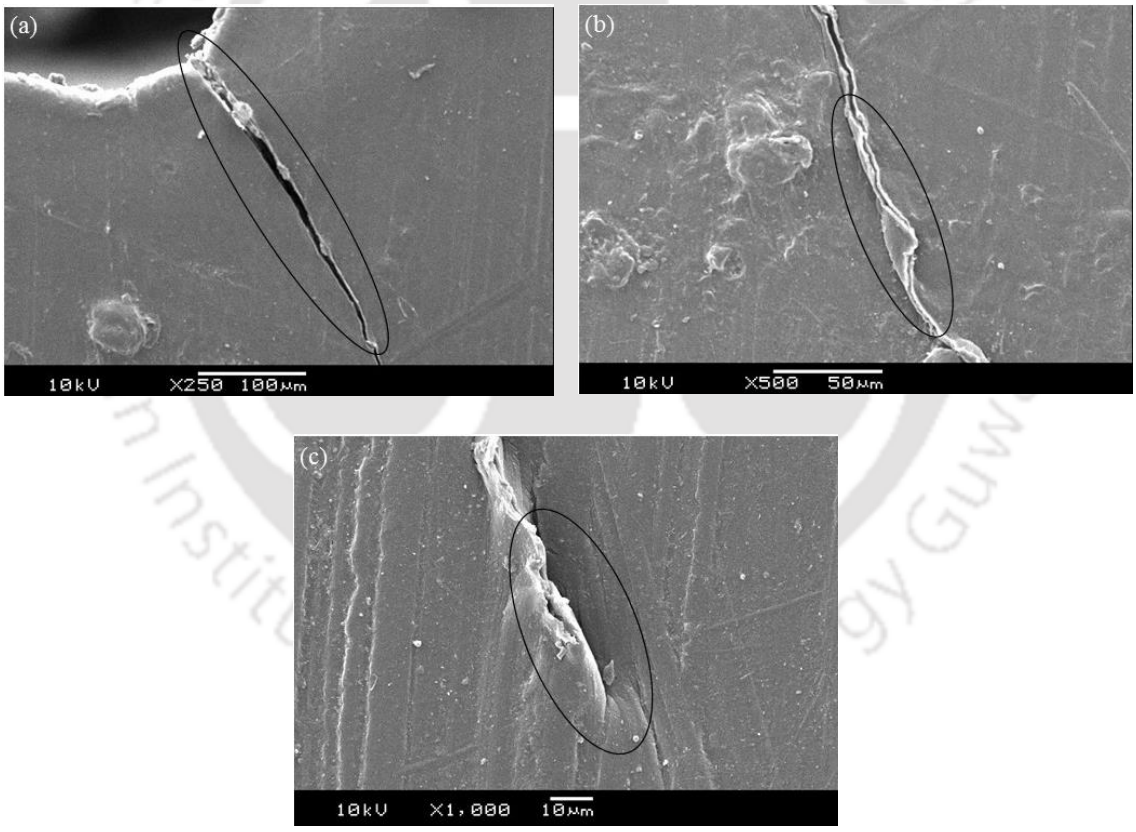

Figure 5.12 Failure morphology at bi-directional 7.5 Nm load (a) root crack of gear showing straight crack, (b) overlapping of fractured surfaces and (c) thermo mechanical failure of gear

The thermo mechanical failures confirmed by tooth deformation and cracks were observed for the gears tested at 7.5 and 8.5 Nm bi-directional loads (Figure 5.11(a)). This behaviour was because of the higher material hysteretic heating under the bi-directional load in addition to the poor thermal conductivity of the polymer material, which increased the temperature as high as the glass transition temperature (50 ºC) of the gear material. The gears tested at 6 Nm bi-directional load and 5, 6, and 7.5 Nm uni-directional loads exhibited only the mechanical root crack failures, as the increase in temperature was insufficient to soften the gear material (Figures 5.11(b)–5.11(d)).

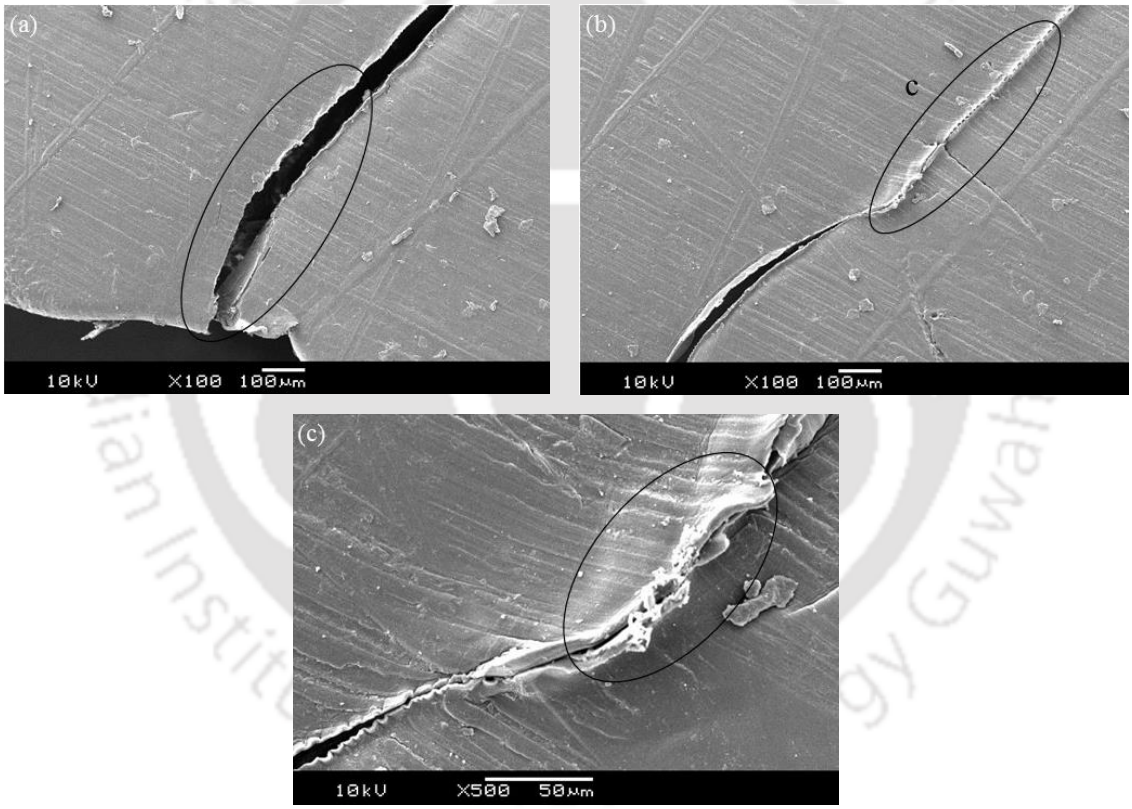

Figure 5.13 Root crack of test gear showing (a) straight crack: uni-directional 7.5 Nm load, (b) overlapping of fractured surfaces: uni-directional 7.5 Nm load and (c) close-up view of region marked as c in the Figure 5.13(b)

The failure morphology of the gears subjected to the bi-directional and uni-directional loads was analysed using a scanning electron microscope. Figures 5.12(a)–5.12(c) and

Figures 5.13(a)–5.13(c) show the images of the crack observed on the gears subjected to 7.5 Nm bi-directional load and 7.5 Nm uni-directional load, respectively. The failure morphology shows that for both bi-directional and uni-directional loads, the cracks initiated at the root, and the straight cracks propagated from the crack tip in the plane perpendicular to the direction of maximum tangential tensile stress and was almost perpendicular to the root fillet radius (Figures 5.12(a) and 5.13(a)). The collision of the cracked/fractured surfaces in subsequent cycles was also observed, increasing the temperature at the fractured surfaces, thereby softening the local material and overlapping of the fractured surfaces (Figures 5.12(b), 5.13(b), and 5.13(c)). More number of collisions at higher test frequencies (7.5 Hz for bi-directional load and 15 Hz for uni-directional load) was responsible for these overlapping characteristics, which were not observed in the gears tested at 5 Hz bi-directional and 10 Hz uni-directional loads (reported in CHAPTER 4). Additionally, thermal softening of the material near the crack tip was observed on the gear subjected to 7.5 Nm bi-directional load (Figure 5.12(c)), which is because of the higher hysteresis heating, increasing the temperature to the level of the glass transition temperature of the material.

5.7 SUMMARY

The hysteretic heating characteristics and bending fatigue performance of the injection molded unreinforced polyamide 66 spur gears under bi-directional (R = −1) and uni-directional (R = 0) loads at different frequencies were conducted using a servo motor driven gear test rig developed in-house. The following are the major conclusions of this study:

- The hysteretic heating and surface temperature increases with the increase in the torque and frequency for both the bi-directional and uni-directional loads.

- Hysteresis heating of gears was more while subjected to bi-directional loads, because of the higher angular displacement, and increased mobility and sliding of the polymer chains.
- The fatigue life of the gear decreases with the increase in the torque under both the bi-directional and uni-directional loads.
- Under both the uni-directional and bi-directional loads, the gears tested at higher frequencies exhibited inferior fatigue life compared to those tested at lower frequencies, which was because of the increased hysteresis heating at higher frequencies.
- At higher test frequencies, both the thermo mechanical and root crack failures were observed under the bi-directional loads. The gears exhibited only the root crack failures under the uni-directional loads.
- The failure morphology studied using the scanning electron microscope confirmed the straight root crack with overlapping fractured surfaces under both the bi-directional and uni-directional loads because of the collision of fractured surfaces during subsequent loadings.

CHAPTER 6

TRANSMISSION AND BENDING CHARACTERISTICS OF UNREINFORCED POLYAMIDE 66 SPUR GEARS

6.1 INTRODUCTION

Transmission and bending characteristics of the gears are the functional requirement, when the gears are used for the precision motion applications. Researchers (Yelle and Burns (1981), Walton *et al.* (1994), Ming and Ying (1997), Meuleman *et al.* (2007), Letzelter *et al.* (2009), Karimpour *et al.* (2010), Atanasiu *et al.* (2011), Cathelin *et al.* (2013)) have carried out the numerical, analytical as well as experimental studies on the transmission characteristics of the polymer gears such as the path of contact, static transmission error and mesh stiffness. When the polymer materials are utilized for the gears, strain rate dependent nonlinear material characteristic affects the contact and deflection behaviour, in turn the performance of gears. Extensive investigations were carried out on the polymer and polymer composite materials to assess the mechanical behaviour under different strain rate conditions (Mourad *et al.* (2004), Guo and Li (2007), Nitta and Nomura, (2014)).

Analytical works and finite element analyses carried out on the polymeric gears were used linear material model only. This chapter investigate the transmission characteristics of the unreinforced polyamide gears using different strain rate linear and nonlinear material models numerically. The experimental results obtained using in-

house developed static transmission error gear test rig are compared with the numerically predicted values.

6.2 TRANSMISSION CHARACTERISTICS: NUMERICAL EVALUATION WITH LINEAR MATERIAL MODEL AND EXPERIMENTAL INVESTIGATION WITH ROTARY POTENTIOMETER SENSOR

6.2.1 Methodology

The unreinforced polyamide 66 (PA) was injection molded into tensile specimens and spur gears using the injection molding machine. The processing, molding conditions, test gear and specimen details, parameters and inspection are explained in Sections 3.2, 3.3 and 3.4 (CHAPTER 3). Finite element analysis details are reported in Section 3.7 (CHAPTER 3).

The numerical simulations were carried out for different loads (0.5, 1.0, 1.5 and 2.0 Nm). The master and slave contact with a coefficient of friction of 0.1 was provided for the driver and driven gears. Analysis was repeated for each roll angle position by rotating the gear by 1º. In order to cover the roll angle from −20º to +20º, a total 41 simulations were carried out for each torque value. From each simulation, coordinates of the surface node of driven gear tooth experiencing maximum contact normal force and angular rotation of driver gear were extracted. The path/line of contact was plotted using the coordinates of contact surface nodes of driven gear. The angular rotation magnitude of a reference node of driver gear is a measure of static transmission error. The gear mesh stiffness is defined as ratio of torque applied to the static transmission error and was calculated from the results.

Figure 6.1(a) shows the in-house developed gear test rig using rotary potentiometer sensor for the evaluation of static transmission error. The details of test rig are explained in Section 3.6 (CHAPTER 3). The desired torque can be applied by adding dead weights on weighing pan. The product of load and pulley radius provides the rotational moment or torque. The rotary position sensor, potentiometer (MCB, PR27M) was connected at the other end of the driver gear shaft to measure angle turned during test. The close-up view of gear mesh is shown in Figure 6.1(b). Tests were carried out for the four different torque values such as 0.5, 1.0, 1.5 and 2.0 Nm at laboratory maintained with the temperature of 296±5 K and relative humidity of 60±5 %. Tests at each torques were conducted on two different identified teeth of three different gears at single tooth contact positions (3 positions) and at double teeth contact positions (6 positions).

Single tooth contact: The three single tooth contact positions with pitch (0º roll angle) as well as pitch−1º and pitch+1º were considered for the tests.

Double teeth contact: The three double teeth contact positions, each at dedendum and addendum sides were considered for the tests. The three positions in dedendum side were pitch−9º, pitch−10º and pitch−11º. Similarly, three positions in the addendum side were pitch+9º, pitch+10º and pitch+11º.

After loosening shaft locking plate, the driven gear was rotated to take test position with the help of rotary sensor and subsequently locked before the load is applied. After applying the load, maximum holding time of 3 s was allowed for measurement. About 5 min time interval was allowed between the successive tests in order to regain elastic

tooth deformation of the previous loading. Almost same output was observed in the rotary sensor before and after loading, ensured no creep/relaxation of polymer gear.

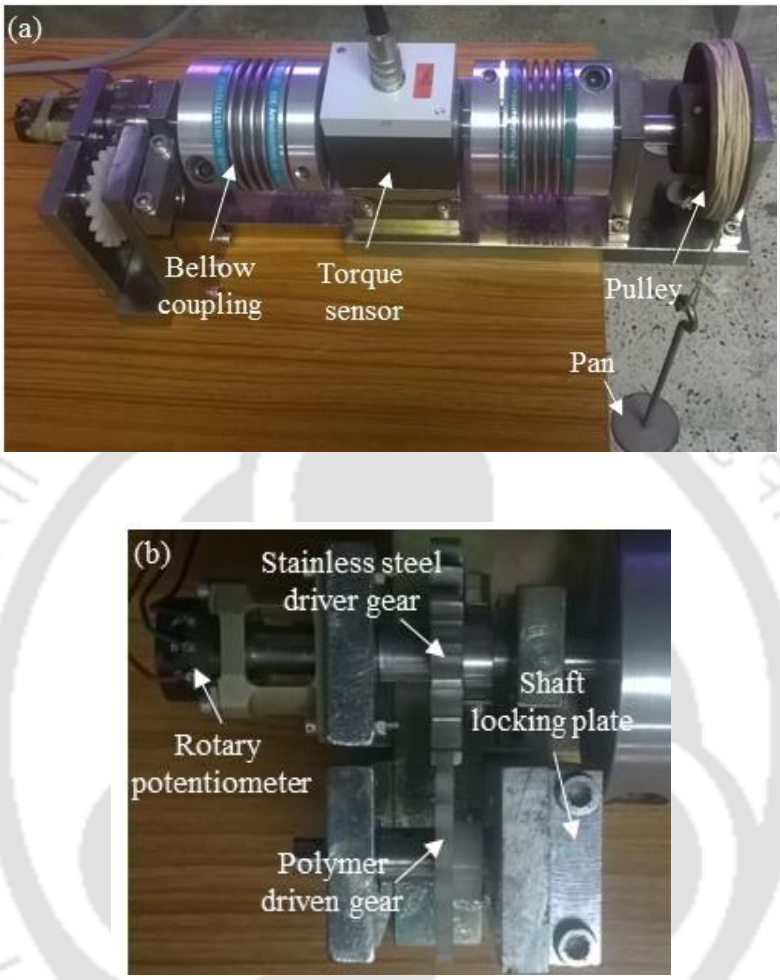

Figure 6.1 Static transmission error (a) experimental set-up and (b) close up view of gear mesh

6.2.2 Mechanical properties of test gear materials

The mechanical properties of unreinforced polyamide 66 material were evaluated at 296±5 K as per ASTM D638 standard under a crosshead speed of 1 mm/min. Table 6.1 shows the properties of gear materials.

Table 6.1 Properties of gear materials

Parameter / material	Stainless steel	Polyamide 66
Young's modulus (GPa)	200	1.147
Density (kg/m^3)	7850	1140
Poisson's ratio	0.3	0.41

6.2.3 Numerical validation with BS ISO 6336

The stainless steel-stainless steel gear pair was considered for validating the numerical model developed. Torque of 2.0 Nm was applied at pitch point. The induced maximum principal stress at the root was 20.31 MPa as against the 20.79 MPa obtained from standard BS ISO 6336 and is given below. Results were closely matching and hence the numerical model was further considered for the evaluation of static transmission error.

Tooth root stress, $$\sigma_{F0} = \frac{F_t}{b\, m_n} Y_F\, Y_S\, Y_\beta\, Y_B\, Y_{DT} \quad = 20.79 \text{ MPa} \qquad (6.1)$$

where

F_t = nominal tangential load $= \dfrac{torque}{pitch\ circle\ radius} = 74.07$ N;

b = facewidth = 4 mm;

m_n = normal module = 3 mm;

Y_F = form factor by which the influence of tooth form on nominal tooth root stress is taken into account = 1.5733;

Y_S = stress correction factor, is used to convert the nominal tooth root stress to local tooth stress = 2.1404;

Y_β = helix angle factor = 1 (because of spur gear);

Y_B = rim thickness factor = 1 (because of no rim in the gear);

Y_{DT} = deep tooth factor 1 (for gear with contact ratio ≤ 2.05 and the accuracy grade > 4);

6.2.4 Static transmission error: numerical prediction

The stainless steel-polyamide gear pair was considered for the analysis of static transmission error. Figure 6.2(a) and Figure 6.2(b) show the schematic of single tooth contact (STC) and double teeth contacts (DTC).

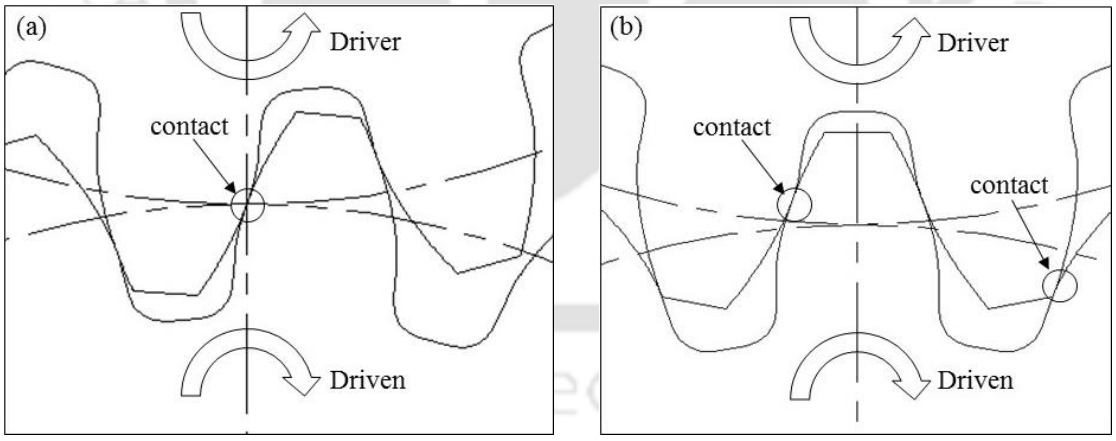

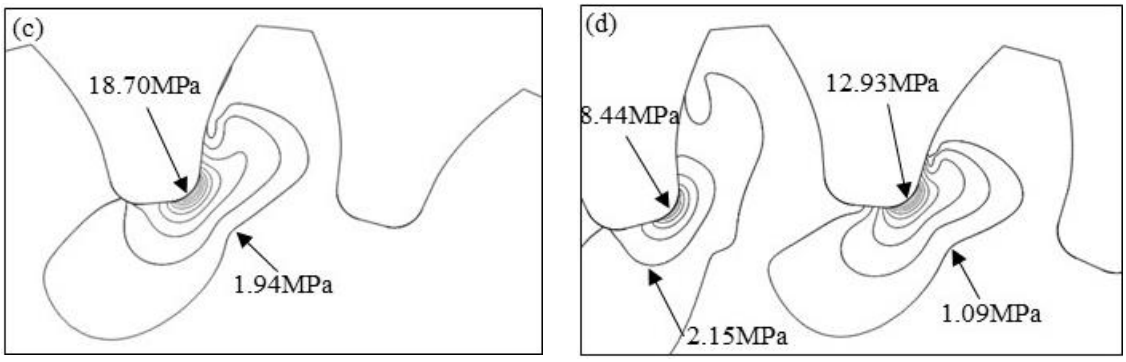

Figure 6.2 Schematic of (a) single tooth contact (STC), (b) double teeth contacts (DTC) and maximum principal stress distribution for (c) single tooth contact and (d) double teeth contacts, at 2 Nm load

Figure 6.2(c) and Figure 6.2(d) show the maximum principal stress distribution at root region when the polyamide gear was subjected to 2.0 Nm for STC and DTC, respectively. Due to the load sharing, maximum principal stress at root was lesser for double teeth contacts compared to the single tooth contact.

Torque is transferred from the driver stainless steel gear to polyamide driven gear. In order to understand that the load is transferred to the driven gear only through the loading side of polyamide gear teeth, contact normal forces were extracted. Figures 6.3(a) and 6.3(b) show the distribution of contact normal force (CNF1) and its close-up view, respectively. It is observed from the contact normal force distribution (CNF1) that there was no contact at the coast sides of polymer gear teeth with stainless steel gear teeth. Figure 6.3(c) shows the close-up of the tooth root region with very fine mesh.

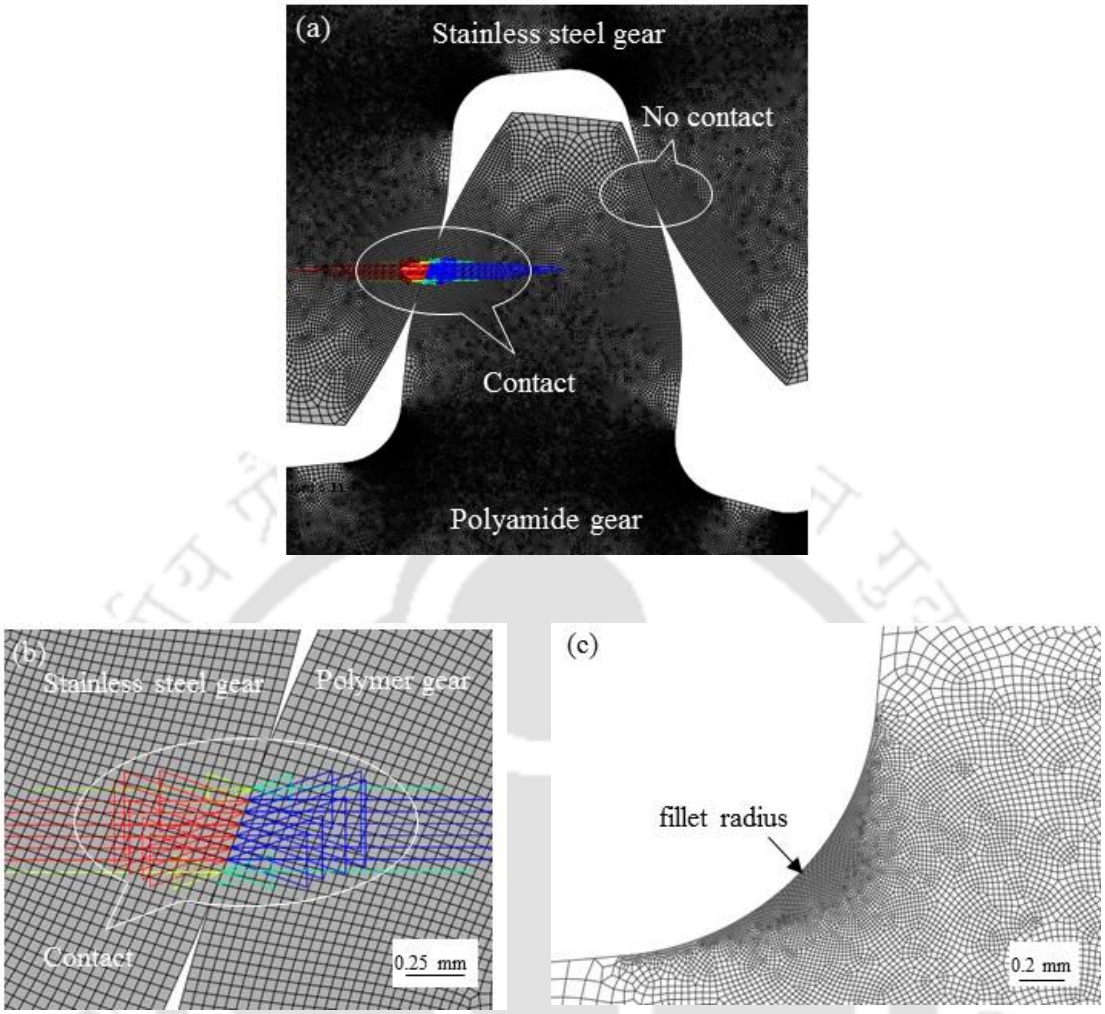

Figure 6.3 Distribution of contact normal force at (a) contact region and close-up view at (b) contact region and (c) tooth root region

Static transmission error is the difference between theoretical position of the output gear with perfect geometric accuracy and rigid drive and actual output position. The figure 6.4 shows the predicted static transmission error/angular rotation of driver of gear pair at various loads. When the stainless steel-polyamide gears are in mesh, static transmission error varies from 1.147–1.304 × 10^{-3} rad at 0.5 Nm in double teeth contacts region and 1.659–1.861 × 10^{-3} rad in single tooth contact region. This varying static transmission error behaviour either in single tooth or double teeth contacts is due to the difference between tooth stiffness of meshing gear pair. As observed, the static

transmission error increases with load increase and is 4.418–5.129 × 10^{-3} rad at 2.0 Nm in double teeth contact region and is 6.386–6.885 × 10^{-3} rad in single tooth contact region. One important behaviour of the increased double teeth contacts (decreased single tooth contact) region as the load increases from 0.5 Nm (roll angle period: 9º) to 2.0 Nm (roll angle period: 10º) was observed. It can be noted that present finding is in line with Meuleman *et al.* (2007) observation on polyoxymethylene-polyoxymethylene gear pair subjected to 5–10 Nm loads, where transmission error was found to increase with load (0.025 mm at 5 Nm was found to increase to 0.05 mm at 10 Nm) including the increased double teeth contacts region at higher loads.

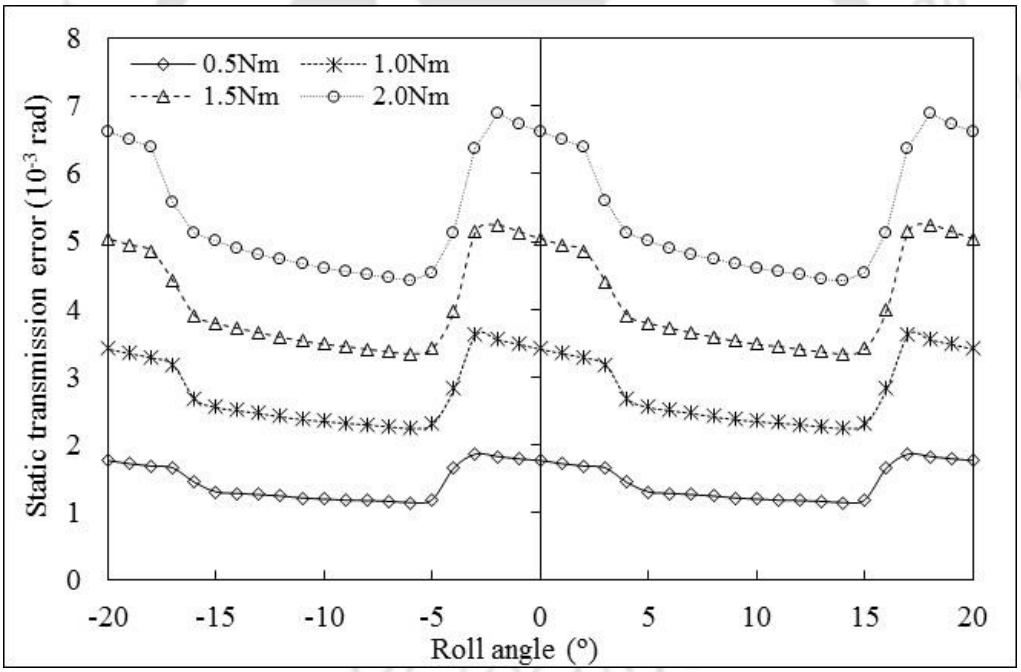

Figure 6.4 Predicted static transmission error at various loads

6.2.5 Static transmission error: experimental evaluation

A backlash of 0.66º was measured for a gear mesh which confirms that there was no contact at the coast sides of polymer gear teeth with stainless steel gear teeth. Figure 6.5 shows the average static transmission error measured for different torques. Measured static transmission errors were repeatable within 14 % deviation among six test cases at both the single tooth contact and double teeth contacts for all the loads.

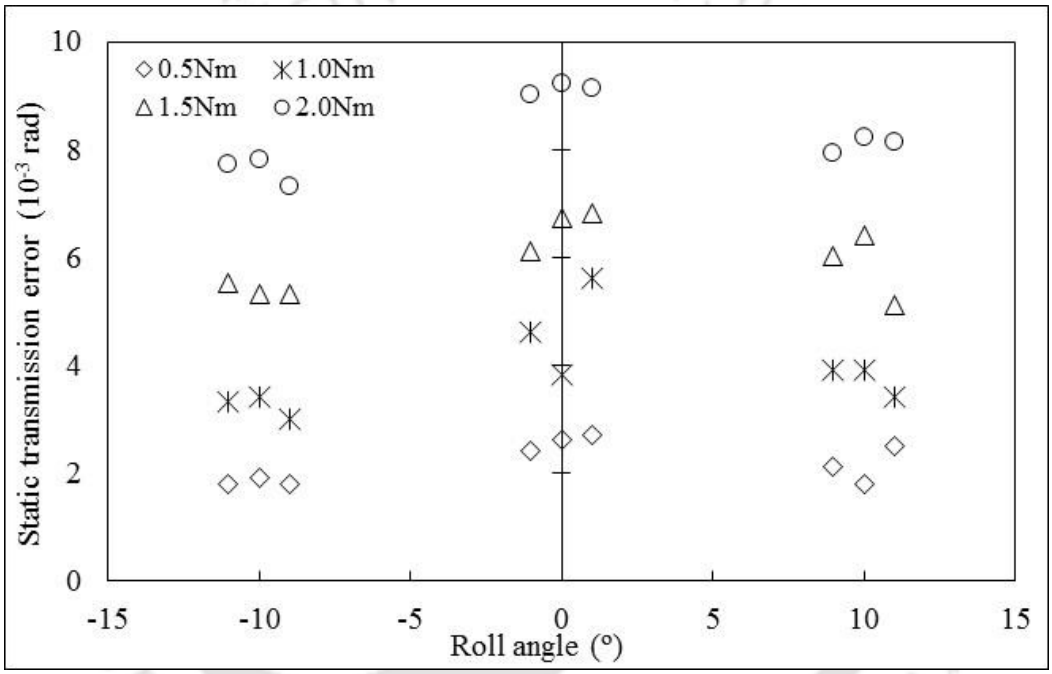

Figure 6.5 Measured static transmission error at various loads

As predicted in finite element analysis (Figure 6.4), static transmission error increases with load during experimental measurements (2.608×10^{-3} rad at 0.5 Nm at pitch point increases to 9.228×10^{-3} rad at 2.0 Nm). For each load in experiment, static transmission error at single tooth contact region is higher by 11.8–36.8 % than the double teeth contact region. The predicted static transmission error was correlated with measured static transmission error for single tooth contact (at 0º roll angle) and double teeth contacts (at –10º roll angle) and are shown in Figures 6.6(a) and 6.6(b),

respectively. It is noticed that static transmission error measured through experiment is always higher than the prediction. Maximum deviation between prediction and experiment is 47.7 % at 0.5 Nm for single tooth contact region and is 69.9 % at 2.0 Nm for double teeth contact region, as shown in Table 6.2. At higher loads, deviation increases between the predicted and measured. The contributing factors for deviation between experimental and finite element analysis (FEA) results include: (a) poor polymer gear quality; in finite element analysis, a gear with ideal tooth profile and geometry without any deviation (DIN 1 class) was considered where as a large variation in the tooth profile (form and total) was observed on the injection molded polymer gears (DIN 12 class). (b) practical difficulties in experiment; the position of gear mesh corresponds to the exact roll angle of 0° (single tooth contact) and −10º (double teeth contact) in FEA, but it is not possible to exactly keep the contact at 0º or −10º roll angle positions, even position variation of 0.5–1º among trials contribute to the deviation with respect to FEA. Moreover, measured static transmission error is only the average of six measurements. (c) static transmission error variation; as shown in Figure 6.4, numerically predicted static transmission error both at single and double tooth contact region is not constant but varies (12 to 14 % at 0.5 Nm and 8 to 16 % at 2.0 Nm) due to the tooth stiffness difference between stainless steel and polymer gears, which cause the deviation when compared to experimental results.

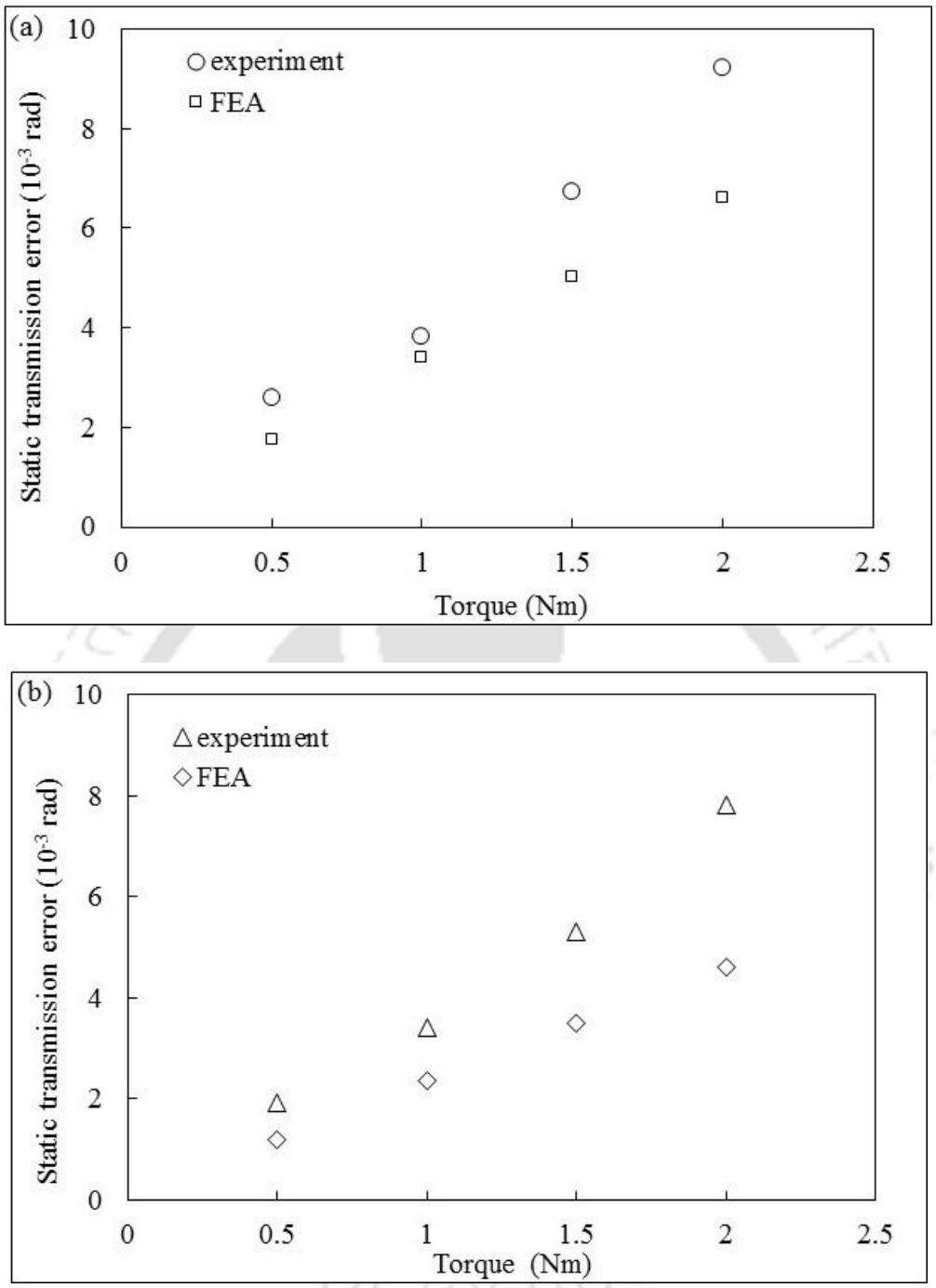

Figure 6.6 Predicted and measured static transmission error for

(a) single tooth contact and (b) double teeth contacts

Table 6.2 Deviation of experimentally measured static transmission error (10^{-3} rad) with respect to prediction

Torque (Nm)	Single tooth contact			Double teeth contacts		
	experiment	FEA	% deviation	experiment	FEA	% deviation
0.5	2.608	1.766	47.7	1.906	1.196	59.4
1.0	3.812	3.416	11.6	3.410	2.349	45.2
1.5	6.721	5.032	33.6	5.316	3.482	52.7
2.0	9.228	6.624	39.3	7.824	4.606	69.9

6.2.6 Premature and extended contacts: numerical prediction

The coordinate details of contact surface nodes of polyamide driven gear were extracted from each simulations. The locus of coordinates of contact nodes has provided the path of contact. The actual path of contact for the gears with higher material modulus such as stainless steel, will follow the ideal contact line drawn at pressure angle. The polymer gears, due to large deflection (because of their lower material modulus), are found to have contacts outside the ideal contact path and are known as premature and extended contacts. The contacts of polymer gear tooth with its mating gear before entering into the ideal contact line is called as premature contact (Figure 6.7(a)). The extended contact (Figure 6.7(b)) for the polymer gear occurs beyond the ideal contact path, where tip of the mating gear digs the flank of driven gear. Figure 6.7(c) shows the predicted path of contact of stainless steel-polyamide gear pair for different torque loads. As shown in Figure 6.7(d) and 6.7(e), due to the polymer gear tooth deflection, premature and extended contacts were observed outside the ideal contact path for stainless steel-polyamide gear pair, whereas for the stainless steel-

stainless steel pair no such behaviour was observed. These premature and extended contacts were found to be increased as the load increases. Due to the premature/extended contact (non conjugate action), tip of the driving gear comes into contact with the flank of driven gear resulting in high contact stress. Senthilvelan and Gnanamoorthy (2004a) observed excessive wear at the flank of nylon gears when meshed with stainless steel gear at 2 Nm, whereas uniform wear was observed at 0.8 Nm. This behaviour was due to increased gear tooth deflection of nylon gear at higher load. Tip of the stainless steel gear digs the flank region of polymer gear due to the non-conjugate action and high contact stresses. Karimpour *et al.* (2010) observed similar behaviour of premature and extended contacts for the POM-POM gear pairs.

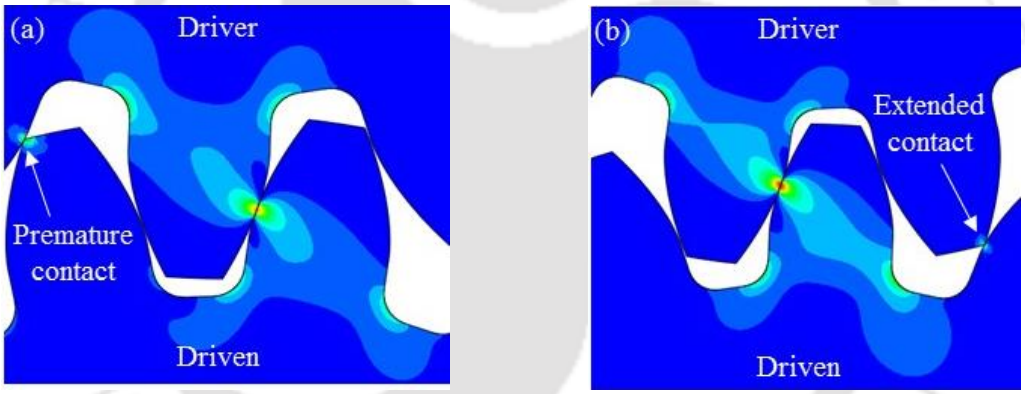

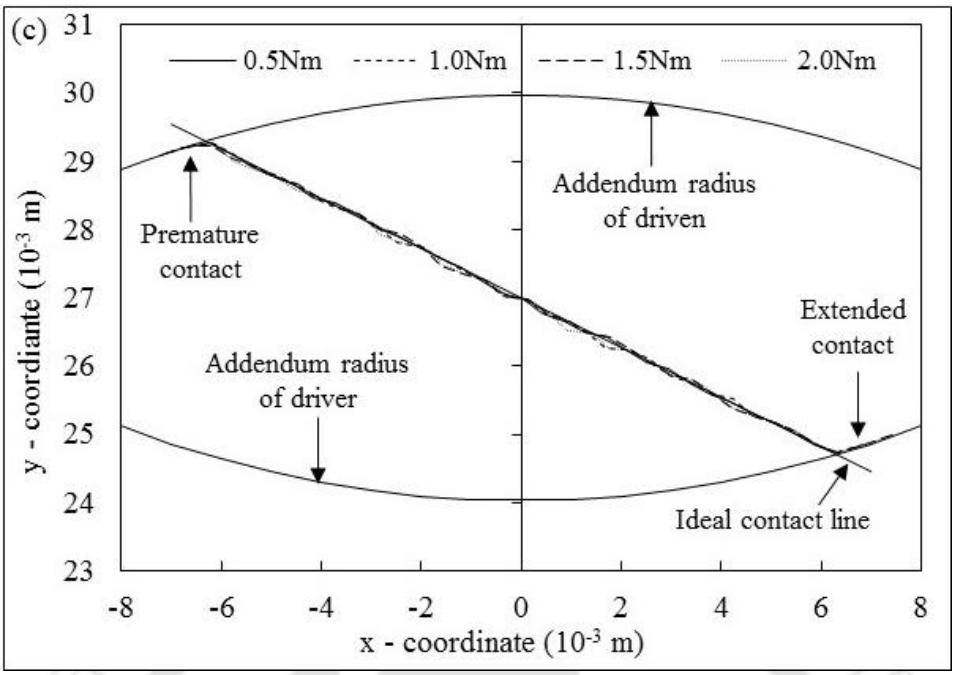

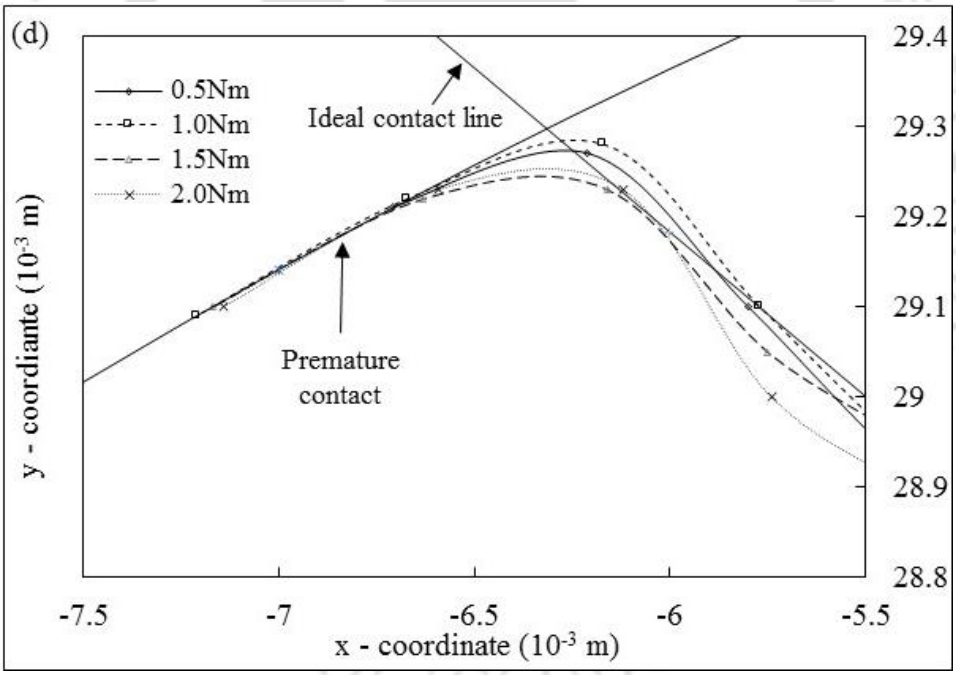

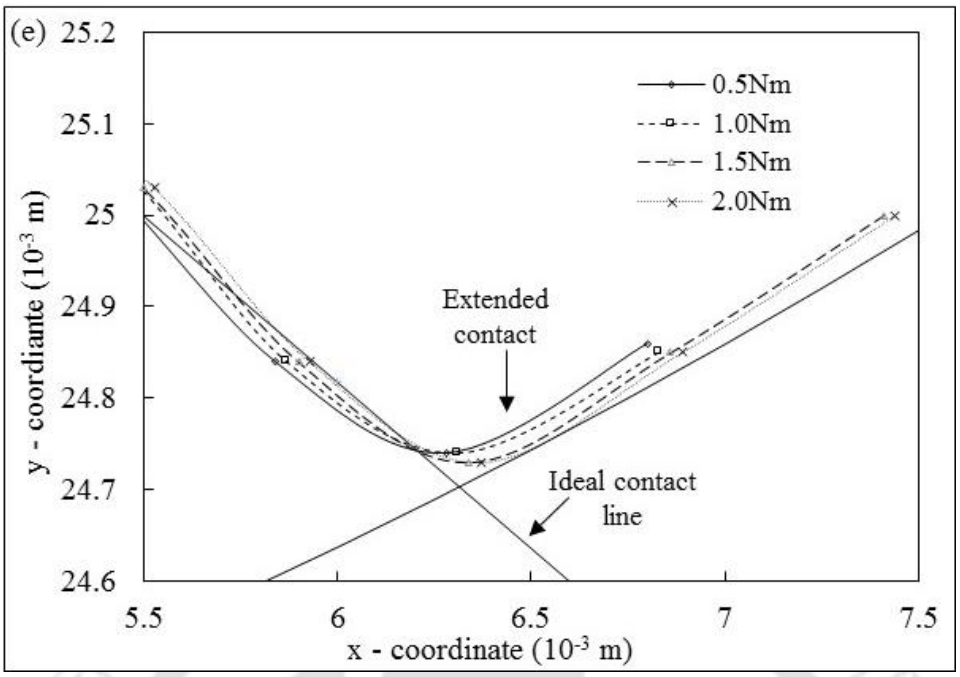

Figure 6.7 Path of contact (a) premature contact, (b) extended contact, (c) predicted path of contact and close-up view of (d) premature contacts and (e) extended contacts, in the gear pair at various loads

As observed in Figures 6.7(a)–6.7(c), the increased tooth deflection of polymer gear increases the roll angle. In order to compare the behaviour of stainless steel-polymer gear pair with that of stainless steel-stainless steel gear pair, numerical analysis was repeated with stainless steel-stainless steel gear pair, the roll angle obtained was 30º for 0.5 Nm torque, it can be noted that roll angle remain constant for all torque value from 0.5 to 2.0 Nm as expected. When one of the gears is polyamide then the observed roll angle for stainless steel-polyamide gear pair is 32º for 0.5 Nm, which is 6.7% increase compared to stainless steel-stainless steel gear pair. Variation of roll angle with different torque is provided in Table 6.3. It can be seen from the table that as torque increases, roll angle increases for stainless steel-polyamide gear mesh. Difference in the gear tooth stiffnesses between stainless steel and polyamide contributed this behaviour. This is in agreement with the work of Karimpour *et al.* (2010), where 30 % roll angle

increase was reported (from 19.84º to 25º), for POM-POM gear mesh subjected to 8 Nm torque loading.

Table 6.3 Variation of roll angle with torque

Torque (Nm)	Roll angle (º)	Percentage increase (compared to stainless steel- stainless steel pair)
0.5	32	6.7
1.0	33	10
1.5	34	13.3
2.0	34	13.3

6.2.7 Gear mesh stiffness: numerical prediction

The ratio of torque applied to the static transmission error provided the gear mesh stiffness. The gear mesh stiffness of stainless steel-polyamide gear pair at various loads is shown in Figure 6.8. It was found that with increase in load, slight increase in stiffness both at the single tooth contact region and double teeth contacts region. The nonlinear gear tooth deflection alongwith contact behaviour contributed this load dependent stiffness characteristics. Change in mesh stiffness with torque is given in Table 6.4. It can be observed from table that the deformation behaviour of gear teeth is nonlinear. Similar results of slight load dependency for the mesh stiffness (1.75×10^5 Nm/rad at 1.0 Nm and 1.81×10^5 Nm/rad at 114.3 Nm for pitch point) was predicted for steel–aluminium gear pair by Wang and Howard (2004).

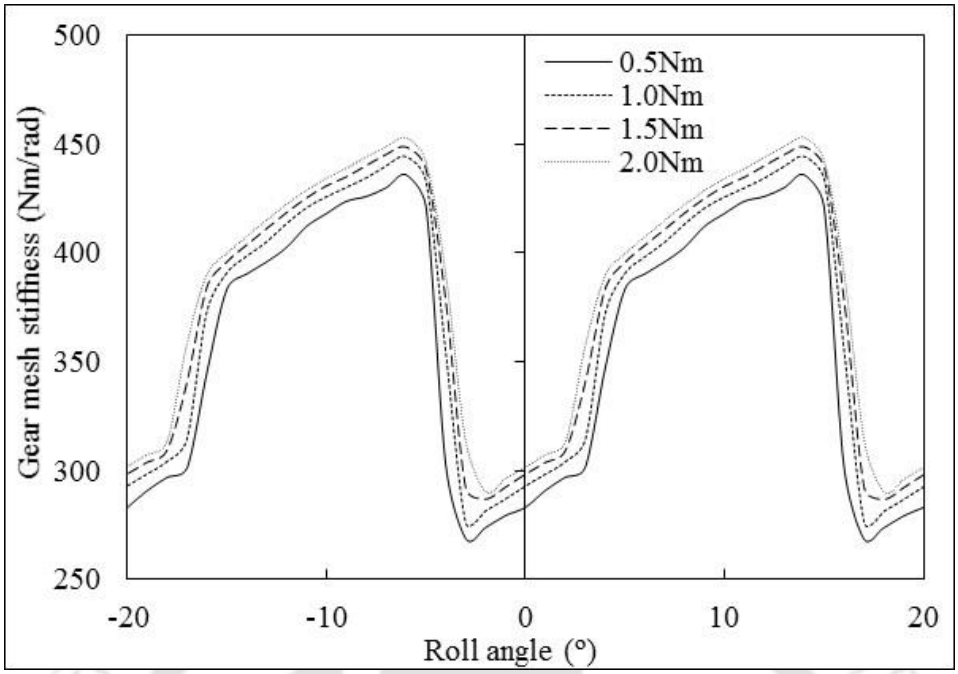

Figure 6.8 Predicted gear mesh stiffness at various loads

Table 6.4 Variation of gear mesh stiffness with load

Torque (Nm)	Mesh Stiffness (Nm/rad)	
	Single tooth contact	Double teeth contacts
0.5	268.7–301.4	383.4–435.0
1.0	275.6–304.0	390.6–444.2
1.5	286.6–309.0	395.7–448.7
2.0	290.5–313.2	399.6–452.7

6.2.8 Gear mesh stiffness: experimental evaluation

Figures 6.9(a) and 6.9(b) show the comparison of gear mesh stiffness predicted in finite element analysis with the results obtained in experiments for single tooth contact (at 0º roll angle) and double teeth contacts (at –10º roll angle). Stiffness observed from the experiments for different torques is lower than the prediction, which is due to the

higher static transmission error measured in experiments. Variation of experimentally measured stiffness with respect to FEA prediction is shown in Table 6.5. Maximum stiffness variation of 32.3 % at single tooth contact and 41.1 % at double teeth contact were observed; (i) poor polymer gear quality, (ii) practical difficulties in experiment and (iii) static transmission error variation are the contributing factors for the stiffness difference observed between experiment and FEA prediction.

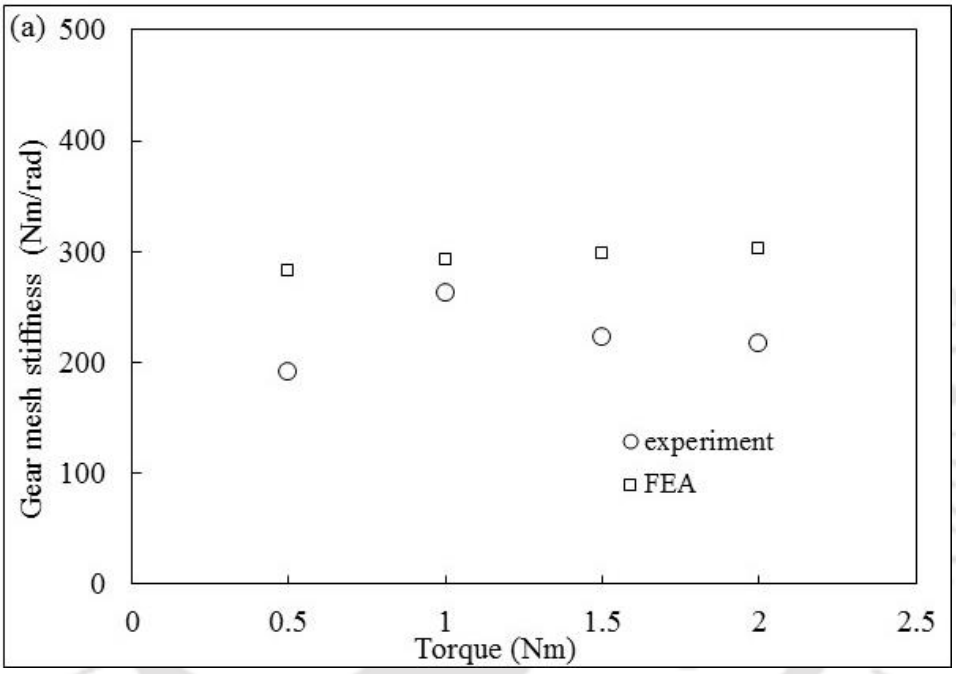

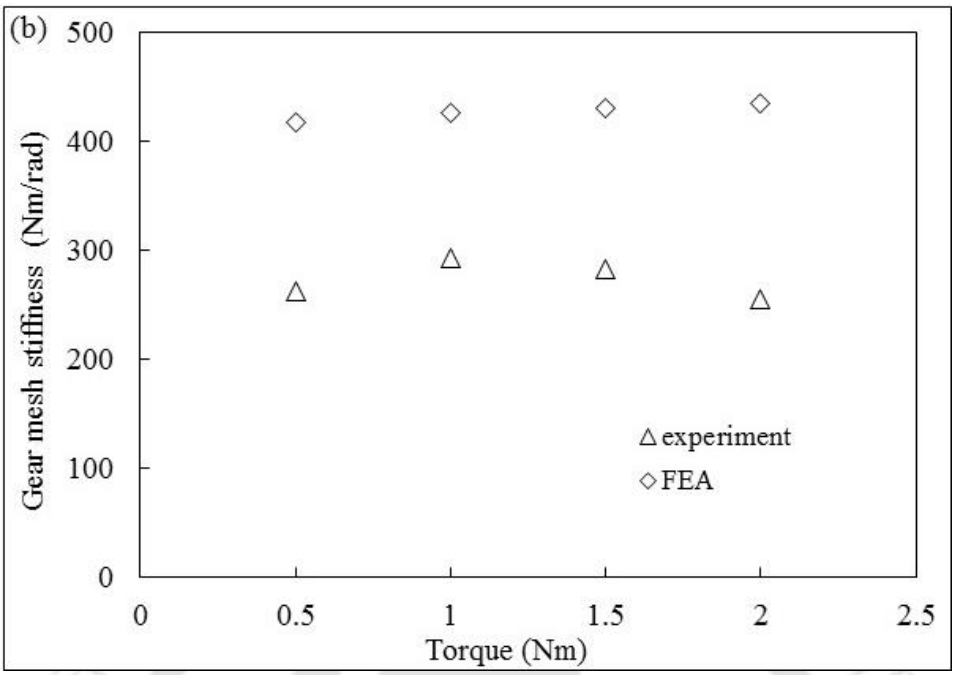

Figure 6.9 Measured and predicted gear mesh stiffnesses for (a) single tooth contact and (b) double teeth contacts

Table 6.5 Variation of experimentally measured stiffness with respect to FEA prediction

Torque (Nm)	Single tooth contact (Nm/rad)			Double teeth contacts (Nm/rad)		
	FEA	experiment	% variation	FEA	experiment	% variation
0.5	283.13	191.72	32.3	418.06	262.36	37.2
1.0	292.74	262.36	10.4	425.71	293.22	31.1
1.5	298.09	223.20	25.1	430.79	282.16	34.5
2.0	301.93	216.73	28.2	434.22	255.63	41.1

6.3 EFFECTS OF STRAIN RATE ON BENDING AND TRANSMISSION CHARACTERISTICS OF INJECTION MOLDED POLYAMIDE 66 SPUR GEARS

6.3.1 Strain rate dependent material characteristics

The unreinforced polyamide 66 was injection molded into tensile specimens. The tensile specimens were tested at laboratory temperature (296±5 K) as per the ASTM D638-10 standard with a servo hydraulic fatigue testing machine (INSTRON, 8801). The mechanical properties of the tensile specimens were evaluated at the crosshead speeds of 1, 10 and 30 mm/min in the fatigue testing machine, corresponding to loading/strain rates of 0.0003, 0.003 and 0.01 s^{-1}, respectively. Three specimens were tested for each strain rate. Figure 6.10 and Table 6.6 show the stress-strain curves and the mechanical properties of test material at different strain rates, respectively. At higher strain rate, the time available for the material response is lesser, this contributes to the higher modulus and strength of polyamide material.

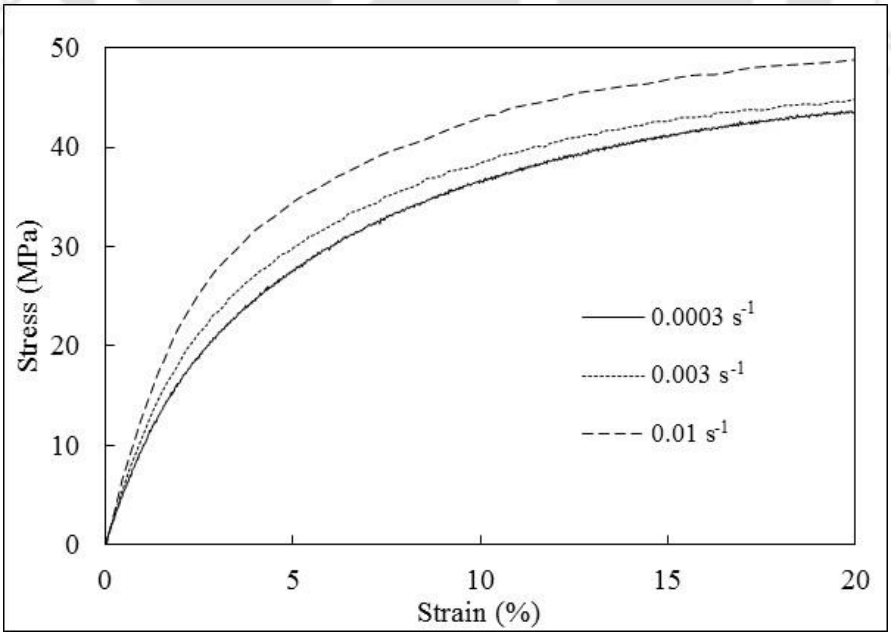

Figure 6.10 Stress strain curves of polyamide 66 at different strain rates

Table 6.6 Mechanical properties of polyamide 66 at different strain rates

Parameter	Strain rates (s^{-1})		
	0.0003	0.003	0.01
Young's modulus (GPa)	1.147±0.01	1.241±0.12	1.458±0.07
Tensile strength (MPa)	45.6±0.10	46.3±0.82	48.8±0.42

6.3.2 Bending stress: numerical prediction

The two-dimensional finite element model of the stainless steel-polyamide 66 gear pair. A disc with five meshing teeth having an ideal involute profile (DIN 1 quality) was modeled to minimize the computational effort, and the finite element analysis was carried out using ABAQUS®. The element size of 8 µm at the root region, 55 µm at the contact region and coarse elements at the disc portion were considered based on a systematic convergence study. The details of numerical study are reported in Section 3.7 (CHAPTER 3). A Young's modulus of 200 GPa, Poisson's ratio of 0.3 and density of 7850 kg/m^3 were used for the stainless steel driver gear. Similarly, Young's modulus of 1.147, 1.241 and 1.458 GPa evaluated, with a Poisson's ratio of 0.41 and a density of 1140 kg/m^3 were used for the polyamide driven gear for the linear material analysis. In addition to the Young's modulus and Poisson's ratio, the stress-strain characteristics (Figure 6.10) are converted to a true stress and plastic strain pair for the polyamide gear for the material nonlinear analysis. The plane stress linear quadrilateral elements (CPS4R) with reduced integration were considered. All degrees of freedom of the driven gear at its hub inner diameter were constrained. For a driver gear, a reference node at the hub center with its degrees of freedom in the x and y directions constrained was created for applying torque. The kinematic coupling was established between the reference node and the hub inner diameter. A coefficient of friction of 0.3 was used for

the surface contact nodes between the driver and driven gears. Karimpour *et al.* (2010) also used a 0.3 coefficient of friction for the polymer-polymer gear pair.

The finite element analysis was carried out at 0° (pitch point) and 10° roll angle positions, which correspond to single tooth contact (STC) and double teeth contacts (DTC), respectively. The simulations were conducted for different torques (1 to 2.5 Nm). From each simulation, the angular rotation of the reference node of the driver gear (which is a measure of static transmission error) and the maximum principal stress of the polyamide gear tooth root were extracted.

Maximum principal stress is a measure of tooth root bending stress. Figures 6.11(a) and 6.11(b) show the maximum principal stress distribution at a single tooth contact and for double teeth contacts, respectively, of the stainless steel-polyamide gear pair subjected to a 2.5 Nm load that was predicted with linear material model obtained at a strain rate of 0.0003 s^{-1}. It was observed that the stress induced in the polyamide gear at the double teeth contacts was less compared to the stress at the single tooth contact.

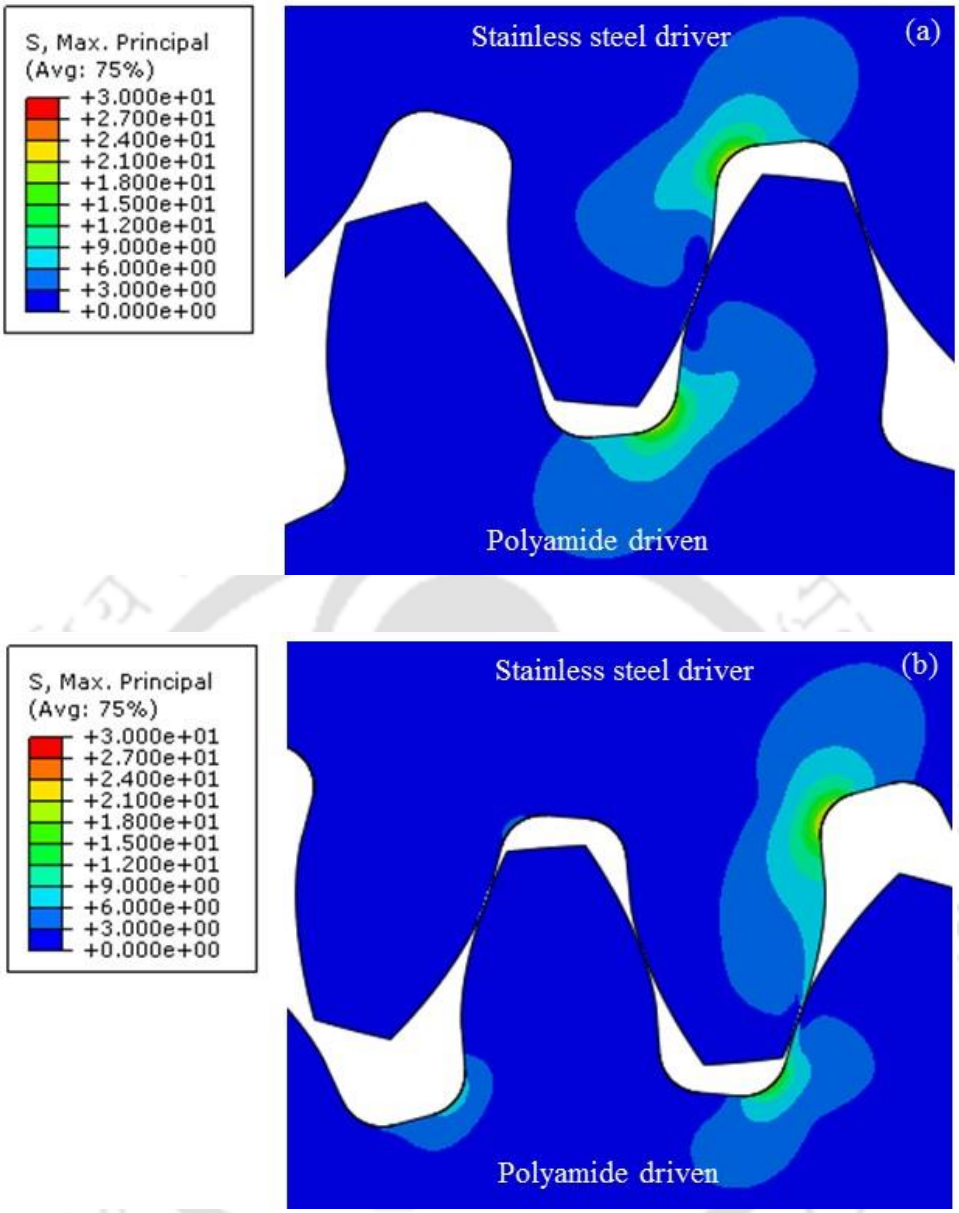

Figure 6.11 Maximum principal stress of stainless steel-polyamide gear pair subjected to 2.5 Nm load, predicted with linear material model obtained at a strain rate of 0.0003 s^{-1} at (a) single tooth contact and (b) double teeth contacts

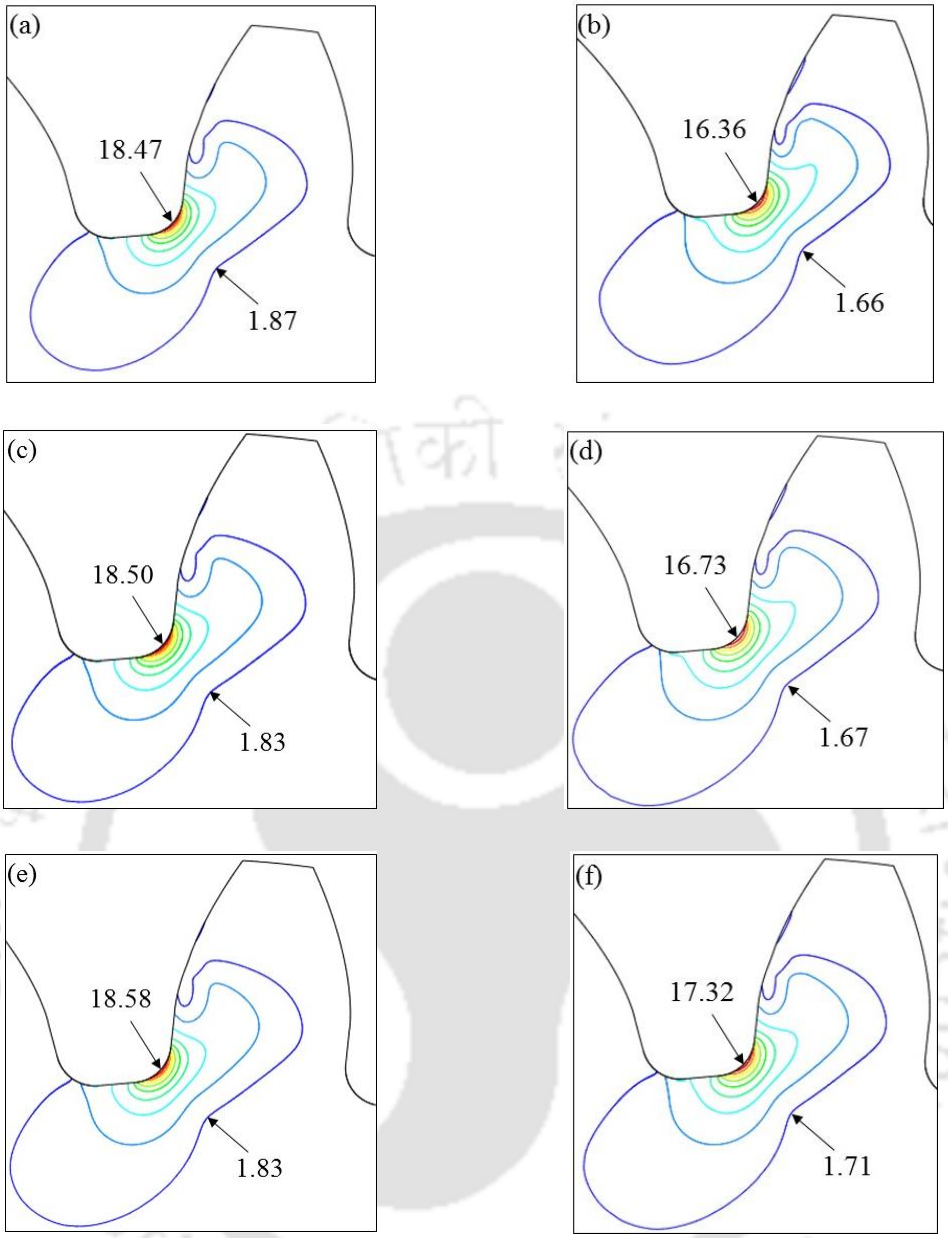

Figure 6.12 Stress contour of polyamide gear at single tooth contact for 2 Nm torque for (a) linear material model at 0.0003 s^{-1} strain rate, (b) nonlinear material model at 0.0003 s^{-1} strain rate, (c) linear material model at 0.003 s^{-1} strain rate, (d) nonlinear material model at 0.003 s^{-1} strain rate, (e) linear material model at 0.01 s^{-1} strain rate and (f) nonlinear material model at 0.01 s^{-1} strain rate

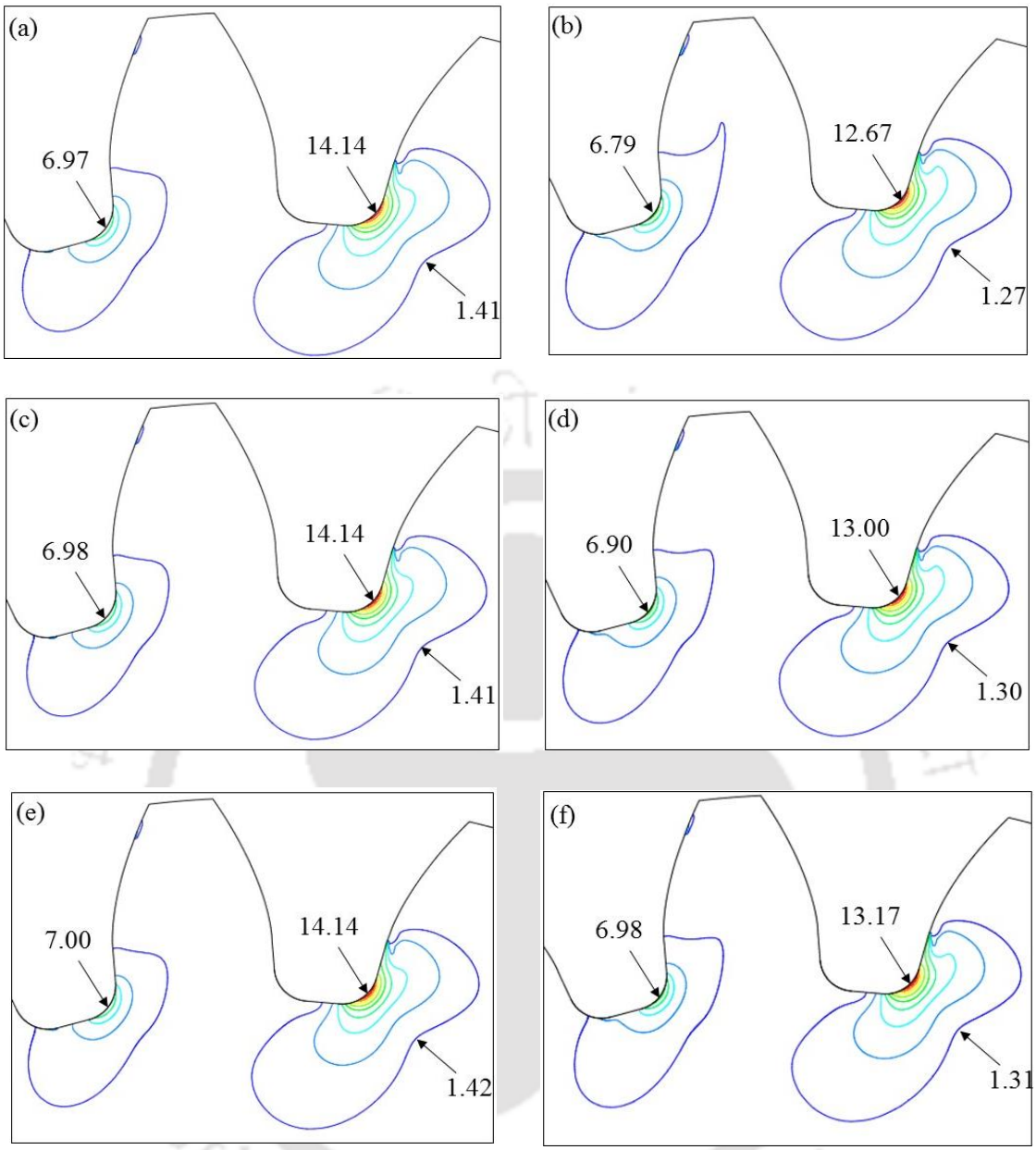

Figure 6.13 Stress contour of polyamide gear at double teeth contacts for 2 Nm torque for (a) linear material model at 0.0003 s^{-1} strain rate, (b) nonlinear material model at 0.0003 s^{-1} strain rate, (c) linear material model at 0.003 s^{-1} strain rate, (d) nonlinear material model at 0.003 s^{-1} strain rate, (e) linear material model at 0.01 s^{-1} strain rate and (f) nonlinear material model at 0.01 s^{-1} strain rate

Figures 6.12(a)–6.12(f) show the contour plots of the maximum principal stress distribution of the polyamide gear at STC for 2 Nm torque with the linear and nonlinear

material models. The root stress for the linear material models was higher than the nonlinear material models due to higher stiffness of the material, which provided more resistance for the linear material models. With the increasing strain rate, an increase in root stress was observed due to higher material modulus at higher strain rates. Similarly, increasing gear tooth root stress (4.5 %) with an increase in material Young's modulus (from 1 to 2 GPa) was reported by Karimpour *et al.* (2010).

Because of the load sharing, the maximum principal stress at the root was lower by 21.9–24.1 % for DTC compared to STC, for all the material models (Figures 6.13(a)–6.13(f)). Similar to the bending stress observed in STC (Figures 6.12(a)–6.12(f)), an increase in bending stress was observed for DTC with the linear material models compared to the nonlinear material models, and it increased as the strain rate increased.

Figure 6.14 shows the bending stress for different loads with the linear and nonlinear material models for STC and DTC. An increase in bending stress with torques at STC and DTC for the linear material models was observed, and the bending stress increases as the strain rate increases in nonlinear material models. Table 6.7 and Table 6.8 show the % difference in the bending stress predicted for the different strain rates with the nonlinear material models with respect to the linear material models at STC and DTC, respectively.

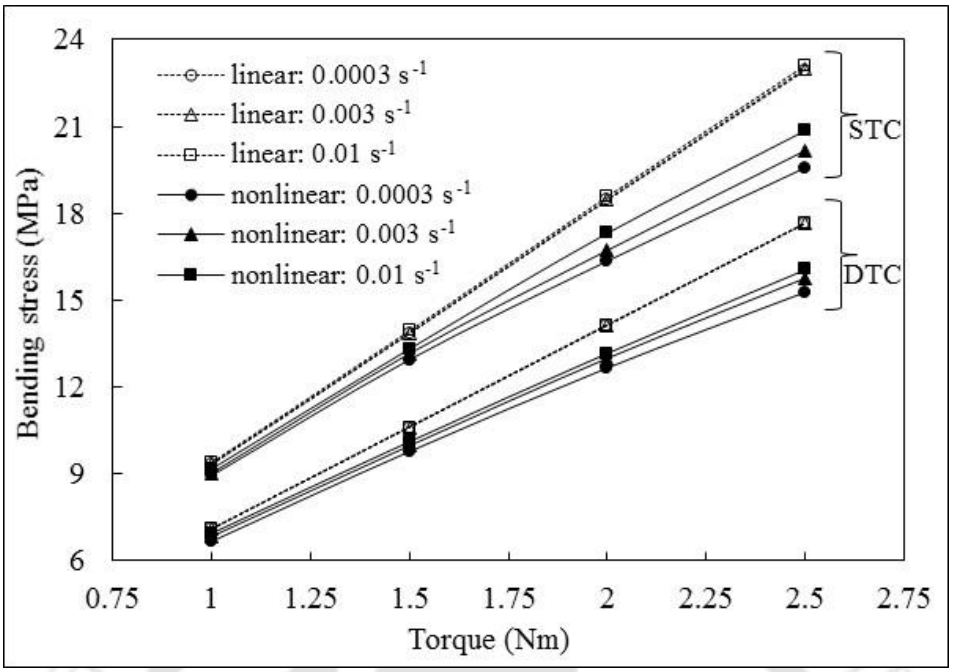

Figure 6.14 Bending stress at single tooth contact and double teeth contacts for different loads

Table 6.7 Bending stress deviation for the different strain rates at STC with the nonlinear material models with respect to the linear material models

Torque (Nm)	% deviation at strain rate of		
	0.0003 s^{-1}	0.003 s^{-1}	0.01 s^{-1}
1	4.28	3.53	2.55
1.5	6.57	5.19	4.52
2	11.42	9.57	6.78
2.5	14.64	12.26	9.61

Table 6.8 Bending stress deviation for the different strain rates at DTC with the nonlinear material models with respect to the linear material models

Torque (Nm)	% deviation at strain rate of		
	0.0003 s^{-1}	0.003 s^{-1}	0.01 s^{-1}
1	5.92	3.66	2.11
1.5	7.91	6.03	4.71
2	10.40	8.06	6.86
2.5	13.32	10.70	9.11

It was observed that the % difference in bending stress at STC and DTC with the nonlinear material models compared to the linear models was decreasing as the strain rate was increasing because of the higher Young's modulus obtained at the higher strain rates.

The bending stresses predicted in numerical analysis at the pitch point were compared to those calculated using the BS ISO 6336 standard (Table 6.9). Deviations of 9.4–14.0 % at 1.0 Nm and 11.1–24.6 % were observed for the stresses predicted in FEA with respect to those obtained using the standard. This result indicates that the standard does not account for the material property variations that occur at different strain rates.

Table 6.9 Comparison of bending stresses between FEA and BS ISO 6336 standard

Torque (Nm)	Linear material models at strain rate of			Nonlinear material models at strain rate of			BS ISO 6336 standard
	0.0003 s^{-1}	0.003 s^{-1}	0.01 s^{-1}	0.0003 s^{-1}	0.003 s^{-1}	0.01 s^{-1}	
1	9.34	9.36	9.41	8.94	9.03	9.17	10.39
1.5	13.86	13.88	13.95	12.95	13.16	13.32	15.59
2	18.47	18.50	18.58	16.36	16.73	17.32	20.79
2.5	22.95	23.00	23.09	19.59	20.18	20.87	25.98

6.3.3 Static transmission error: numerical prediction

The prediction of static transmission error of polymer gears indicates the measure of gear tooth deflection, and in turn, the position accuracy. The angular rotation of a reference node of the driver gear is a measure of static transmission error. Figures 6.15(a) and 6.15(b) show the static transmission errors for different loads at STC and DTC with the linear and nonlinear material models, respectively. The static transmission error at STC was higher compared to that at DTC and increased with torque. The static transmission error with the nonlinear material models was higher by 1.29–9.28 % compared to that of the linear material models for STC, and it was 0.63–4.21 % for DTC for all strain rates because of the higher deflection of material in the nonlinear material analysis.

Table 6.10 and Table 6.11 show the % difference in static transmission error predicted with the nonlinear material models with respect to their corresponding linear material models at STC and DTC, respectively. The % difference with a negative sign observed

indicated that the bending deflection behavior of the gear for the nonlinear material models was higher compared to that of the linear material models.

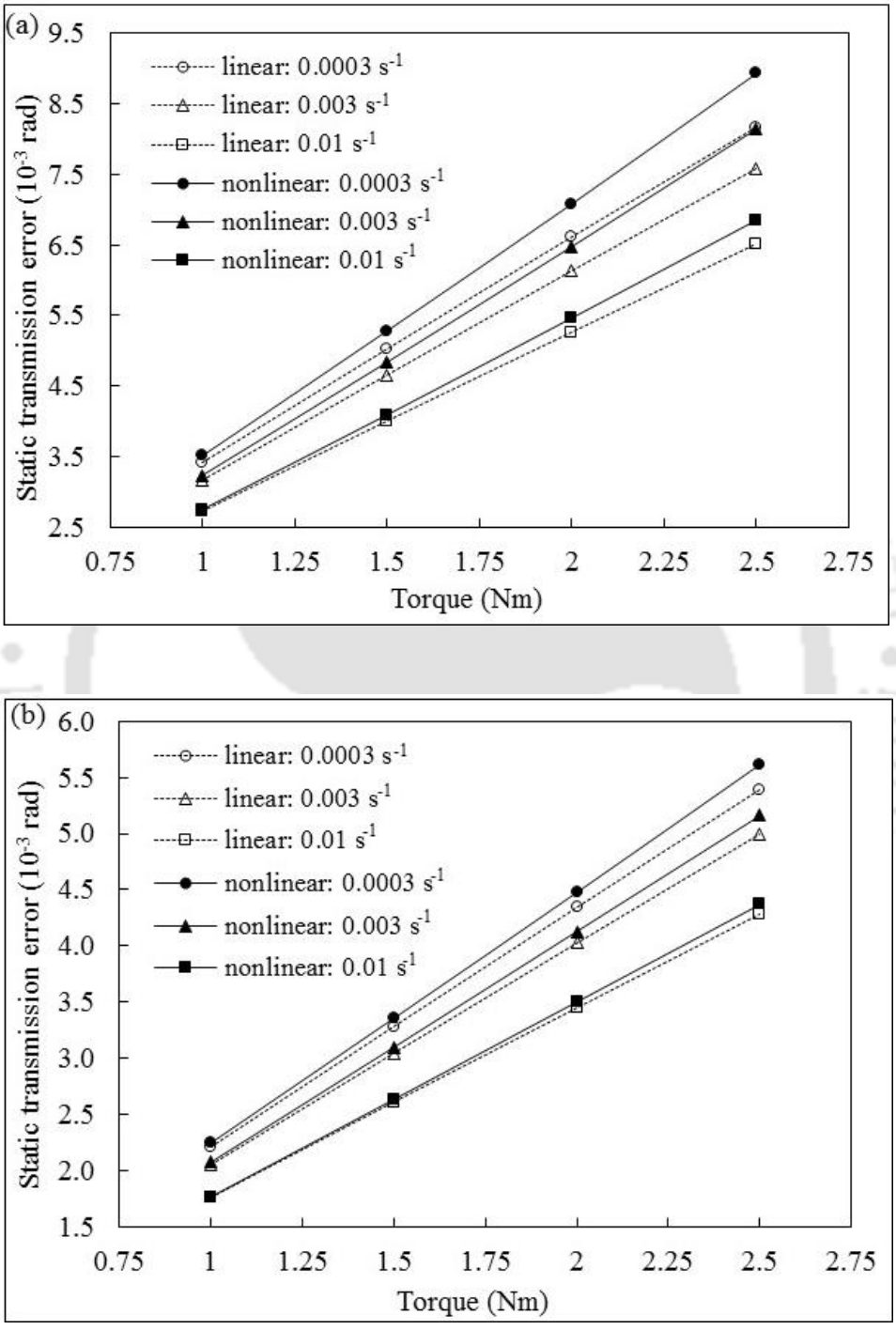

Figure 6.15 Static transmission error for different loads at (a) single tooth contact and (b) double teeth contacts

Table 6.10 Static transmission error deviation at STC with the nonlinear material models with respect to the linear material models (10^{-3} rad)

Torque (Nm)	% deviation at strain rate of		
	0.0003 s^{-1}	0.003 s^{-1}	0.01 s^{-1}
1	–3.08	–2.24	–1.29
1.5	–5.22	–3.88	–2.32
2	–7.09	–5.55	–3.82
2.5	–9.28	–7.34	–5.12

Table 6.11 Static transmission error deviation at DTC with the nonlinear material models with respect to the linear material models (10^{-3} rad)

Torque (Nm)	% deviation at strain rate of		
	0.0003 s^{-1}	0.003 s^{-1}	0.01 s^{-1}
1	–1.49	–1.17	–0.63
1.5	–2.19	–1.74	–1.04
2	–3.11	–2.58	–1.63
2.5	–4.21	–3.26	–2.06

It was observed that the % difference in static transmission error at STC and DTC with the nonlinear material models compared to the linear material models was lower for lower torque, and that the higher strain rate increased as the torque increased. Trobentar *et al.* (2016) carried out a finite element analysis of a Delrin gear with linear and nonlinear models. With the normal force of 421 N, the nonlinear model predicted

higher deflection (0.323 mm) compared to the deflection predicted by the linear material model (0.308 mm).

6.3.4 Static transmission error: experimental evaluation

The static transmission error of stainless steel-polyamide gear pair was measured with the help of in-house developed test rig using optical encoder sensor. The details of test rig are reported in Section 3.6 (CHAPTER 3). Figure 6.16 shows the measured static transmission error at different loads. It can be observed that the static transmission error increased with torque. It can also be noted that the static transmission error was higher for STC than DTC, as predicted by the numerical analysis (Figures 6.15(a) and 6.15(b)). Figures 6.17(a) and 6.17(b) show the comparison of static transmission error between the predicted and measured values for STC (pitch) and DTC (pitch−10°), respectively. Table 6.12 and Table 6.13 show the % difference between the measured static transmission error and numerical results with the different material models at STC and DTC, respectively. The static transmission error observed between the numerical results and the experimentally measured values shows a good trend with a maximum difference of 27.93 % for STC and 33.51 % for DTC.

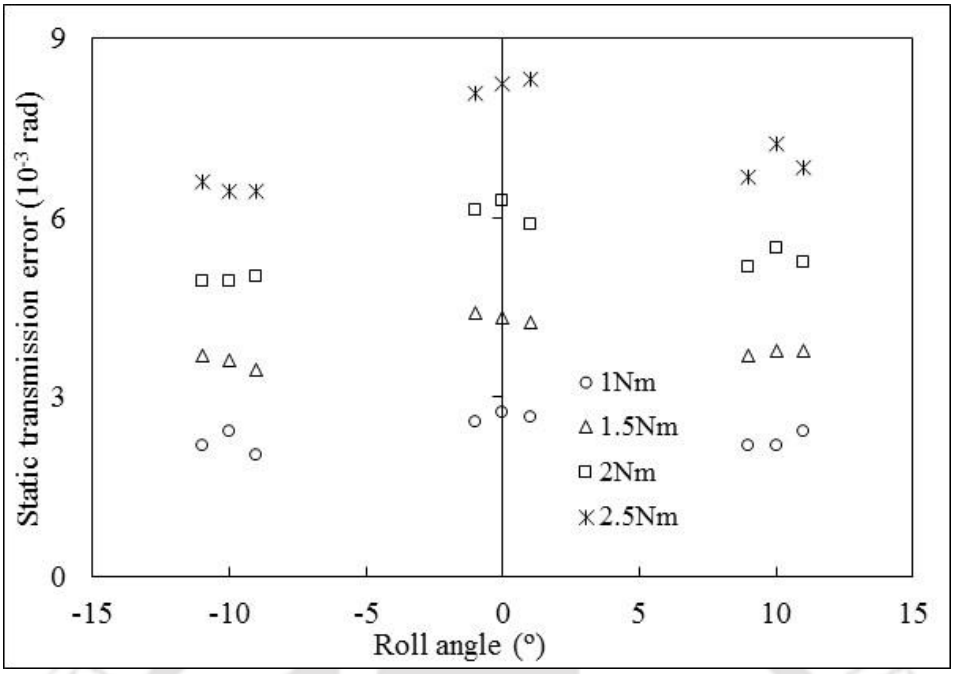

Figure 6.16 Measured static transmission error at different loads

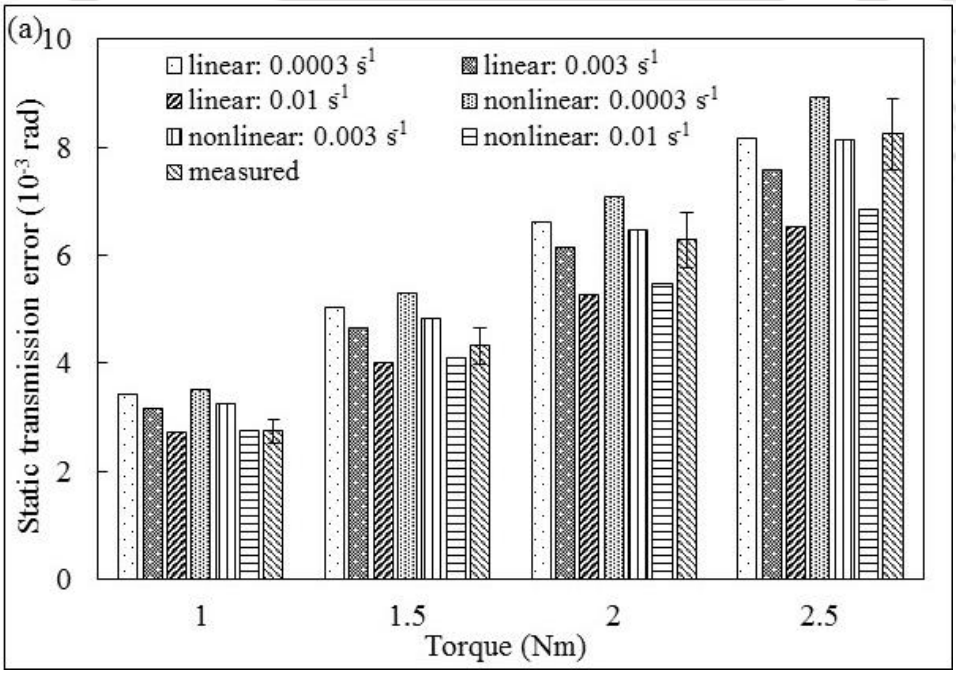

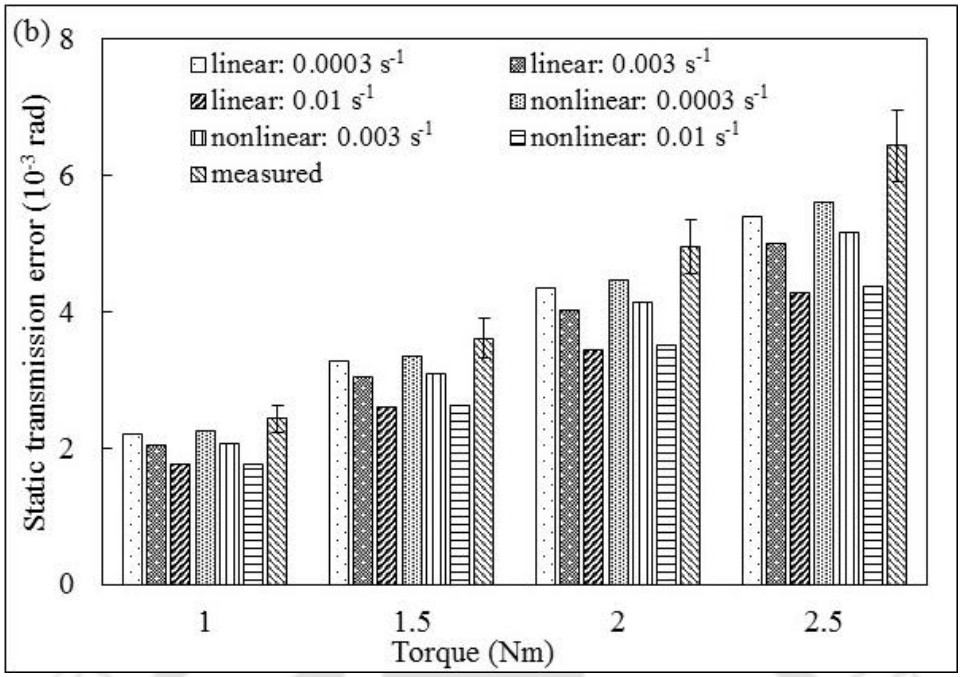

Figure 6.17 Static transmission error comparison between the predicted and measured at different loads for (a) single tooth contact and (b) double teeth contacts

Table 6.12 Variation of the predicted static transmission error at STC (pitch) with respect to measured values

Torque (Nm)	% variation for linear material model at strain rate of			% variation for nonlinear material model at strain rate of		
	0.0003 s^{-1}	0.003 s^{-1}	0.01 s^{-1}	0.0003 s^{-1}	0.003 s^{-1}	0.01 s^{-1}
1	–24.11	–15.23	1.07	–27.93	–17.82	–0.20
1.5	–16.34	–7.96	7.31	–22.41	–12.15	5.15
2	–5.35	2.25	16.15	–12.82	–3.18	12.95
2.5	0.81	7.90	20.89	–8.40	1.15	16.83

Table 6.13 Variation of the predicted static transmission error at DTC (pitch–10º) with respect to measured values

Torque (Nm)	% variation for linear material model at strain rate of			% variation for nonlinear material model at strain rate of		
	0.0003 s^{-1}	0.003 s^{-1}	0.0003 s^{-1}	0.003 s^{-1}	0.0003 s^{-1}	0.003 s^{-1}
1	9.14	15.80	27.92	7.79	14.81	27.47
1.5	9.08	15.70	27.83	7.09	14.23	27.08
2	12.22	18.61	30.34	9.49	16.51	29.21
2.5	16.30	22.39	33.51	12.77	19.85	32.14

The nonlinear material models with a 0.01 s^{-1} strain rate predicted the lower static transmission errors for both STC and DTC (Table 6.10 and Table 6.11), because of the higher Young's modulus of the material. It should be noted that the poor gear quality (DIN 8–12) increased the measured static transmission error compared to the ideal gear quality (DIN 1), which was considered for the numerical model. The polymer gears experienced higher strain rates in the experiments since the load was abruptly applied by keeping dead weight on the loading pan. Hence, the measured static transmission errors closely matched the results obtained with higher strain rate (0.01 s^{-1}) nonlinear material models, as observed in Table 6.11. Meuleman *et al.* (2007) also observed a higher transmission error (50 µm) for POM gears due to their poor gear quality (DIN 7) compared to the predicted error (20 µm) for a 10 Nm load.

6.4 SUMMARY

A numerical analysis of stainless steel-polyamide gear pairs with linear and nonlinear material models obtained at different strain rates was carried out at different loads. The

experiments were also carried out to measure the static transmission error of the gear pairs at three different discrete positions. The following major conclusions can be drawn from the present study:

- Premature and extended contacts occurred in the stainless steel-polyamide gear mesh were responsible for roll angle increase. Roll angle of stainless steel-polyamide gear pair was increased by 6.7 % at 0.5 Nm and 13.3 % at 2.0 Nm when compared to that of stainless steel- stainless steel gear pair.
- Static transmission error and gear mesh stiffness increased nonlinearly with load increase for both the numerical and experimental works. The nonlinear deformation of polymer gear tooth and contact behaviour of polymer gear tooth surface contributed these characteristics. Gear mesh stiffness of 268.7–301.4 Nm/rad at 0.5 Nm was increased to 290.5–313.2 Nm/rad at 2.0 Nm for the single tooth contact.
- Bending stress with nonlinear material models was lower by 2.55–14.64 % as compared to that of linear material models. With an increasing strain rate, an increase in the bending stress was observed for nonlinear material models because of the higher material modulus at higher strain rates.
- Static transmission error with linear material models was lower by 0.63–9.28 % than that of nonlinear material models, and it further decreased with increased strain rate, for both STC and DTC.
- The nonlinear material model obtained at the strain rate corresponding to the desired application can be used for predicting the bending stress and static transmission error of polymer gears more accurately.

CHAPTER 7

SUMMARY AND CONCLUSIONS

7.1 SUMMARY

Bi-directional and uni-directional bending fatigue performance evaluation of the unreinforced and carbon fiber reinforced polyamide gears were carried out using in-house developed servo motor based gear test rig for different load magnitudes. The effects of frequency on the hysteretic heating and bending fatigue performance were evaluated for unreinforced polyamide gears. The net surface temperature of test gears, torque exerted and angular displacement of gears were continuously measured and recorded. Temperature rise was correlated to the hysteresis loop plotted using acquired torque and angular displacement of gears. Failure morphology of the failed test gears was analysed.

Bending and transmission behaviours of stainless steel-polyamide gear pair using linear and nonlinear material models with a help of commercial finite element analysis software were carried out. Injection molded unreinforced polyamide gears were used in the experimental evaluation of static transmission error using in-house developed test rig and compared with the predicted results. Following major conclusion were drawn from these investigations.

7.2 CONCLUSIONS

Bi-directional bending fatigue performance of unreinforced and carbon fiber reinforced polyamide gears and static transmission characteristics of polyamide gears were investigated. The following are the conclusions of the studies

7.2.1 Bi-directional bending fatigue performance of polymer composite gears

- Unreinforced polyamide gears exhibited thermo mechanical and mechanical root crack failures. The root crack failures occurred when the heat generated under the bending loads was not sufficient to soften the gear material. However, carbon fiber reinforced polyamide gears exhibited root crack mechanical fatigue failures only.
- In unreinforced polyamide gears, due to their lower stiffness, crack direction was almost perpendicular to the fillet radius of gear tooth root. Orientation of reinforcing fibers and their failures were responsible for the tortuous crack path in the case of carbon fiber reinforced polyamide gears.
- Carbon fiber reinforced polyamide gears exhibited higher bending load carrying capability and fatigue life than unreinforced polyamide gears.
- Unreinforced and carbon fiber reinforced polyamide gears exhibited decreased fatigue life in bi-directional loads (83–99 %) when compared to uni-directional loads.
- Hysteretic heating and surface temperature of unreinforced polyamide gears increased with torque and frequency for both the bi-directional and uni-directional loads. Hysteresis heating of gears was more while subjected to bi-directional loads, because of the higher angular displacement, and increased mobility and sliding of the polymer chains.

- At higher test frequency, unreinforced polyamide gears exhibited both the thermo mechanical and mechanical root crack failures. In addition, the straight root crack with overlapping fractured surfaces was observed for both the bi-directional and uni-directional loads due to repeated collision of fractured surfaces during subsequent loadings.
- In both the uni-directional and bi-directional loads, gears tested at higher frequency exhibited inferior fatigue life as compared to lower frequency. Gears shown inferior life in bi-directional loads than uni-directional loads. This was because of the increased hysteresis heating at higher frequency.

7.2.2 Static transmission characteristics of polymer gear

- Premature and extended contacts occurred in the stainless steel-polyamide gear mesh due to higher deflection of lower material modulus polymer gear. These contacts were responsible for roll angle increase. Roll angle of stainless steel-polyamide gear pair was increased by 6.7% at 0.5 Nm and 13.3% at 2.0 Nm when compared to that of stainless steel- stainless steel gear pair
- Static transmission error and gear mesh stiffness increased nonlinearly with load increase for both the numerical and experimental works. The nonlinear deformation of polymer gear tooth and contact behaviour of polymer gear tooth surface contributed these characteristics. Gear mesh stiffness of 268.7–301.4 Nm/rad at 0.5 Nm was increased to 290.5–313.2 Nm/rad at 2.0 Nm for the single tooth contact.
- Bending stress with nonlinear material models was lower by 2.55–14.64 % compared to that of linear material models. With an increasing strain rate, an increase in the bending stress was observed for nonlinear material models because of the higher material modulus at higher strain rates.

- The static transmission error with the linear material models was lower by 0.63–9.28 % than that of the nonlinear material models, and it further decreased with increased strain rate, for both STC and DTC.
- The nonlinear material model obtained at the strain rate corresponding to the desired application can be used for predicting the bending stress and static transmission error of polymer gears more accurately.

7.3 FUTURE SCOPE

- In the present investigation, bending fatigue tests and static transmission studies were conducted on unreinforced and carbon fiber reinforced polyamide gears while meshing with stainless steel gear. In future, both tests and studies on the gears may be of same polymer/polymer composite gear material.
- Damage tolerant studies including crack growth investigation on unreinforced and carbon fiber reinforced polyamide gears can be attempted.
- Ideal involute profile without tooth errors was considered for the numerical analysis. Measured tooth features can be used for numerical analysis, in future and compared with the experimental results.
- Numerical analysis can be carried out for assessing the bending and transmission behaviour of polymer gears using viscoelastic material models. Numerical analysis can also be extended for thermal studies on polymer gears.

REFERENCES

1. **Akata E, Altynbalyk MT and Can Y** (2004) Three point load application in single tooth bending fatigue test for evaluation of gear blank manufacturing methods. *International Journal of Fatigue*, **26**(7): 785-789.

2. **Atanasiu V, Doroftei I, Iacob MR and Leohchi D** (2011) Nonlinear dynamics of steel/plastic gears of servomechanism structures. *Materiale Plastice*, **48**(1): 98-103.

3. **Bernasconi A, Davoli P, Basile A and Filippi A** (2007) Effect of fibre orientation on the fatigue behaviour of a short glass fibre reinforced polyamide-6. *International Journal of Fatigue*, **29**(2): 199–208.

4. **Bernasconi A and Kulin RM** (2009) Effect of frequency upon fatigue strength of a short glass fiber reinforced polyamide 6: A superposition method based on cyclic creep parameters. *Polymer Composites*, **30**(2): 154-161.

5. **Bernasconi A, Conrado E and Hine P** (2015) An experimental investigation of the combined influence of notch size and fibre orientation on the fatigue strength of a short glass fibre reinforced polyamide 6. *Polymer Testing*, **47**: 12–21.

6. **Boccardi S, Carlomagno GM, Meola C, Simeoli G and Russo P** (2015) Infrared thermography to evaluate thermoplastic composites under bending load. *Composite Structures*, **134**: 900–904.

7. **Bravo A, Koffi D, Toubal L and Erchiqui F** (2015) Life and damage mode modeling applied to plastic gears. *Engineering Failure Analysis*, **58**(1): 113–133.

8. **Breeds AR, Kukureka SN, Mao K, Walton D and Hooke CJ** (1993) Wear behaviour of acetal gear pairs. *Wear*, **166**(1): 85–91.

9. **British Standards Institution** (2006) BS ISO 6336-3:2006: Calculation of load capacity of spur and helical gears – Part 3: Calculation of tooth bending strength. London, BSI.

10. **Brunbauer J, Mosenbach A, Guster C and Pinter G** (2014) Fundamental influences on quasistatic and cyclic material behavior of short glass fiber reinforced polyamide illustrated on microscopic scale. *Journal of Applied Polymer Science*, **131**(19): 40842.

11. **Brunbauer J and Pinter G** (2015) Effects of mean stress and fibre volume content on the fatigue-induced damage mechanisms in CFRP. *International Journal of Fatigue*, **75**: 28-38.

12. **Cao K, Ma X, Zhang B, Wang Y and Wang Yu** (2010) Tensile behavior of polycarbonate over a wide range of strain rates. *Materials Science and Engineering A*, **527**(16-17): 4056–4061.

13. **Cathelin J, Letzelter E, Guingand M, Vaujany JP de and Chazeau L** (2013) Experimental and numerical study of a loaded cylindrical PA66 gear. *Journal of Mechanical Design*, **135**(4): 1-9.

14. **Chandran KSR** (2016) Mechanical fatigue of polymers: A new approach to characterize the S-N behavior on the basis of macroscopic crack growth mechanism. *Polymer*, **91**: 222-238.

15. **Crippa G and Davoli P** (1995) Comparative fatigue resistance of fiber reinforced nylon 6 gears. *Journal of Mechanical Design*, **117**(1): 193–198.

16. **Daniewicz SR and Moore DH** (1998) Increasing the bending fatigue resistance of spur gear teeth using a presetting process. *International Journal of Fatigue*, **20**(7): 537-542.

17. **Duzcukoglu H** (2009) PA 66 spur gear durability improvement with tooth width modification. *Materials and Design*, **30**(4): 1060–1067.

18. **Duzcukoglu H** (2009) Study on development of polyamide gears for improvement of load-carrying capacity. *Tribology International*, **42**(8): 1146–1153.

19. **Eyercioglu O, Walton D and Dean T** (1997) Comparative bending fatigue strength of precision forged spur gears. *Proceedings of the Institution of Mechanical Engineers, Part C: Journal of Mechanical Engineering Science*, **211**(4): 293-299.

20. **Fan JT, Weerheijm J and Sluys LJ** (2015) High-strain-rate tensile mechanical response of a polyurethane elastomeric material. *Polymer*, **65**: 72-80.

21. **Florin P, Facchinetti M, Doudard C and Calloch S** (2013) Fast fatigue properties identification by "Self-Heating" method: Application to automotive welded joints. *5th Fatigue Design Conference, Fatigue Design 2013*, **66**: 676-683.

22. **German Standards** (1978) DIN 3962: Tolerances for cylindrical gear teeth. Berlin, DIN.

23. **Goel A, Chawla KK, Vaidya UK, Chawla N and Koopman M** (2009) Characterization of fatigue behaviour of long fiber reinforced thermoplastic (LFT) composites. *Materials Characterization*, **60**(6): 537–544.

24. **Gorla C, Rosa F, Concli F and Alertini H** (2012) Bending fatigue strength of innovative gear materials for wind turbines gearboxes: effect of surface coatings. *Proceedings of IMECE2012,* **86513**: 1-7.

25. **Guo Y and Li Y** (2007) Quasi-static/dynamic response of SiO_2–epoxy nanocomposites. *Materials Science Engineering: A*, **458**(1-2): 330–335.

26. **Hakimian E and Sulong AB** (2012) Analysis of warpage and shrinkage properties of injection-molded micro gears polymer composites using numerical simulations assisted by the taguchi method. *Materials and Design*, **42**: 62–71.

27. **Handa K, Kato A and Narisawa I** (1999) Fatigue characteristics of a glass-fiber-reinforced polyamide. *Journal of Applied Polymer Science*, **72**(13): 1783-1793.

28. **Handschuh RF, Krantz TL, Lerch BA and Burke CS** (2007) Investigation of low-cycle bending fatigue of AISI 9310 steel spur gears. *Proceedings of ASME 2007 International Design Engineering Technical Conferences and Computers and Information in Engineering Conference*, **7**:871-877.

29. **Hooke CJ, Mao K, Walton D, Breeds AR and Kukureka SN** (1993) Measurement and prediction of the surface temperature in polymer gears and its relationship to gear wear. *Journal of Tribology*, **115**(1): 119–124.

30. **Hossan MR and Hu Z** (2008) Strength evaluation of polymer composite spur gear by finite element analysis. *Proceedings of IMECE2008*, **66617**: 1–8.

31. **Hoskins TJ, Dearn KD, Kukureka SN and Walton D** (2011) Acoustic Noise from Polymer Gears - A Tribological Investigation. *Materials and Design*, **32**(6): 3509-3515.

32. **Hoskins TJ, Dearn KD, Chen YK and Kukureka SN** (2014) The wear of PEEK in rolling-sliding contact - Simulation of polymer gear applications. *Wear*, **309**(1-2): 35–42.

33. **Hu Z and Hossan MR** (2013) Strength evaluation and failure prediction of short carbon fiber reinforced nylon spur gears by finite element modelling. *Applied Composite Materials*, **20**(3): 315-330.

34. **Imrek H** (2009) Performance improvement method for Nylon 6 spur gears. *Tribology International*, **42**(3): 503–510.

35. **Jegou L, Marco Y, SauxVLe and Calloch S** (2013) Fast prediction of the wohler curve from heat build-up measurements on short fiber reinforced plastic. *International Journal of Fatigue*, **47**: 259-267.

36. **Karimpour M, Dearn KD and Walton D** (2010) A kinematic analysis of meshing polymer gear teeth. *Proceedings of the Institution of Mechanical Engineers, Part L: Journal of Materials Design and Applications*, **224**(3): 101–115.

37. **Katunin A, Hufenbach W, Kostka P and Holeczek K** (2010) Frequency dependence of the self-heating effect in polymer-based composites. *Journal of Achievements in Materials and Manufacturing Engineering*, **41**(1-2): 9-15.

38. **Kawagoe M, Nomiya M, Qiu J and Morita M** (1997) Fatigue behaviour of injection-moulded polymer blends of polypropylene and liquid crystalline polyester. *Polymer*, **38**(1): 113-118.

39. **Kim CH** (2006) Durability improvement method for plastic spur gears. *Tribology International*, **39**(11): 1454–1461.

40. **Kim SH, Shin MC, Byun JW, Hwan OK and Chu CN** (2012) Efficiency prediction of worm gear with plastic worm wheel. *International Journal of Precision Engineering and Manufacturing*, **13**(2): 167–174.

41. **Kirupasankar S, Gurunathan C and Gnanamoorthy R** (2012) Transmission efficiency of polyamide nanocomposite spur gears. *Materials and Design*, **39**: 338–343.

42. **Koffi D, Gauvin R and Yelle H** (1985) Heat generation in thermoplastic spur gears. *Journal of Mechanisms Transmissions and Automation in Design*, **107**(1): 31–36.

43. **Koricho EG, Belingardi G and Beyene AT** (2014) Bending fatigue behavior of twill fabric E-glass/epoxy composite. *Composite Structures*, **111**: 169-178.

44. **Kurokawa M, Uchiyama Y and Nagai S** (1999) Performance of plastic gear made of carbon fiber reinforced poly-ether-ether-ketone. *Tribology International*, **32**(9): 491–497.

45. **Kurokawa M, Uchiyama Y and Nagai S** (2000) Performance of plastic gear made of carbon fiber reinforced poly-ether-ether-ketone: Part 2. *Tribology International*, **33**(10): 715–721.

46. **Kurokawa M, Uchiyama Y and Nagai S** (2000) Tribological properties and gear performance of polyoxymethylene composites. *Journal of Tribology*, **122**(4): 809–814.

47. **Kurokawa M, Uchiyama Y, Iwai T and Nagai S** (2003) Performance of plastic gear made of carbon fiber reinforced polyamide 12. *Wear*, **254**(5-6): 468–473.

48. **Letzelter E, Vaujany JP de, Chazeau Land Guingand M** (2009) Quasi-static load sharing model in the case of nylon 6/6 cylindrical gears. *Materials and Design*, **30**(10):4360-4368.

49. **Letzelter E, Guingand M, Vaujany JPD and Schlosser P** (2010) A new experimental approach for measuring thermal behaviour in the case of nylon 6/6 cylindrical gears. *Polymer Testing*, **29**(8): 1041–1051.

50. **Li W, Wood A, Weidig R and Mao K** (2011) An investigation on the wear behaviour of dissimilar polymer gear engagements. *Wear*, **271**(9-10): 2176–2183.

51. **Lin A-D and Kuang JH** (2008) Dynamic interaction between contact loads and tooth wear of engaged plastic gear pairs. *International Journal of Mechanical Sciences*, **50**(2): 205–213.

52. **Mao K** (2007) A new approach for polymer composite gear design. *Wear*, **262**(3-4): 432–441.

53. **Mao K, Li W, Hooke C and Walton D** (2009) Friction and wear behaviour of acetal and nylon gears. *Wear*, **267**(1): 639-645**.**

54. **Mao K, Li W, Hooke CJ and Walton D** (2010) Polymer gear surface thermal wear and its performance prediction. *Tribology International*, **43**(1-2): 433–439.

55. **Mao K, Langlois P, Hu Z, Alharbi K, Xu X, Milson M, Li W, Hooke CJ and Chetwynd D** (2015) The wear and thermal mechanical contact behaviour of machine cut polymer gears. *Wear*, **332-333**: 822-826.

56. **Mathieson H and Fam A** (2014) High cycle fatigue under reversed bending of sandwich panels with GFRP skins and polyurethane foam core. *Composite Structures*, **113**: 31-39.

57. **Meuleman PK, Walton D, Deran KD, Weale DJ and Driessen I** (2007) Minimization of transmission errors in highly loaded plastic gear trains. *Proceedings of the Institution of Mechanical Engineers, Part C: Journal of Mechanical Engineering Science*, **221**(9):1117-1129.

58. **Ming HT and Ying CT** (1997) A method for calculating static transmission errors of plastic spur gears using FEM evaluation. *Finite Elements in Analysis and Design*, **27**(4): 345-357.

59. **Mohan NA and Senthilvelan S** (2014) Preliminary bending fatigue performance evaluation of asymmetric composite gears. *Mechanism and Machine Theory*, **78**: 92–104.

60. **Mortazavian S and Fatemi A** (2015) Fatigue behavior and modelling of short fiber reinforced polymer composites: A literature review. *International Journal of Fatigue*, **70**: 297-321.

61. **Mortazavian S and Fatemi A** (2015) Effects of fiber orientation and anisotropy on tensile strength and elastic modulus of short fiber reinforced polymer composites. *Composites: Part B*, **72**: 116-129.

62. **Mortazavian S, Fatemi A, Mellott SR and Khosrovaneh A** (2015) Effect of cycling frequency and self-heating on fatigue behaviour of reinforced and unreinforced thermoplastic polymers. *Polymer Engineering and Science*, **55**(10):2355-2367.

63. **Mortazavian S and Fatemi A** (2016) Effects of mean stress and stress concentration on fatigue behaviour of short fiber reinforced polymer composites. *Fatigue and Fracture of Engineering Materials and Structures*, **39**(2):149-166.

64. **Mourad AHI, Elsayed HF and Barton DC** (2004) Semicrystalline polymers deformation and fracture behaviour under quasi static strain rates and triaxial states of stress. *Strength, Fracture and Complexity*, **2**(4):149–162.

65. **Munier R, Doudard C, Calloch S and Weber B** (2014) Determination of high cycle fatigue properties of a wide range of steel sheet grades from self-heating measurements. *International Journal of Fatigue*, **63**: 46–61.

66. **Naebe M, Abolhassani MM, Khayyam H, Amini A and Fox B** (2016) Crack damage in polymers and composites: A review. *Polymer Reviews*, **56**(1): 31-69.

67. **Nitta K-H and Nomura H** (2014) Stress-strain behaviour of cold-drawn isotactic polypropylene subjected to various drawn histories. *Polymer*, **55**(25): 6614-6622.

68. **Peyrac C, Jollivet T, Leray N, Lefebvre F, Westphal O and Gornet L** (2015) Self-heating method for fatigue limit determination on thermoplastic composites. *Procedia Engineering*, **133**: 129–135.

69. **Pegoretti A and Ricco T** (2000) Fatigue fracture of neat and short glass fiber reinforced polypropylene: Effect of frequency and material orientation. *Journal of Composite Materials*, **34**(12): 1009-1027.

70. **Pogacnik A and Tavcar J** (2015) An accelerated multilevel test and design procedure for polymer gears. *Materials and Design*, **65**: 961–973.

71. **Rittel D, Eliash N and Halary JL** (2003) Hysteretic heating of modified poly (methylmethacrylate). *Polymer*, **44(**9): 2817-2822.

72. **Rosa G La and Risitano A** (2000) Thermographic methodology for rapid determination of the fatigue limit of materials and mechanical components. *International Journal of Fatigue*, **22**(1): 65–73.

73. **Senthilvelan S and Gnanamoorthy R** (2004) Wear characteristics of injection-moulded unfilled and glass-filled nylon 6 spur gears. *Proceedings of the Institution of Mechanical Engineers, Part J: Journal of Engineering Tribology*, **218**(6): 495–502.

74. **Senthilvelan S and Gnanamoorthy R** (2004) Damage mechanisms in injection molded unreinforced, glass and carbon reinforced nylon 66 spur gears. *Applied Composite Materials*, **11**(6): 377–397.

75. **Senthilvelan S and Gnanamoorthy R** (2006) Effect of gear tooth fillet radius on the performance of injection molded nylon 6/6 gears. *Materials and Design*, **27**(8): 632-639.

76. **Senthilvelan S and Gnanamoorthy R** (2006) Damping characteristics of unreinforced, glass and carbon fiber reinforced nylon 6/6 spur gears. *Polymer Testing*, **25**(1): 56–62.

77. **Senthilvelan S and Gnanamoorthy R** (2006) Fiber reinforcement in injection molded nylon 6/6 spur gears. *Applied Composite Materials*, **13**(4): 237–248.

78. **Senthilvelan S and Gnanamoorthy R** (2007) Effect of rotational speed on the performance of unreinforced and glass fiber reinforced Nylon 6 spur gears. *Materials and Design*, **28**(3): 765–772.

79. **Senthilvelan S and Gnanamoorthy R** (2008) Influence of reinforcement on composite gear metrology. *Mechanism and Machine Theory*, **43**(9): 1198–1209.

80. **Senthilvelan S and Gnanamoorthy R** (2009) Efficiency of injection-moulded polymer composite spur gears. *Proceedings of the Institution of Mechanical Engineers, Part J: Journal of Engineering Tribology*, **223**(6): 925–928.

81. **Shan G-F, Yang W, Yang M-bo, Xie B-hu, Feng J-min and Fu Q** (2007) Effect of temperature and strain rate on the tensile deformation of polyamide 6. *Polymer*, **48**(10): 2958-2968.

82. **Starkova O, Zhang Z, Zhang H and Park H-W** (2008) Limits of the linear viscoelastic behaviour of polyamide 66 filled with TiO_2 nanoparticles: Effect of strain rate, temperature, and moisture. *Materials Science and Engineering A*, **498**(1-2): 242–247.

83. **Shrestha R, Simsiriwong J, Shamsaei N and Moser R** (2016) Cyclic deformation and fatigue behavior of polyether ether ketone. *International Journal of Fatigue*, **82**(3): 411-427.

84. **Stringer DB, Dykas BD, LaBerge KE, Zakrajsek AJ and Handschuh RF** (2011) A new high-speed, high-cycle, gear-tooth bending fatigue test capability. *NASA Glenn Research Center*, Report No. NASA/TM-2011-217039, ARL-TR-5506: 1-9.

85. **Sweeney PJ and Randall RB** (1996) Gear transmission error measurement using phase demodulation. *Proceedings of the Institution of Mechanical Engineers, Part C: Journal of Mechanical Engineering Science*, **210**(3): 201-213.

86. **Taburdagitan M and Akkok M** (2006) Determination of surface temperature rise with thermo-elastic analysis of spur gears. *Wear*, **261**(5-6): 656–665.

87. **Takahara A, Magome T and Kajiyama T** (1994) Effect of glass fiber-matrix polymer interaction on fatigue characteristics of short glass fiber-reinforced poly (butylene terephthalate) based on dynamic viscoelastic measurement during the fatigue process. *Journal of Polymer Science: Part B: Polymer Physics*, **32**(5): 839-849.

88. **Teisuke B, Hiroshi S and Taku A** (2001) Wear of plastic spur gear made by injection molding. *Journal of Japanese Society of Tribologists*, **46**(11): 889–896.

89. **Trobentar B, Glodez S and Zafosnik B** (2015) Deflection analysis of spur polymer gear teeth. *Journal of Multidisciplinary Engineering and Technology*, **2**(4): 847-853.

90. **Walton D, Tessema AA, Hooke CT and Shippen JM** (1994) Load sharing in metallic and non-metallic gears, *Proceedings of the Institution of Mechanical Engineers, Part C: Journal of Mechanical Engineering Science*, **208**(2): 81-87.

91. **Walton D, Cropper AB, Weale DJ and Meuleman PK** (2002) The efficiency and friction of plastic cylindrical gears Part 1: Influence of materials. *Proceedings of the Institution of Mechanical Engineers, Part J: Journal of Engineering Tribology*, **216**(2): 75–92.

92. **Walton D, Cropper AB, Weale DJ and Meuleman PK** (2002) The efficiency and friction of plastic cylindrical gears Part 2 : Influence of tooth geometry. *Proceedings of the Institution of Mechanical Engineers, Part J: Journal of Engineering Tribology*, **216**(2): 93–103.

93. **Wang J and Howard I** (2004) The torsional stiffness of involute spur gears. *Proceedings of the Institution of Mechanical Engineers, Part C: Journal of Mechanical Engineering Science*, **218**(1): 131-142.

94. **Wang L, Shi S, Fu S, Chen G and Chen Xu** (2014) Evaluation of multiaxial fatigue life prediction criteria for PEEK. *Theoretical and Applied Fracture Mechanics*, **73**: 128-135.

95. **Weale DJ, White J and Walton D** (1999) The effect of fiber orientation and distribution on the tooth stiffness of a polymer composite gear. *Journal of Reinforced Plastics and Composites*, **18**(5): 454–463.

96. **Wright NA and Kukureka S** (2001) Wear testing and measurement techniques for polymer composite gears. *Wear*, **251**(1-12): 1567–1578.

97. **Xi L** (2010) Investigation of the region of fatigue crack initiation in a transmission gear. *Materials Science and Engineering A*, **527**(6): 1377-1382.

98. **Yelle H and Burns DJ** (1981) Calculation of contact ratios for plastic/plastic or plastic/steel spur gear pairs. *Journal of Mechanical Design*, **103**(2): 528-542.

99. **Yousef SS, Burns DJ and McKinlay W** (1973) Techniques for assessing the running temperature and fatigue strength of thermoplastic gears. *Mechanism and Machine Theory*, **8**(2): 175–185.

100. **Zainudin ES, Sapuan SM, Sulaiman S and Ahmad MMHM** (2002) Fiber orientation of short fiber reinforced injection molded thermoplastic composites: A Review. *Journal of Injection Molding Technology*, **6**(1): 1-10.

101. **Zhang J, Zhang Q, Xu Z-Z, Shin G-S and Lyu S** (2013) A Study on the Evaluation of Bending Fatigue Strength for 20CrMoH Gear, *International Journal of Precision Engineering and Manufacturing*, **14**(8): 1339-1343.

102. **Zhou J, D'Amore A, Yang Y, He T, Li B and Nicolais L** (1994) Flexural fatigue of short glass fiber reinforced a blend of polyphenylene ether ketone and polyphenylenesulfide. *Applied Composite Materials*, **1**(3): 183-195.

LIST OF PUBLICATIONS BASED ON THE RESEARCH WORK

REFEREED JOURNALS

1. **Kodeeswaran M, Arnika Verma, Suresh R and Senthilvelan S** (2016) Bi-directional and uni-directional bending fatigue performance of unreinforced and carbon fiber reinforced polyamide 66 spur gears. *International Journal of Precision Engineering and Manufacturing*, **17**(8):1025-1033.

2. **Kodeeswaran M, Suresh R and Senthilvelan S** (2016) Transmission characteristics of Injection molded polymer spur gears: Experimental and Numerical Evaluation. *International Journal of Powertrains*, **5**(3): 246-263.

3. **Kodeeswaran M, Arnika Verma, Suresh R and Senthilvelan S** (2017) Effects of frequency on hysteretic heating and fatigue life of unreinforced injection molded polyamide 66 spur gears. *Proceedings of the Institution of Mechanical Engineers, Part L: Journal of Materials: Design and Applications*, Available online from 09 April 2017.

4. **Kodeeswaran M, Suresh R and Senthilvelan S (2017)** Effect of strain rate on bending and transmission characteristics of injection molded polyamide 66 spur gears. *Proceedings of the Institution of Mechanical Engineers, Part L: Journal of Materials: Design and Applications*, Available online from 13 August 2017.

PRESENTATION IN CONFERENCES

1. **Kodeeswaran M, Suresh R and Senthilvelan S** (2013) Test rig design for bending fatigue performance evaluation of polymer based composite gears. *Proceedings of the 1st International and 16th National Conference on Machines and Mechanisms (iNaCoMM 2013)*, 434-438.

2. **Kodeeswaran M, Suresh R and Senthilvelan S** (2014) Finite element analysis of polymeric gear mesh stiffness. *17th International conference on Advances in Materials and Processing Technologies (AMPT 2014),* Dubai, UAE.

3. **Kodeeswaran M, Anurag Mishra, Suresh R and Senthilvelan S** (2015) Bending fatigue performance of polymeric composite gears under bi-directional loading, *23rd Annual International Conference on Composites/Nano Engineering (ICCE-23),* Chengdu, China.

4. **Kodeeswaran M, Arnika Verma, Suresh R and Senthilvelan S** (2016) Hysteresis heating of polymer gear. *2nd International Conference on Polymer Tribology (PolyTrib 2016),* Ljubljana, Slovenia.

CURRICULUM VITAE

1.	Name	:	**M. Kodeeswaran**
2.	Date of Birth	:	11.05.1975
3.	Permanent Address	:	TC: 10/1665(7) Harmony Gardens Chenchery Kurumkulam Road Nalanchira Thiruvananthapuram Kerala – 695015 Ph. No.: +91-9496258389, 0471-2534289 Email: kodees_vssc@yahoo.com

4. Educational Qualifications:

1992–1996	**:**	**Bachelor of Engineering**
Institution	:	Govt. College of Technology Coimbatore–641013, India
Specialization	:	Mechanical Engineering
2006–2008	**:**	**Master of Technology**
Institution	:	Indian Institute of Technology Madras Chennai–600036, India
Specialization	:	Mechanical Engineering
2012–2017	**:**	**Doctor of Philosophy**
Institution	:	Indian Institute of Technology Guwahati Guwahati–781039, India
Registration Date	:	30.07.2012
Thesis Submission Date	:	02.08.2017
Viva-Voce Date	:	05.02.2018

DOCTORAL COMMITTEE

Supervisors	:	**Dr. S. Senthilvelan** Professor Department of Mechanical Engineering Indian Institute of Technology Guwahati
		Dr. R. Suresh Head, Composite and Thermal Structures Section Structural Design & Analysis Division Vikram Sarabhai Space Centre
Chairperson	:	**Dr. U. S. Dixit** Professor Department of Mechanical Engineering Indian Institute of Technology Guwahati
Members	:	**Dr. Sukhomay Pal** Associate Professor Department of Mechanical Engineering Indian Institute of Technology Guwahati
		Dr. A. Perumal Professor Department of Physics Indian Institute of Technology Guwahati